EPA-600/3-76-029
April 1976

Ecological Research Series

SMOG CHAMBER CONFERENCE PROCEEDINGS

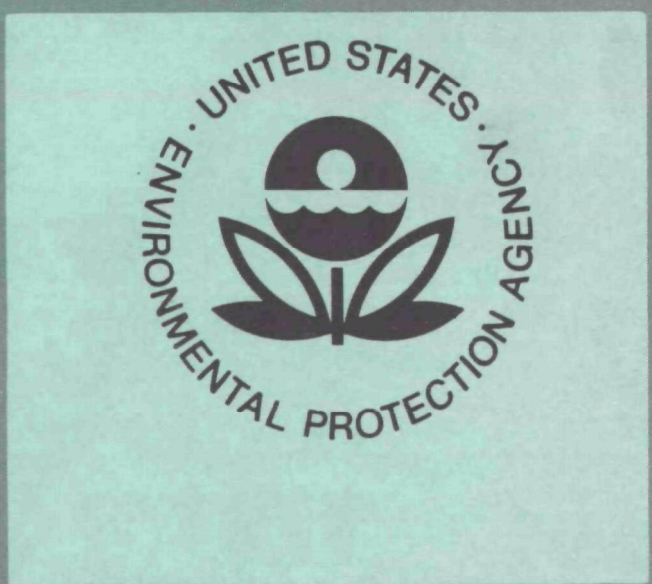

Environmental Sciences Research Laboratory
Office of Research and Development
U.S. Environmental Protection Agency
Research Triangle Park, North Carolina 27711

RESEARCH REPORTING SERIES

Research reports of the Office of Research and Development, U.S. Environmental Protection Agency, have been grouped into five series. These five broad categories were established to facilitate further development and application of environmental technology. Elimination of traditional grouping was consciously planned to foster technology transfer and a maximum interface in related fields. The five series are:

1. Environmental Health Effects Research
2. Environmental Protection Technology
3. Ecological Research
4. Environmental Monitoring
5. Socioeconomic Environmental Studies

This report has been assigned to the ECOLOGICAL RESEARCH series. This series describes research on the effects of pollution on humans, plant and animal species, and materials. Problems are assessed for their long- and short-term influences. Investigations include formation, transport, and pathway studies to determine the fate of pollutants and their effects. This work provides the technical basis for setting standards to minimize undesirable changes in living organisms in the aquatic, terrestrial, and atmospheric environments.

This document is available to the public through the National Technical Information Service, Springfield, Virginia 22161.

EPA-600/3-76-029
April 1976

SMOG CHAMBER CONFERENCE PROCEEDINGS

B. Dimitriades
(Chariman)

U.S. ENVIRONMENTAL PROTECTION AGENCY
Office of Research and Development
Environmental Sciences Research Laboratory
Research Triangle Park, North Carolina 27711

April 1976

DISCLAIMER

This report has been reviewed by the Environmental Sciences Research Laboratory, U.S. Environmental Protection Agency, and approved for publication. Mention of trade names or commercial products does not constitute endorsement or recommendation for use.

CONTENTS

	Page
LIST OF FIGURES	v
LIST OF TABLES	viii
1. INTRODUCTORY REMARKS	1
2. SMOG CHAMBER PERFORMANCE	3
COMPARISON OF SMOG CHAMBERS	3
EFFECTS OF CHAMBER DESIGN FACTORS	4
INTERPRETATIONS OF CHAMBER DESIGN EFFECTS	6
DISCUSSION	18
REFERENCES FOR CHAPTER 2	22
3. ANALYTICAL TECHNIQUES IN SMOG CHAMBER STUDIES	25
MEASUREMENT OF NITROGEN OXIDES	25
Colorimetric Analyzers	25
Chemiluminescence Analyzers	25
Calibration	26
Interferences	26
Comparison of Methods	26
Discussion	28
IN SITU MEASUREMENTS	29
DISCUSSION	35
AEROSOL MEASUREMENT	37
MEASUREMENT OF OXYGENATED SULFUR COMPOUNDS	40
Sulfur Dioxide	43
Sulfate Aerosols	45
Discussion	46
QUALITY CONTROL	46
Calibration	46
Statistical Approach	47
Measures of Reactivity	50
REFERENCES FOR CHAPTER 3	53
4. BACKGROUND REACTIVITY	57
INTERPRETATION OF BACKGROUND REACTIVITY DATA	57
DISCUSSION	59
REFERENCES FOR CHAPTER 4	61
5. COMPARABILITY OF SMOG CHAMBER ATMOSPHERE AND REAL ATMOSPHERE	63
A METHOD FOR COMPARING SMOG CHAMBER DATA WITH ATMOSPHERIC DATA	63
Sampling and Data Collection	64

Page

Discussion 66
STATIC AND DYNAMIC SMOG CHAMBER TESTS 67
SIMULATION OF NATURAL SUNLIGHT 71
OUTDOOR SMOG CHAMBERS 72
REFERENCES FOR CHAPTER 5 90
6. VALIDITY AND UTILITY OF SMOG CHAMBER DATA 91
INTRODUCTORY REMARKS 91
THE LACAPCD VIEWPOINT (HAMMING TRANSFORM) 92
Summary 92
Presentation 93
Discussion 94
THE EPA VIEWPOINT 98
CALIFORNIA AIR RESOURCES BOARD VIEWPOINT 102
Introduction 102
Environmental Chamber Studies 103
Conclusions 112
Unresolved Questions 113
SMOG CHAMBER STUDIES OF POLLUTANT PRECURSOR RELATIONSHIPS 113
REFERENCES FOR CHAPTER 6 114
7. CONCLUSION 115
LIST OF ATTENDANTS 117

LIST OF FIGURES

Figure		Page
1	Composite Photochemical Test Results for Teflon Film Surfaces	5
2	Composite Photochemical Test Results for Pyrex Surfaces	5
3	Composite Photochemical Test Results for Aluminum Surfaces	6
4	Composite Photochemical Test Results for Stainless Steel Surfaces	6
5	Species in Irradiated Propylene/NO_x System that Dissociate on Absorption of Radiation Present	7
6	Comparison of Full and Cut Spectrum Model Simulations	9
7	Effective Quantum Yields for Propylene Destruction by Absorption of Photolytic Energy by Nitrogen Dioxide	11
8	Simulation of Full Spectrum Runs for Various Heterogeneous Rates, $NO + NO_2 + H_2O \xrightarrow{k} 2\ HONO$	13
9	Relative Importance of $O + C_3H_6$ and $HONO + h\nu$ in Initiating Reaction	14
10	Simulation of Full Spectrum Runs With Preestablished HONO Equilibrium and Without Preestablished HONO Equilibrium	15
11	Reactions Controlling Ozone Production	15
12	Graphs of the $(O_3)(NO)/(NO_2)$ Function Versus Time for Different Surfaces	16
13	Reactions of Radical Species with Nitric Oxide	16
14	Alternative Reactions of Peroxy Radicals Leading to Ozone Formation	17
15	Concentration-time Profiles for NO, NO_2, O_3, and Propylene at 15° and 35° C.	20
16	Predicted Concentration-time Profiles for NO, NO_2, O_3, and Propylene at 0, 50, and 100 Percent Relative Humidity	21
17	Comparison of Methods for Monitoring NO and NO_2 During a Smog-chamber Experiment	27
18	Nitrogen Balance During Irradiation of Propylene-NO_x	28
19	Nitrogen Balance During Irradiation of Synthetic Auto Exhaust	29
20	Single Beam Plot in CH Absorption Region for 1 Atmosphere of Tank Air with Addition of 5 ppm 1,1 Dichlorethylene and 0.1 ppm Molecular Chlorine, Before Irradiation. Path Length, 500 Meters; Resolution, 1 cm^{-1}	34

Figure		Page
21	Single Beam Plot in CH Absorption Region for 1 Atmosphere of Tank Air with Addition of 5 ppm 1,1 Dichlorethylene and 0.1 ppm Molecular Chlorine, after 15 Minutes of Irradiation. Path length, 500 Meters; Resolution, 1 cm^{-1}	35
22	Ratio Plot, Spectrum of Products over Spectrum of Reactants; 5 ppm 1,1 Dichlorethylene and 0.1 ppm Molecular Chlorine in Air, after 15 Minutes of Irradiation. Path Length, 500 Meters; Resolution, 1 cm^{-1}	36
23	Ratio Plot, Spectrum of Reactants over Spectrum of Tank Air; 5 ppm 1,1 Dichlorethylene and 0.1 ppm Molecular Chlorine in Air, Before Irradiation. Path Length, 500 Meters; Resolution, 1 cm^{-1}	37
24	Ratio Plot, Spectrum of Products over Spectrum of Tank Air; 5 ppm 1,1 Dichlorethylene and 0.1 ppm Molecular Chlorine in Air, after 10 Minutes Irridiation. Path Length, 500 Meters; Resolution, 1 cm^{-1}	38
25	Ratio Plot, Spectrum of Products over Spectrum of Reactants; 5 ppm 1,1 Dichlorethylene and 0.1 ppm Molecular Chlorine in Air, after 10 Minutes Irradiation. Path Length, 500 Meters; Resolution, 4 cm^{-1}	39
26	Sulfur Dioxide Removal During Irradiation of Propylene-NO_x	43
27	Comparison of Methods for Sulfur Dioxide Analyses During Smog-Chamber Irradiations.	44
28	Calibration Methods Used for Chemiluminescent NO_x and O_3 Instruments.	46
29	Comparison of Typical Reaction Data for Indoor and Outdoor Smog Chambers	54
30	Injection and Back Flush of Ambient Air Sample	65
31	Ambient Air Photolysis	67
32	Maximum 4-hour-average Ozone, Kane, Pennsylvania, Versus Maximum Temperature at Nearest Reporting Stations, October 1974	68
33	Effect on Ozone Generation by Dilution of Reactants: NO, $_2$, and O_3, October 7, 1974	69
34	Effect of Reaction and Dilution on a Simulated Urban Mix of Hydrocarbons, October 7, 1974	70
35	Chamber Simulation of Extended Urban Influence on Surface Ozone Concentration	71
36	The University of North Carolina Smog Chamber	73
37	Comparison of Total Solar Radiation on Horizontal Surface with Rate of Photolysis of NO_2 (K_1) (Latitude 35.72°), September 19, 1974.	76
38	Diurnal Variation of Solar Radiation and Temperature, May 7, 1974	76
39	Diurnal Variations of Solar Radiation and Temperature, May 19, 1974	77
40	Comparison of Concentration-time Profiles from the Two Chamber Compartments (Red and Blue), May 7, 1974	77
41	Concentration-time Profiles, May 19, 1974	78

Figure		Page
42	Rate of NO Disappearance and NO_2 Appearance for a Clear Day, October 13, 1974	78
43	Rate of NO Disappearance and NO_2 Appearance for a Partly Cloudy Day, May 19, 1974	79
44	Comparison of Ozone Profiles and Solar Radiation Profiles for Propylene Runs	80
45	Diurnal Variation of Solar Radiation and Temperature, September 19, 1974	81
46	Concentration-time Profiles, September 19, 1974	81
47	Diurnal Variations of Solar Radiation and Temperature, September 23, 1974	82
48	Concentration-time Profiles, September 23, 1974	82
49	Comparison of Ozone and Solar Radiation Profiles for Mix Runs	84
50	Effect of Temperature on Maximum Rate of NO Disappearance	85
51	Comparison of Kinetics Model and Actual Data for May 7, 1974	86
52	Model Results for Constant K_1=0.1, 0.3, May 7, 1974, Conditions	87
53	Model Results for Constant K_1=0.2, 0.4, May 7, 1974, Conditions	88
54	Concentration-time Profiles for Dual Run in University of North Carolina Chamber, Effect of Initial NO_2/NO_x, May 19, 1974	89
55	Ozone as a Function of HC and NO_x, from Smog Chamber Data	95
56	Time to Maximum NO_2 as a Function of HC and NO_x, from Smog Chamber Data	96
57	Variation of $[O_3]_{air}/[O_3]_{ch}$ With Year	98
58	Upper Limit Oxidant Values in the South Coast Air Basin as a Function of Average 6 to 9 a.m. Nonmethane Hydrocarbon Concentrations, 1971 Data. Oxidant Concentrations are Maximum 1-hour Values for 12 Stations; NMHC Concentrations are Average Values for 8 Stations	99
59	Smog Chamber Data on Dependence of Oxidant on NMHC under Constant NO_x or HC/NO_x Conditions	100
60	Equal Response Lines Representing All Combinations of NMHC and NO_x Concentrations Corresponding to 0.08 ppm O_3 of Oxidant	101
61	Reaction Profile for SAPRC Run No. 42E, 6-hour Irradiation	105
62	Reaction Profile for SAPRC Run No. 48E, 10-hour Irradiation	106
63	Ozone Isopleths from 6-hour Irradiations of HC-NO_x Mixtures, SAPRC Runs 10-48(E). $[O_3]$ Values Are Final 6-hour Ozone Concentrations (ppm)	108
64	Ozone Isopleths from 10-hour Irradiations of HC-NO_x mixtures, SAPRC Runs 10-48(E). $[O_3]$ Values Are Final 10-hour Ozone Concentrations Plus 3 Times the Final Rate of Ozone Formation	109

Figure | Page

65 Ozone Rate Isopleths from 10-hour Irradiations of HC-NO_x Mixtures, SAPRC Runs 10-48(E) . . . 110

66 Oxidant-dosage Reactivity of Exhaust as a Function of NO_x at Various HC:NO_x Ratios . . . 111

LIST OF TABLES

Table | Page

1 Range and Average Values of Propylene/NO_x Reactivity Data Obtained with Various (9) Smog Chambers . . . 3

2 Reactivity Rankings of Hydrocarbons as Measured in Various (7) Smog Chambers . . . 3

3 Ratio Values for Cut-to-fit Spectrum Parameters . . . 10

4 Ratio Values for Deleted-to-complete Model (Full Spectrum) Parameters . . . 10

5 Activation Energies of Reactions in the General Mechanism . . . 19

6 Colorimetric NO_2 Analyzer: Ozone Interference, $[NO_2]$ = 0.23 ppm . . . 26

7 Infrared Detection of Pollutants . . . 32

8 Aerosol Sampling Procedures . . . 41

9 Characteristics of Selected Samplers . . . 42

10 Confidential Interval on Bias in Measuring Ozone at the Federal Air Quality Standard with a Chemiluminescent Instrument Calibrated by Replicated NBKI Measurements . . . 49

11 Inorganic Reactions of Photochemical Smog Formation . . . 51

12 Reactions Participating in the Total Ozone Decay Process . . . 61

13 Summary of Measurements to be Made at University of California, Riverside . . . 66

14 Derivation of Continuous Chemical Actionometer for NO_x (CCANOX) . . . 75

15 Ozone Formation, SAPRC Glass Chamber . . . 107

SMOG CHAMBER CONFERENCE PROCEEDINGS

1. INTRODUCTORY REMARKS

B. Dimitriades, EPA

Following a welcome address to the conference, Dr. Dimitriades explained briefly the purposes and theme of the Smog Chamber Conference. One of the purposes of the conference relates to the U.S. Environmental Protection Agency's practice of holding regular conference-type meetings to which all EPA contractors and grantees working in a certain problem area are invited to present and discuss with EPA work progress and future plans and to coordinate the various research projects.

Another reason for organizing this event and setting the theme to be "smog chamber studies" is the strong needs that have developed lately for smog chamber evidence. In the past, smog chamber studies focused on exploring the photochemical smog phenomenon, on making reactivity characterizations of emissions, and on generating mechanistic evidence. Presently, it is believed that the most important use of smog chambers is in generating evidence on the relationships between photochemical pollutants and their precursors. Such evidence serves as a part of the scientific basis, and in some cases, perhaps, as the entire scientific basis of a photochemical pollutant control strategy.

Smog chambers have already been used in this latter fashion. Specifically, smog chamber data have been used to derive such relationships between photochemical oxidant (O_x) and its precursors, hydrocarbons (HC) and nitrogen oxides (NO_x). In this case, it so happened that it was possible to derive such relationships from aerometric data also. Furthermore, it so happened that EPA felt--not in agreement with everyone else--that the aerometric data relationships should be used as the primary basis for an oxidant control strategy. However, such preference for the aerometric data, in this instance, should not--and did not--degrade the utility of the smog chamber method. It should be borne in mind that the O_x/HC/NO_x relationships are relatively simple and can be defined to a degree from aerometric data. However, this, in all probability, is not going to be the case with the other

photochemical pollution problems, e.g., photochemical aerosol, sulfate, etc. The enormous complexity of these problems could very well make smog chamber experimentation the only feasible source of definitive, useful information.

For these reasons, EPA has initiated, in the last year, a fairly comprehensive program of smog chamber studies. It is hoped and expected that this conference will provide an opportunity to review the smog chamber method and associated procedures, to identify and correct possibly existing problems, and, finally and most importantly, to closely examine and discuss the validity and utility of the smog chamber data that are to be obtained.

2. SMOG CHAMBER PERFORMANCE

COMPARISON OF SMOG CHAMBERS -- *B. Dimitriades, EPA*

One systematic comparison of smog chambers and smog chamber data was completed in 1969, as a part of a cooperative effort sponsored by the Coordinating Research Council (CRC). The participating research groups used nine smog chambers to test a number of standard HC/NO_x mixtures. Ranges and averages of test results are shown in Tables 1 and 2.

Table 1. RANGE AND AVERAGE VALUES OF PROPYLENE/NO_x REACTIVITY DATA OBTAINED WITH VARIOUS (9) SMOG CHAMBERS

Initial concentrations of propylene/NO_x, ppmC/ppm	R_{NO_2}, ppb/min		Maximum oxidant, ppm	
	Range	Average	Range	Average
9/3	14-39	25.3	0.5-1.4	0.79
9/1.5	18-42	28.9	0.5-1.4	1.0
9/0.5	7-52	22.2	0.2-1.0	0.59
1.5/0.25	5-50	13.4	0.2-0.6	0.39

Table 2. REACTIVITY RANKINGS OF HYDROCARBONS AS MEASURED IN VARIOUS (7) SMOG CHAMBERS
(Rankings of most and least reactive hydrocarbons: 1 and 7 respectively)

Hydrocarbon	R_{NO_2}	Maximum oxidant
n-hexane	6-7	6-7
Isooctane	6-7	6-7
Ethylene	4-5	3-5
Propylene	3	1-3
2-me-2-butene	1	1-4
O-xylene	4-5	3-5
Mesitylene	2	1-4

Such an intercomparison of smog chambers is lacking in the following respects: (1) All chambers were operated under constant light intensity conditions; simulation of the diurnal variation of sunlight intensity was not attempted. (2) Reactant concentrations were considerably higher than those of the background contaminants; therefore, differences in results caused by differences in chamber contamination levels could not be seen, although

*Inquiries concerning this effort and results should be addressed to Coordinating Research Council, Rockerfeller Plaza (30), New York, N. Y. 10020.

they were certain to exist. (3) The comparison data do not include data on photochemical aerosol formation; this is important since it is almost certain that aerosol reactivity differences among the various chambers do not parallel the rate of NO_2 formation (R_{NO_2}) and oxidant reactivity differences shown in Tables 1 and 2.

The observed disagreement in results among the various chambers (Tables 1 and 2), unless explainable, causes the smog chamber method and data to be looked at with distrust. Before smog chambers can be used with confidence for this intended purpose, it is necessary that the following questions be answered satisfactorily:

1. Why do test results from chambers of various designs disagree?
2. Which chamber design gives valid results, that is, results applicable to the real atmosphere?

Both questions have received some research attention and speculative answers have been offered. Thus, the disagreement in results among chambers was investigated by Lockheed under a CRC-EPA contract. Lockheed[1] found that smog chamber design factors such as wall material, surface-to-volume ratio, and radiation spectrum affect smog chamber test results. Effects are also known to be caused by radiation intensity, condition of chamber wall surface, and background contamination. The significance of these results is obvious considering that in the CRC study the intercompared chambers differed considerably in design. Thus, chamber surface-to-volume ratio ranged from 0.78 ft^{-1} to 4.6 ft^{-1}, light intensity (in terms of the NO_2 photolysis k_d factor) ranged from 0.2 min^{-1} to 0.4 min^{-1}, and wall materials included stainless steel, glass, Teflon, Tedlar, aluminum, and nickel. Whether the evidence obtained by Lockheed and others, i.e., the evidence regarding the effect of chamber design on chamber results, can explain completely the observed disagreements in results among chambers (Tables 1 and 2) is not known at this time--no attempt ha been made yet. However, one can reasonably infer that such disagreement is to be expected anc nence, it is not necessarily a reason for distrusting the smog chamber data.

The question "which smog chamber design gives valid results" is discussed elsewhere.[2] Briefly, it is proposed that (1) acceptably valid results can be obtained using a smog chamber such that real atmosphere conditions are closely simulated, and (2) for more confidence, a smog chamber could be checked for "validity" by comparison with real atmosphere. More specifically, it is proposed that a chamber be made of Teflon film, have a volume of 1000 ft^3 or so, be operated outdoors (or indoors, provided the diurnal variation of sunlight is simulated), and be operated under those conditions, static or dynamic, that favor oxidant formation; it is also proposed that field data and smog chamber data be obtained that would depict the time profiles of the oxidant forming process in the real atmosphere and in the smog chamber under consideration.

EFFECTS OF CHAMBER DESIGN FACTORS -- *R.J. Jaffe, Lockheed*

An experimental study has been conducted of effects of materials, spectrum, surface-to-volume ratio, and cleaning technique on the photochemical reactions observed in a smog

chamber.[1] A unique chamber and lighting system was used, which permitted independent variation in chamber materials and in light conditions. A xenon arc lamp-parabolic reflector combination provided a collimated light beam. By orienting plates of materials parallel to the beam, it has been possible to independently vary light conditions and materials.

The study included four materials--aluminum, Pyrex, Teflon, and stainless steel, and two conditions each of spectrum, surface-to-volume ratio, and cleaning. A complete factorial testing sequence was performed. All photochemical runs were at k_d of 0.3 min^{-1} as determined by frequent NO_2 in N_2 photolysis tests. The propylene (3 ppm)/NO_x (1.5 ppm) reaction system was used, at 95° F and 25 percent relative humidity. Initial NO_2 content was nominally 10 percent of NO_x. Chamber background was 0.1 ppmC. Tests were also conducted at lower relative humidity. Several runs were made for the n-butane(3 ppm)/NO_x(0.6 ppm) system. A graphical depiction of some results is shown in Figures 1 through 4.

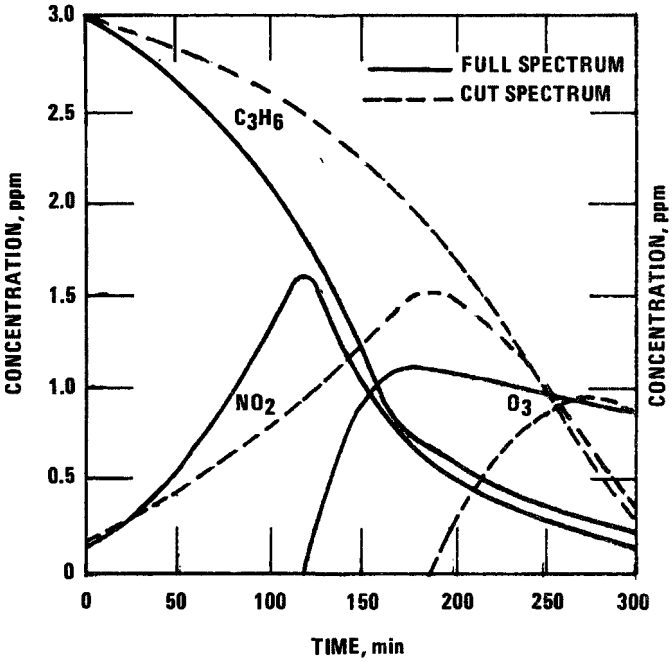

Figure 1. Composite photochemical test results for Teflon film surfaces.

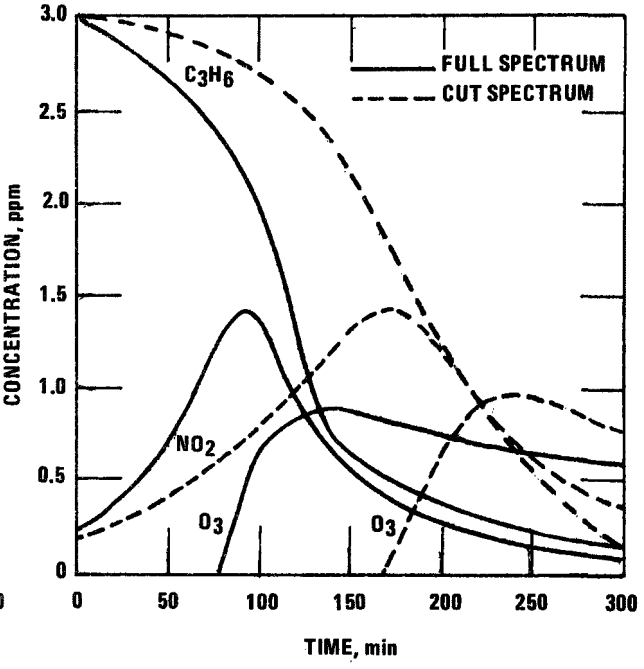

Figure 2. Composite photochemical test results for Pyrex surfaces.

Effects of the different materials and of the two levels of each parameter have been determined. The time to NO_2 maximum is shortest for stainless steel (70 min) followed by aluminum (106 min), Pyrex (131 min), and Teflon (154 min). Maximum ozone concentration increases in the order: Pyrex, aluminum, stainless steel, Teflon (for the full spectrum condition).

The cutoff spectrum (little energy below 350 nm wavelength) strikingly lowers reaction rates compared to the full spectrum. Surface-to-volume ratio measurably affects the reactions. The variations in the two cleaning techniques do not affect as many of the run characteristics except for stainless steel.

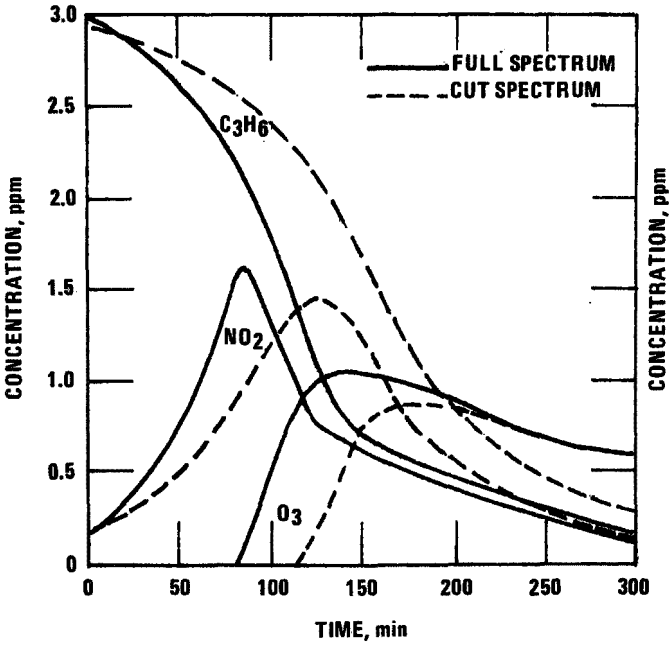

Figure 3. Composite photochemical test results for aluminum surfaces.

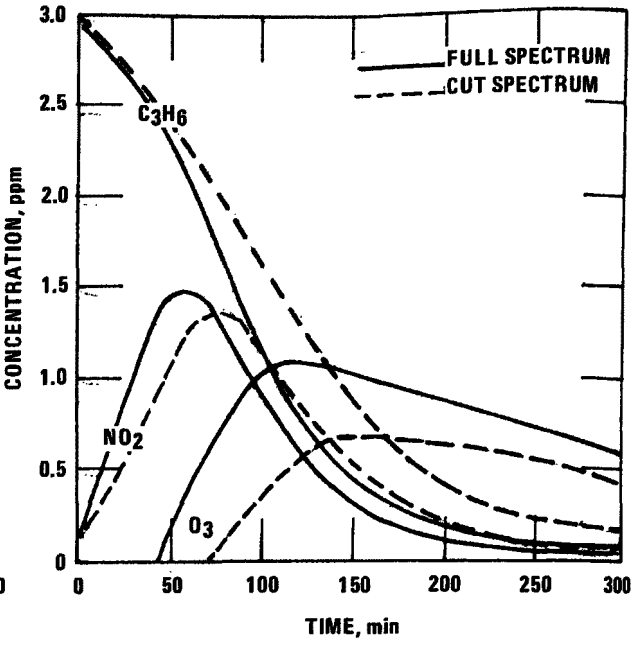

Figure 4. Composite photochemical test results for stainless steel surfaces.

The presence of this large spectral effect (at constant k_d) was not anticipated. It is reproduced in kinetic model simulations by changes in photolysis rate for nitrous acid, formaldehyde, acetaldehyde, and hydrogen peroxide. It appears that heterogeneous catalysis effects in nitrous acid production are responsible for the materials differences.

INTERPRETATIONS OF CHAMBER DESIGN EFFECTS -- *P.S. Connell and H.S. Johnston, U.C. Berkeley*

For about 20 years, the smog chamber has been used as a tool first for understanding the reactions that generate photochemical smog, and second for developing strategies of smog abatement. The first of these goals seems nearly prerequisite for intelligent approaches to the second. To this end of understanding the smog reaction, complete chemical mechanisms have been proposed and tested by comparison with experimental smog chamber data. These mathematical models are of two types, corresponding to atmospheric-mix smog chambers and specific reactant hydrocarbon chambers.

Our model is presented as an attempt to include all important elementary reactions occuring in the propene-NO_x system studied in the Lockheed project.[1] While "lumped" mechanisms, describing atmospheric-mix smog reactions, can only be validated by direct comparison of the model prediction with chamber experiment, specific mechanisms composed of elementary reactions, that is, reactions that actually occur on a microscopic level, can be tested in both this fashion and by independent experiments in other systems, which yield information on the reactions and their rates. Both bases of model testing pose problems. Experimental data lack consistency from chamber to chamber in the major parameters of characterization, such as time to NO_2 maximum. Dependence on the material of construction, history, techniques, and other factors, which are often not well characterized, has been

demonstrated in the Lockheed study. Construction of a model based on reaction rates measured specifically in other systems produces an incomplete picture at present, of necessity, since many of the reactions involved have not been treated. It is important here to remark that any serious model should, however, incorporate such direct experimental data where it is available.

What is most immediately evident in the Lockheed project data is that chamber design effects do exist and are indeed significant in affecting the commonly used descriptive smog chamber reaction parameters. The two major effects encountered have been described as the spectral intensity distribution effect and the dependence of the reaction rate on the nature of surfaces included in the chamber. A third factor in the design of a smog chamber experiment is less tractable to explanation by a model, the effect of techniques involved in performing the run and the nature of analytical methods used to produce the data.

Two different spectral distributions were studied, one with energy down to about 300 nm (full spectrum) and one with wavelengths smaller than 350 nm effectively eliminated (cut spectrum). By increasing the intensity in the cut spectrum case, the NO_2 absorption is held fixed. Full spectrum runs are faster than cut spectrum runs for all surfaces.

Figure 5 shows species that are present in significant concentrations and show dissociation on absorption for wavelengths present. The spectral effect perhaps admits to the simplest explanation. The important light-absorbing species can be identified and the absorptions and photolysis quantum yields can be measured in separate experiments. Knowing the intensity of the light used in the chamber as a function of wavelength, the product of the intensity, cross section, and quantum yield curves gives the rate constants of the photolytic reactions. The proper model should then show quantitatively the same response to the changing spectral distribution. The model's response depends on both the primary photolytic steps and the secondary reaction of the mechanism to changing these steps.

(1)	$HONO + h\nu\,(300\text{-}390\ nm)$	$\longrightarrow HO + NO$
(2)	$H_2CO + h\nu\,(290\text{-}360\ nm)$	$\longrightarrow H + HCO$
(2a)	$(300\text{-}370\ nm)_i$	$\longrightarrow H_2 + CO$
(3)	$CH_3CHO + h\nu\,(300\text{-}350\ nm)$	$\longrightarrow CH_3 + HCO$
(3a)	$(300\text{-}350\ nm)$	$\longrightarrow CH_4 + CO$
(4)	$HOOH + h\nu\,(300\text{-}370\ nm)_i$	$\longrightarrow 2HO$
(5)	$O_3 + h\nu\,(290\text{-}310\ nm)$	$\longrightarrow O(^1D_2) + O_2$

Figure 5. Species in irradiated propylene/NO_x system that dissociate on absorption of radiation present.

Surface effects present greater problems since heterogeneous rates and mechanisms are not well known and depend on individual surface history, for example the "virgin surface" effect for aluminum and stainless steel. Several reactions that must occur in smog chambers are known to be largely or entirely heterogeneous. The direction of the materials

effect must in this case be matched by reasonable adjustment of the rates of these known heterogeneous reactions.

The data produced in the Lockheed study show certain peculiarities that cannot be reproduced in a model mechanism. The apparent growth of the total amount of NO_x species during the first portion of the reaction cannot, of course, be accounted for in any model conserving matter. Changes of species concentration as a result of reaction during sampling and sampling lag, as with ozone and NO, introduce uncertainty into the data, making direct comparison with predicted concentrations more difficult.

The computer program used in this study is a chemical kinetics solving package developed by G. Z. Whitten.[3] It employs a coupled differential equation-solving algorithm written by Gear.[4] This uses an Adams-Bashforth-Moulton[5] predictor-corrector method of numerical integration to generate concentration versus time profiles for the species involved in the mechanism. The chemical mechanism derives largely from the modeling work of Demerjian, Kerr, and Calvert[6] and that of Niki, Daby, and Weinstock.[7] Climatic Impact Assessment Program (CIAP)[8] rate constants were used if tabulated, as well as more recent experimental work, as for the mutual recombination reaction of methyl-peroxy radicals. The photolytic rate constants used for the full and cut spectral distributions for HONO and $O(^1D)$ production were obtained from work in our laboratory. Other photolytic constants were obtained from Demerjian et al.[6] Constants for which no experimental basis exists were taken mostly from Demerjian et al.[6] Figure 6 is a graph of propene, nitrogen dioxide, and ozone concentrations generated by the model for full and cut spectral distributions. For comparison with the experimental data, the effect can be made partially independent of possible deficiencies in the model by considering the ratio of cut to full spectrum time parameters, characteristically around 1.6 for the smog chamber runs. These ratios are shown in Table 3. Model results bracket the experimental numbers, except in the case of propylene destruction half-times. This ratio is lower than observed because the model tends not to account for propylene loss toward the end of the reaction, allowing full and cut spectrum propene concentrations to approach each other for long times.

Determination of which reactions are most responsible for the spectral effect was undertaken by deletion, one by one, of full spectrum photolysis rates and replacement by the corresponding cut spectrum rate. The ratio between the time parameters of the deleted model to the full spectrum complete model was calculated. If the system is insensitive to the reaction replaced at the rate assigned, the ratio will be one and the reaction is unimportant. For more important reactions the ratio will approach the corresponding cut-to-full-spectrum ratio. Table 4 shows these ratios. The photolysis of nitrous acid appears most significant in accounting for the spectral effect, followed by H_2CO, CH_3CHO, and HOOH. The production of $O(^1D)$ is seen to be unimportant in the present instance.

Although the validity of these results depends upon the validity of the rest of the model, the spectral effect appears to be essentially explained by the reactions considered.

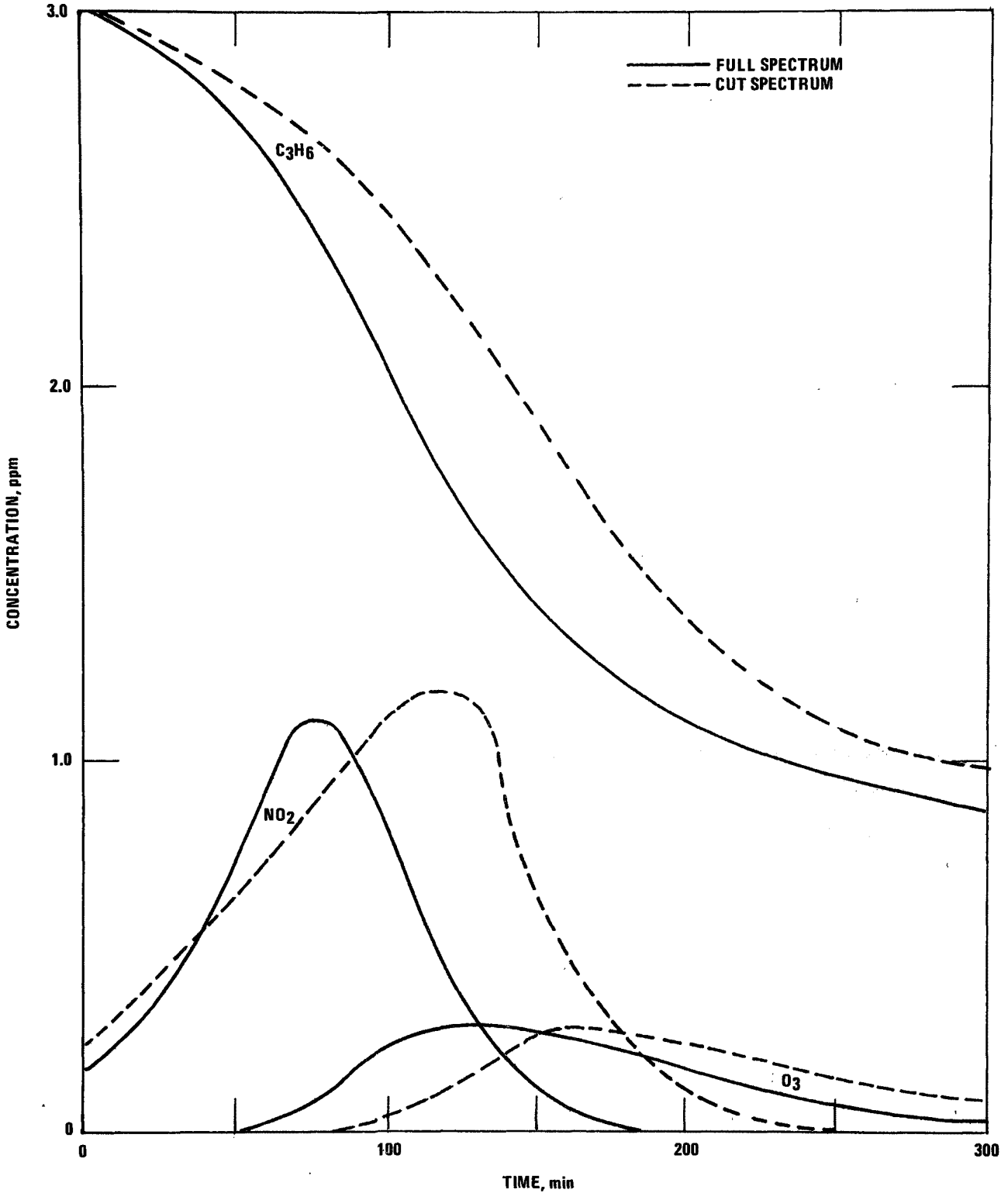

Figure 6. Comparison of full and cut spectrum model simulations.

More difficult to explain than the spectral effect is the great difference observed between runs with Teflon surfaces and those with a stainless steel surface present. While the origin of the spectral effect is identified in principle and requires only knowledge of cross sections, quantum yields, and spectral intensities for explanation, surface reactions are less well

Table 3. RATIO VALUES FOR CUT-TO-FULL SPECTRUM PARAMETERS

	Teflon	Stainless steel	Model	
			Fast NO + NO_2 + H_2O	Slow NO + NO_2 + H_2O
NO_2 T_{max}	1.58	1.49	1.81	1.37
O_3 T_{max}	1.49	1.39	1.51	1.38
50% propylene destruction time	1.50	1.43	1.39	1.31

Table 4. RATIO VALUES FOR THE DELETED-TO-COMPLETE MODEL (FULL SPECTRUM) PARAMETERS

	Deleted compound				
	HONO	H_2CO	CH_3CHO	HOOH	$O_3 \rightarrow O('D)$
NO_2 T_{max}	1.50	1.26	1.17	1.12	1.0
O_3 T_{max}	1.28	1.0	1.04	1.01	1.0
50% propylene destruction time	1.26	1.14	1.03	1.00	1.0

understood, and attempted explanations can be only speculative. It is, however, clear from the Lockheed work that modeling without considering the extent of heterogeneous contributions is unwise.

Generally speaking, stainless steel should be the most active surface, both for promoting reaction rates catalytically by helping to overcome activational energy barriers and for quenching radicals and removing species from the gas phase by adsorption on the wall. Teflon should be the most inert of the surfaces used. Indeed, radicals are capable of bouncing off Teflon without being quenched.

Observation of the smog reaction rate in a chamber with stainless steel surfaces enclosed shows it to be much faster than the same chamber containing Teflon surfaces instead. Since quenching of radicals would result in slowing the overall rate of reaction, lengthening the time to NO_2 maximum, the surface effect must be a combination of opposing factors. The ability of the metal surface to promote certain reactions must overcome its ability to destroy the radical chain carriers.

By considering the NO_2 dose as a function of time from the start of the run, the number of photons absorbed by NO_2 and, therefore, the number of reaction-initiating oxygen atoms can be deduced for any time period. This value, ϕ, is the product of the photolytic rate constant, in this case, 0.2 min^{-1}, and the NO_2 concentration integrated from time T_1 to T_2. Knowing the number of oxygen atoms produced and the number of propene molecules destroyed, the quotient is an effective quantum yield for propene destruction by absorption of photolytic energy by NO_2. In Figure 7, we see this plotted for the four surfaces for various

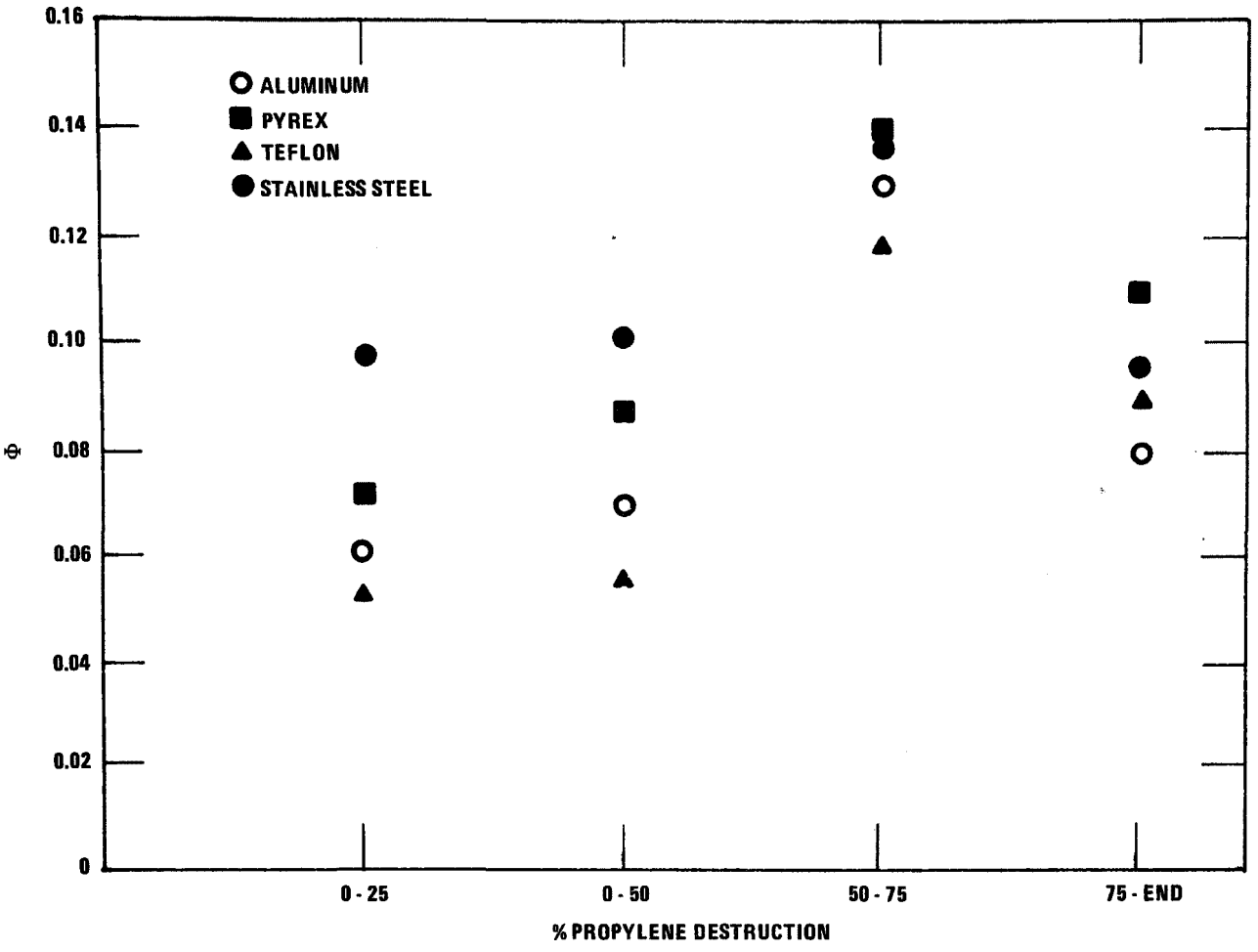

Figure 7. Effective quantum yields for propylene destruction by absorption of photolytic energy by nitrogen dioxide.

time periods during the run. Points were obtained by averaging results for a particular set of runs. The quantum yield does not exceed 0.15 in any case, showing that radical termination reactions predominate over chain propagation steps throughout the reaction. The quantum yield for all surfaces converges to around 0.1 late in the reaction, the major observable difference between the surfaces being the larger initial quantum yield for stainless steel runs. Evidently the stainless steel surface speeds the initiation of reaction.

Of the species known to be present, N_2O_5, HOOH, and O_3 will decompose on the walls. N_2O_5 reacts with adsorbed water to yield nitric acid, which will probably remain stuck. The reaction of NO, NO_2, and H_2O is also thought to be surface catalyzed. An upper limit of 1.3E-20, in cm^3/molecule-sec, (where E is the activation energy in kcal/mole) has been placed on the homogeneous reaction of nitrogen pentoxide, while decomposition half-times for N_2O_5 even in a "dry" system are on the order of minutes, so that in the chamber this reaction is largely heterogeneous. Data from the NO_x reducing column late in a run show that most of the nitrogen-containing species are no longer in the gas phase, since the efficiency of the column for converting alkyl nitrates, nitrites, NO_2, and HNO_3 to observable NO should be high.

The principle nitrogen-containing product, nitric acid, is made both homogeneously, sticking on the wall subsequent to collisions with it, and heterogeneously. Ozone decay half-times were measured for the various surfaces, and these results were used to derive first-order decay constants.

The importance of HONO photolysis in explaining the spectral effect suggests that the surface catalyzed reaction of NO, NO_2, and H_2O to give two molecules of nitrous acid may also contribute to the materials effect. The HONO photolysis product HO is an initiator and radical chain carrier and as such could account for the increased initial quantum yield. The result of heterogeneously catalyzed nitrous acid formation is to increase the HO radical concentration at the outset of the reaction, providing an alternative pathway for initiation. Measurements of the rate of this reaction as a homogeneous trimolecular reaction have in the past been on the order of 1E-34 with a large heterogeneous component. These values have been used by some modelers who generate times to NO_2 maximum characteristic of stainless steel runs. Longer times to NO_2 maximum, encountered in Teflon runs, seem to be incompatible with this large value for the rate constant. The existence of a nonvanishing homogeneous rate is not established, but an unpublished study of the reaction shows it to be much more rapid in a quartz-stainless steel system than in a strictly quartz cell.

Figure 8 shows full spectrum model results for varying rates of the nitrous acid forming reaction. The "active" surface (higher rate) is seen to give a faster system, as is observed experimentally. The relative importance of O+propene and HONO+hν in initiating the reaction in a fast system is shown in Figure 9. For this model system, the production of HO by photolysis of HONO is more important than the O+propene reactions. A further aspect of the HONO effect is the waiting time before the lights are turned on in the chamber. In a fast system, an equilibrium amount of HONO can be produced in the dark in about 20 minutes. In a slow system, it would take longer than 2 hours. Figure 10 shows the difference in rate for a system with a preestablished equilibrium concentration of HONO and for a system with no initial NO.

The focus of abatement strategy has been an oxidant (ozone) level as the primary deleterious component of photochemical smog. Ozone enters into the smog reaction upon the photolysis of NO_2 to produce oxygen atoms, which then mostly combine with oxygen to give ozone. It participates at first by reconverting NO to NO_2, then by reaction with HC to give organic free radical species.[2] The production of ozone in this regime is controlled by the three reactions shown in Figure 11. We can assume that O atoms are present at a steady state concentration. A photostationary ozone concentration expression can then be derived, which is a function of the NO_2/NO concentration ratio and of the quotient of the constants j_1 and k_3. Thus the expression $(O_3)(NO)/(NO_2)$ is constant if the photostationary state applies.

Figure 12 is a graph of this function versus time for various runs with different surfaces. The plots are made only during that period for which O_3 and NO are measurable with some accuracy, so that the total error probably does not exceed 50 percent. This period is during and after the NO_2 maximum. For each of the runs shown, the function exceeds the

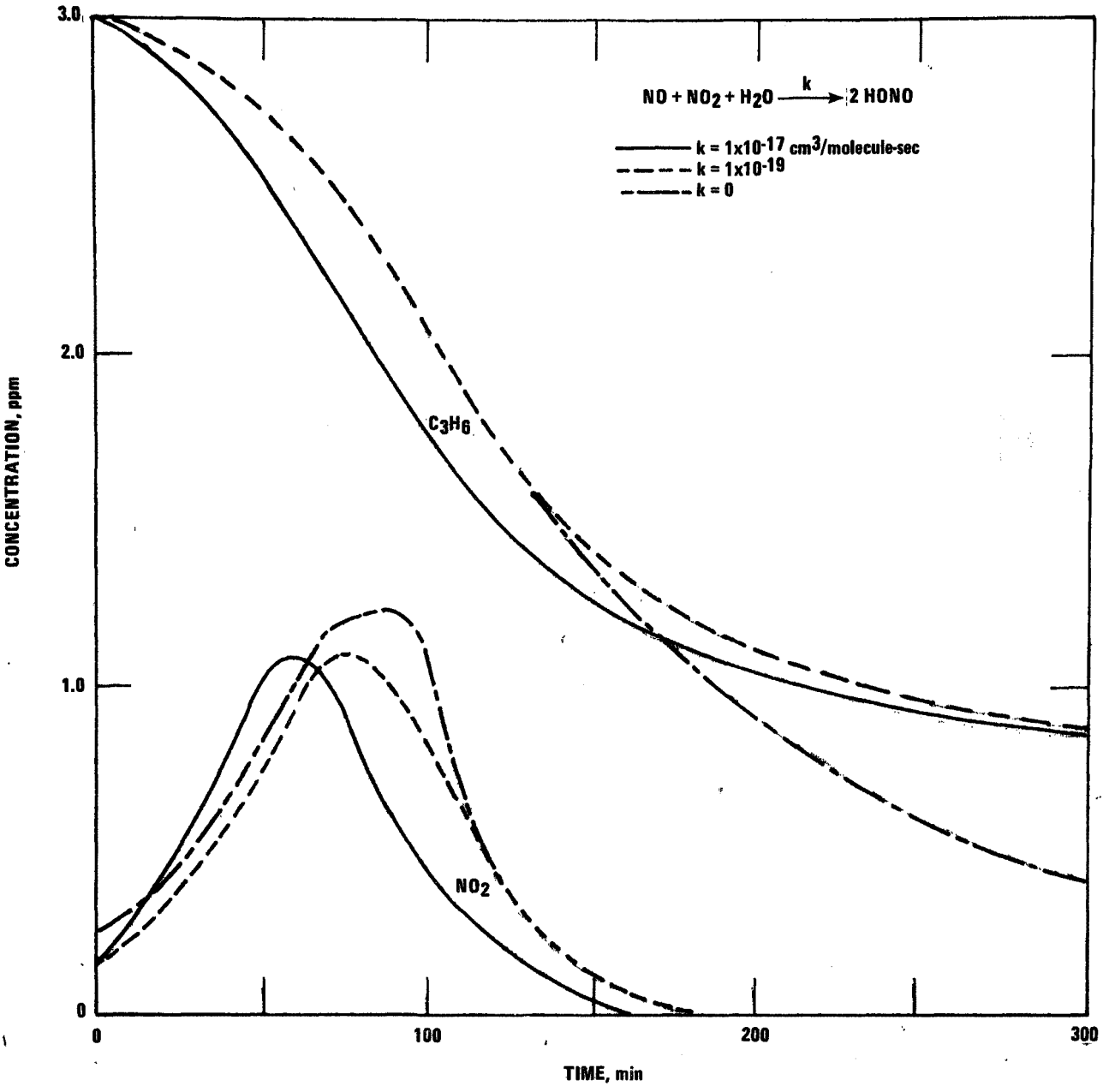

Figure 8. Simulation of full spectrum runs for various heterogeneous rates, $NO + NO_2 + H_2O \xrightarrow{k} 2\ HONO$.

photostationary value, indicated by the dotted horizontal line, shortly after the appearance of ozone and subsequently increases rapidly. It seems that ozone buildup is accelerated by some other mechanism.

A major characteristic of smog reactions is the "excess" conversion of NO to NO_2 by radical species, which, when rapid, provides a mechanism for pumping up the ozone concentration. This reaction is shown in Figure 13. Including this reaction in our prior three step scheme and reforming the same concentration ratio, the new factor appears in the denominator. Thus if conversion by peroxy radicals competes equally with conversion by ozone, the ratio is reduced by a factor of two. The ozone concentration is increased by

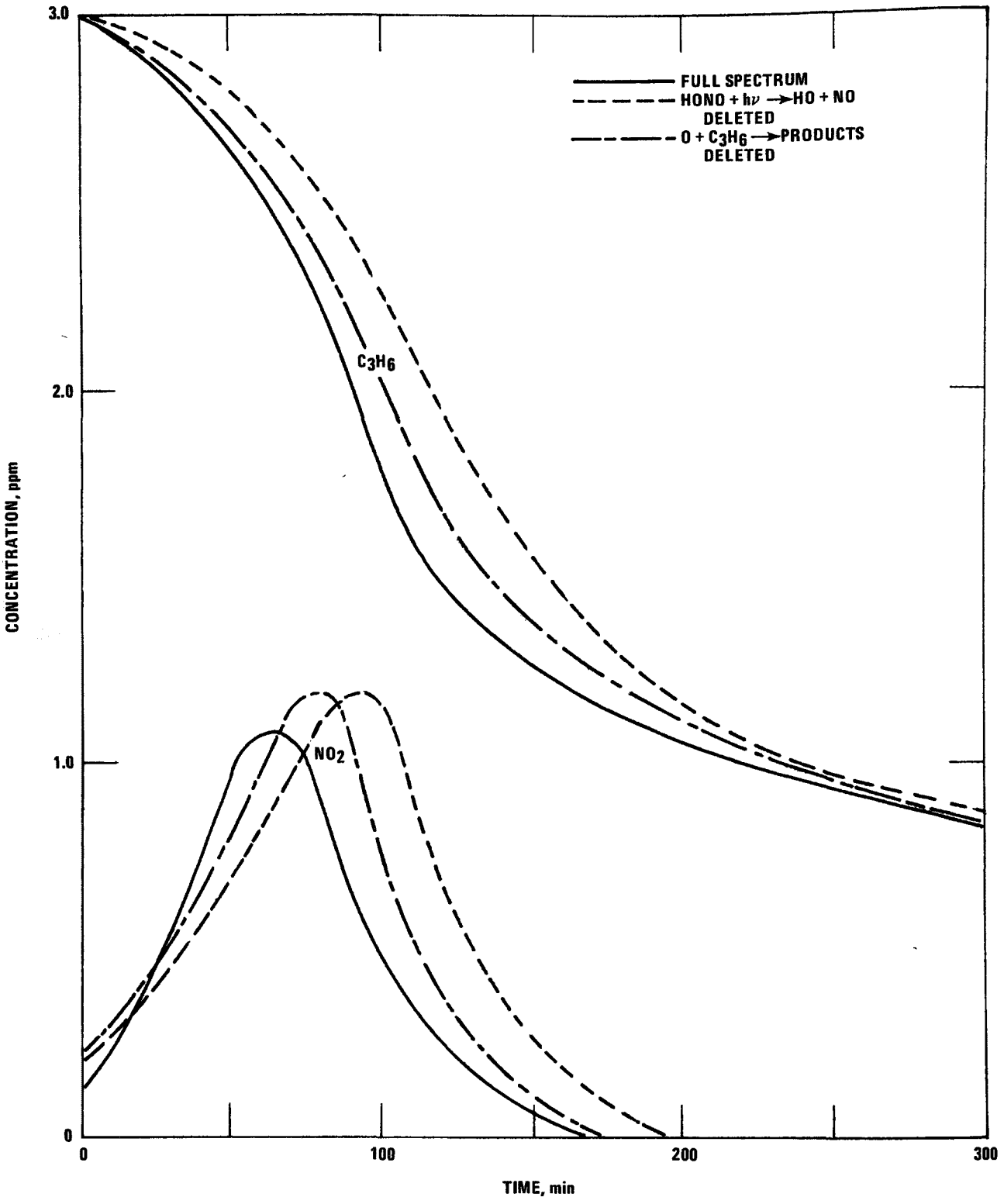

Figure 9. Relative importance of O + C_3H_6 and HONO + hν in initiating reaction.

virtue of increasing the NO_2/NO ratio, but the increase is not as rapid as the increase in the ratio itself.

What is needed to produce both excess ozone and the large $(O_3)(NO)/(NO_2)$ ratio is an ozone forming reaction that is independent of the gas-phase NO_2-NO mechanism. A possibility is photolysis of peroxy radicals to form O atoms. Another alternative is the

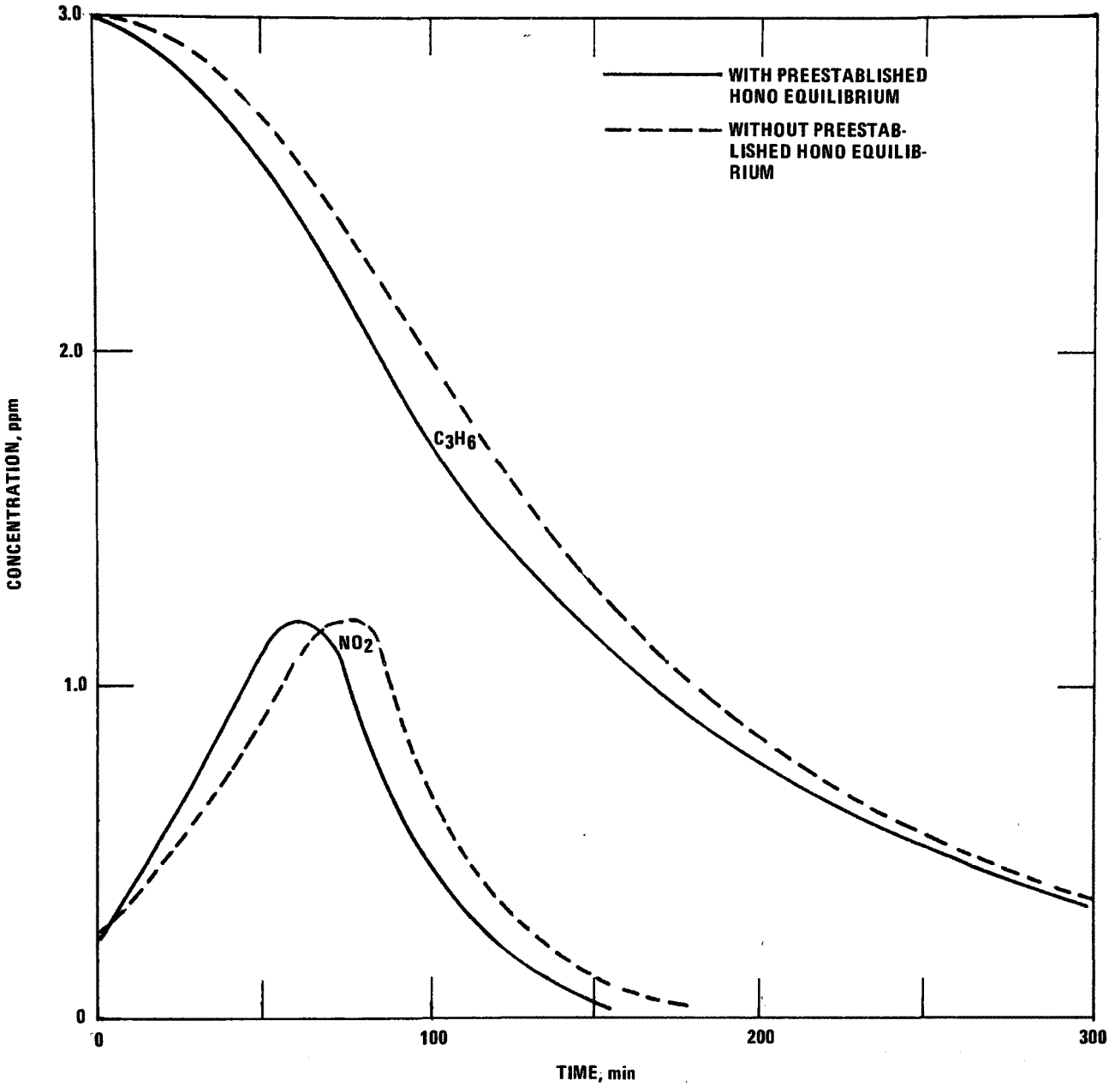

Figure 10. Simulation of full spectrum runs with preestablished HONO equilibrium and without preestablished HONO equilibrium.

1. $NO_2 + h\nu \xrightarrow{j_1} NO + O$
2. $O + O_2 + M \longrightarrow O_3 + M$
3. $NO + O_3 \xrightarrow{k_3} NO_2 + O_2$

$$\frac{[O_3]_{ss}[NO]}{[NO_2]} = \frac{j_1}{k_3}$$

Figure 11. Reactions controlling ozone production.

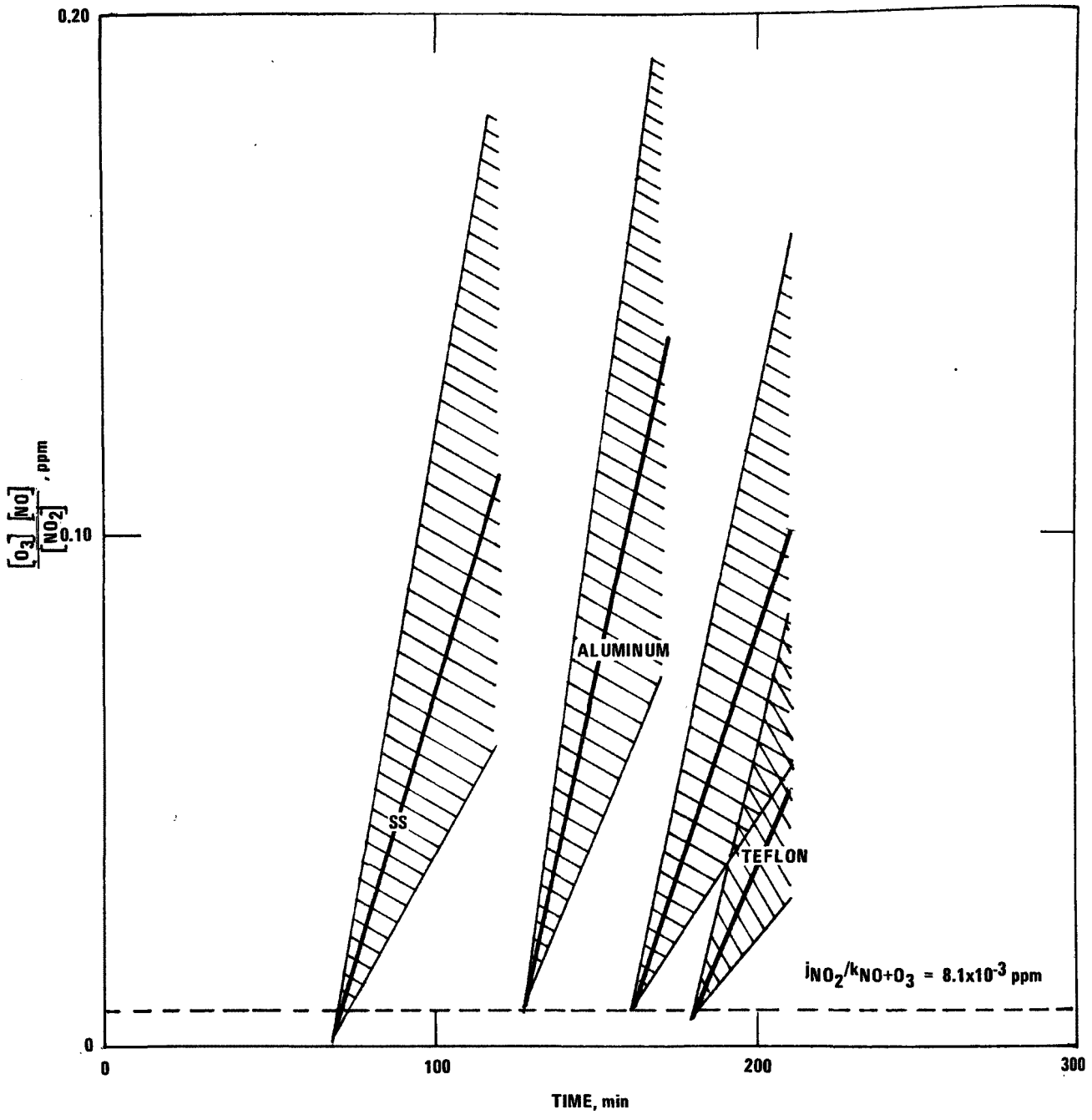

Figure 12. Graphs of the $(O_3)(NO)/(NO_2)$ function versus time for different surfaces.

4. $NO + ROO\cdot \xrightarrow{k_4} NO_2 + RO\cdot$

$$\frac{[O_3]\,[NO]_{ss}}{[NO_2]} = \frac{j_1}{k_3}\left(1/1 + \frac{k_4[ROO\cdot]}{k_3[O_3]}\right)$$

Figure 13. Reactions of radical species with nitric oxide.

production of ozone by the reaction of peroxy radicals with molecular oxygen (Figure 14). This reaction can double the ratio for radicals present at the 1E-10 level if k_6 is on the order of 1E-18. This is a small required value, but the reaction appears to be endothermic for CH_3OO and experimental work shows that it does not occur for the peroxyacetyl radical.

5. $ROO\cdot + h\nu \xrightarrow{j_5} RO\cdot + O$

$$\frac{[O_3]_{ss}[NO]}{[NO_2]} = \frac{j_1}{k_3}\left(1 + \frac{j_5[ROO\cdot]}{j_1[NO_2]}\right)$$

$$= \frac{j_1}{k_3} \quad (2)$$

IF $j_5 \approx 1.0\ sec^{-1}$

6. $ROO\cdot + O_2 \xrightarrow{k_6} RO\cdot + O_3$

$$\frac{[O_3]_{ss}[NO]}{[NO_2]} = \frac{j_1}{k_3}\left(1 + \frac{k_6[ROO\cdot][O_2]}{j_1[NO_2]}\right)$$

$$= \frac{j_1}{k_3} \quad (2)$$

IF $k_6 \approx \frac{1}{[O_2]} = 2 \times 10^{-18}$ MOLECULES/cm^3-sec

Figure 14. Alternative reactions of peroxy radicals leading to ozone formation.

The validity of the photostationary state in large chambers and out of doors in the ambient atmosphere has apparently been established. The discrepancy in the data here is then either due to a systematic overestimation of small NO concentrations or to wall effects minimized in larger chambers.

The Lockheed data, as we have seen, point up several questions related to an attempt to chemically model the findings. The effect of spectral intensity distribution on the rate of reaction can be explained largely by change in HONO and H_2CO photolytic rates. The surface effect appears to be one of heterogeneous formation of nitrogen oxyacids, which speed both the initiation of reaction and the removal of NO_2 after maximum. The ozone concentration problem in small chambers has not submitted to explanation. More accurate techniques for measuring small levels of NO and O_3 as well as faster more direct techniques for NO_2 should help to define the actual existence of a discrepancy. The importance of nitrous acid initiation shows the necessity of obtaining quantitative rate data on its heterogeneous formation reaction as a function of surface or chamber, before this effect can be eliminated as a source of difference between model and experimental results.

DISCUSSION

Dr. T. A. Hecht of Systems Applications, Inc., reported on recent SAI modeling studies addressed to the effects of temperature and water vapor upon smog chamber measurement results. Dr. Hecht's presentation entitled "On the Predicted Effects of Changes in Temperature and Water Concentration on Smog Kinetics," was as follows:

In a recent study, mathematical simulations of a smog chamber experiment were carried out using a kinetic mechanism[9] to determine what effect changes in temperature or water concentration have on the predictions. The base values used were those of a smog chamber run conducted by EPA (Run 333):

$$[NO]_o = 1.25 \text{ ppm}, [NO_2]_o = 0.08 \text{ ppm}, [C_3H_6] = 0.23 \text{ ppm},$$

$$[n\text{-}C_4H_{10}] = 3.41 \text{ ppm}, [H_2O] = 16{,}000 \text{ ppm, and } T = 25^oC$$

For each simulation run, only one parameter was changed from the base values.

Simulations were performed for two different temperatures, 15°C and 35°C, with all other factors kept the same. The rate constants at the new temperatures were calculated from the base values of the rate constants (25°C) and from measured or estimated reaction activation energies, shown in Table 5.[6,8,10] Because the majority of the reactions in the mechanism are thermal and have small positive activation energies, raising the temperature resulted in an accelerated conversion of NO to NO_2 and a decrease in the time to the onset of O_3 accumulation, as expected. Conversely, lowering the temperature noticeably slowed the smog formation process. Concentration-time profiles for NO, NO_3, O_3, and propylene for each of these two runs are presented in Figure 15.

Similar runs were carried out at two extreme conditions of relative humidity--0 and 100 percent--at the base temperature (25°C). These percentages correspond to 0 and 32,000 ppm of H_2O, respectively. Predicted concentration-time profiles for these two cases are compared with the profile for the base case in Figure 16. The increase in the water concentration results in a faster conversion of NO to NO_2, whereas complete elimination of water results in a dramatic slowdown in the overall smog kinetics. Both of these effects are attributable to changes in the production rate and equilibrium level of nitrous acid, governed by the reactions

$$NO + NO_2 + H_2O \rightleftharpoons HNO_2$$

Because it is virturally impossible--even with pumping and baking--to obtain a water concentration of 0 ppm in existing smog chambers, one final run was carried out at 3.2 ppm of water. The concentration-time profile obtained under these conditions differed from those of the completely dry run by less than 2 percent after 6 hours of simulation time.

In urban areas, ambient temperatures and water concentrations change considerably during the day and from one day to the next. Thus, the results of these simulation runs suggest that it may be necessary to account for variations in temperature and water concentration when modeling urban photochemical smog. Toward this end, smog chamber experiments conducted at various constant levels of temperature and water concentration would

Table 5. ACTIVATION ENERGIES OF REACTIONS IN THE GENERAL MECHANISM

No.	Reaction	E_A, cal/mole	Reference
1	$NO_2 + h\nu \rightarrow NO + O$	0	Estimate
2	$O + O_2 + M \rightarrow O_3 + M$	-1	10
3	$O_3 + NO \rightarrow NO_2 + O_2$	2.4	10
4	$O + NO \xrightarrow{M} NO_2$	-1.9	6
5	$O + NO_2 \rightarrow NO + O_2$	0.6	10
6	$O + NO_2 \xrightarrow{M} NO_3$	-1	Estimate
7	$O_3 + NO_2 \rightarrow NO_3 + O_2$	4.9	10
8	$NO_3 + NO \rightarrow 2NO_2$	1.4	11
9[a]	$NO_3 + NO_2 \rightarrow N_2O_5$	-2	6
10[a]	$N_2O_5 \rightarrow NO_2 + NO_3$	19.4	10
11[a]	$N_2O_5 + H_2O \rightarrow 2HNO_3$	0	Estimate
12	$NO + NO_2 + H_2O \rightarrow 2HNO_2$	0	6
13	$2HNO_2 \rightarrow NO + NO_2 + H_2O$	9	6
14	$HNO_2 + h\nu \rightarrow OH + NO$	0	Estimate
15	$OH + NO_2 \xrightarrow{M} HNO_3$	-2.2	10
16	$OH + NO \xrightarrow{M} HNO_2$	-2.2	10
17	$HO_2 + NO \rightarrow OH + NO_2$	2	Estimate
18	$H_2O_2 + h\nu \rightarrow 2OH$	0	Estimate
19	Propylene + $O \rightarrow RO_2 + \frac{1}{2}RCO_3 + \frac{1}{2}HO_2$	0.1	10
20	Propylene + $O_3 \rightarrow RCO_3 + RO + ALD$	3.8	10
21	Propylene + $OH \rightarrow RO_2 + ALD$	1	Estimate
22	n-butane + $O \rightarrow RO_2 + OH$	5	Estimate
23	n-butane + $OH \rightarrow RO_2 + H_2O$	1	Estimate
24	$ALD + h\nu \rightarrow 0.6RO_2 + 1.4HO_2$	0	Estimate
25	$ALD + OH \rightarrow 0.6RCO_3 + 0.4HO_2 + H_2O$	0	Estimate
26	$RO_2 + NO \rightarrow RO + NO_2$	1	Estimate
27	$RCO_3 + NO \rightarrow RO_2 + NO_2 + CO_2$	0	Estimate
28	$RCO_3 + NO_2 \rightarrow PAN$	0	Estimate
29	$RO + O_2 \rightarrow HO_2 + ALD$	6	10
30	$RO + NO_2 \rightarrow RONO_2$	0	Estimate
31	$RO + NO \rightarrow RONO$	0	Estimate
32	$HO_2 + HO_2 \rightarrow H_2O_2 + O_2$	0	Estimate
33	$HO_2 + RO_2 \rightarrow RO + OH + O_2$	0	Estimate
34	$RO_2 + RO_2 \rightarrow 2RO + O_2$	0	Estimate

[a]For these simulations, Reactions 9 through 11 were combined into the single reaction:

$$NO_3 + NO_2 + H_2O \rightarrow 2HNO_3$$

having the rate constant

$$k = \frac{k_9 k_{11}}{k_{10} + k_{11}[H_2O]}$$

and an activation energy of -1.9 kcal/mole.

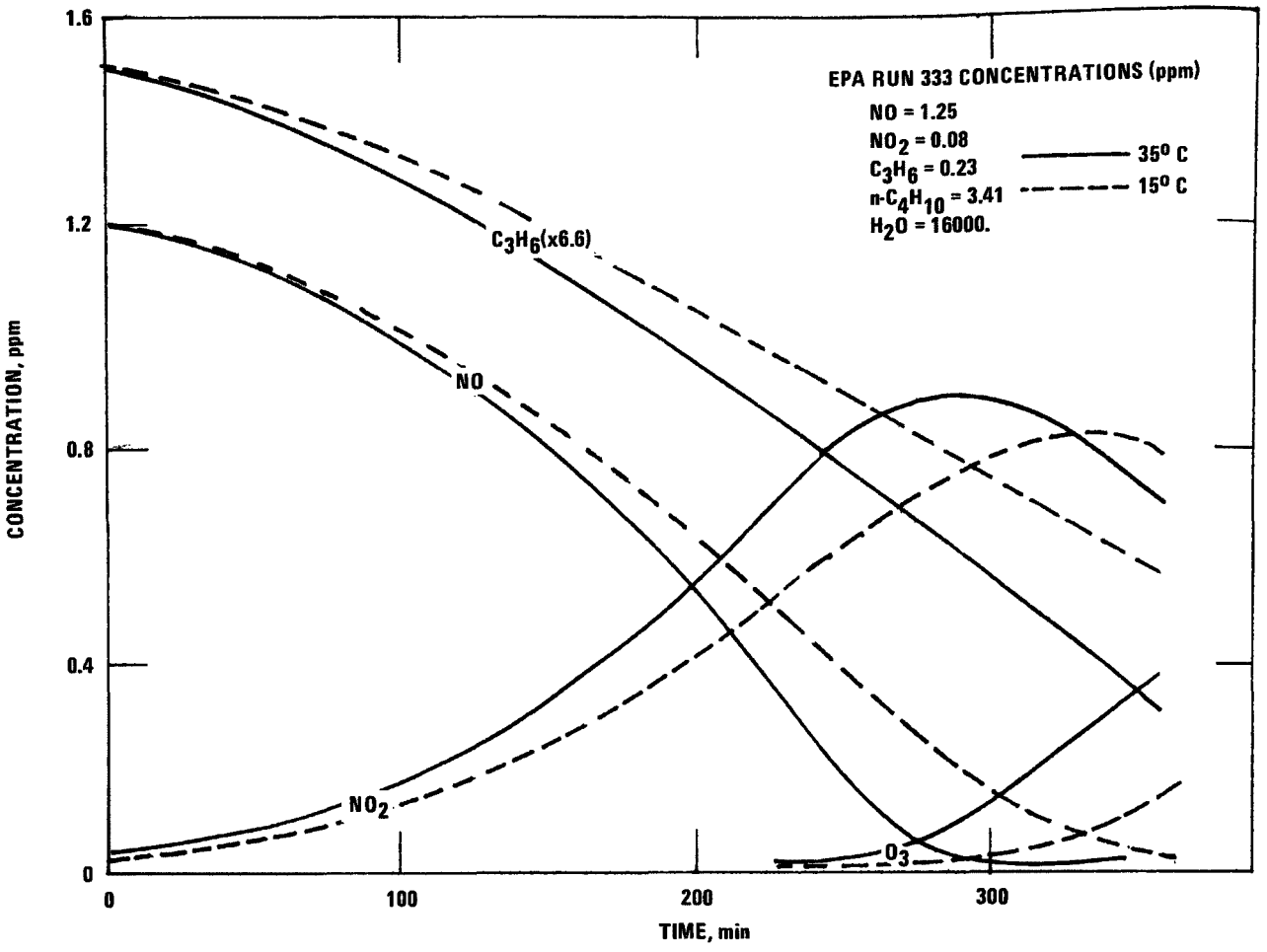

Figure 15. Concentration-time profiles for NO, NO_2, O_3, and propylene at 15° C and 35° C.

be most useful in ascertaining the effects of variations of these two parameters on smog kinetics.

Dr. T. E. Graedel (Bell Laboratories, Murray Hill, N. J.) did not attend the conference. However, he did send some comments pertaining to factors affecting smog chamber results. Dr. Graedel's comments were as follows:

1. The results of smog chamber chemistry depend very much on accurate and complete determinations of the flux and spectral characteristics of the radiation. Absolute radiation measurements, rather than rate of decrease of a single photochemically sensitive species, are required.

2. The presence of H_2O, NO, and NO_2 in smog chambers prior to irradiation is likely to result in the formation of HNO_2 and HNO_3, with subsequent production of free radicals by photodissociation. Complete information on pre-irradiation "induction periods" is thus desirable, as are measurements of the inorganic acid concentrations.

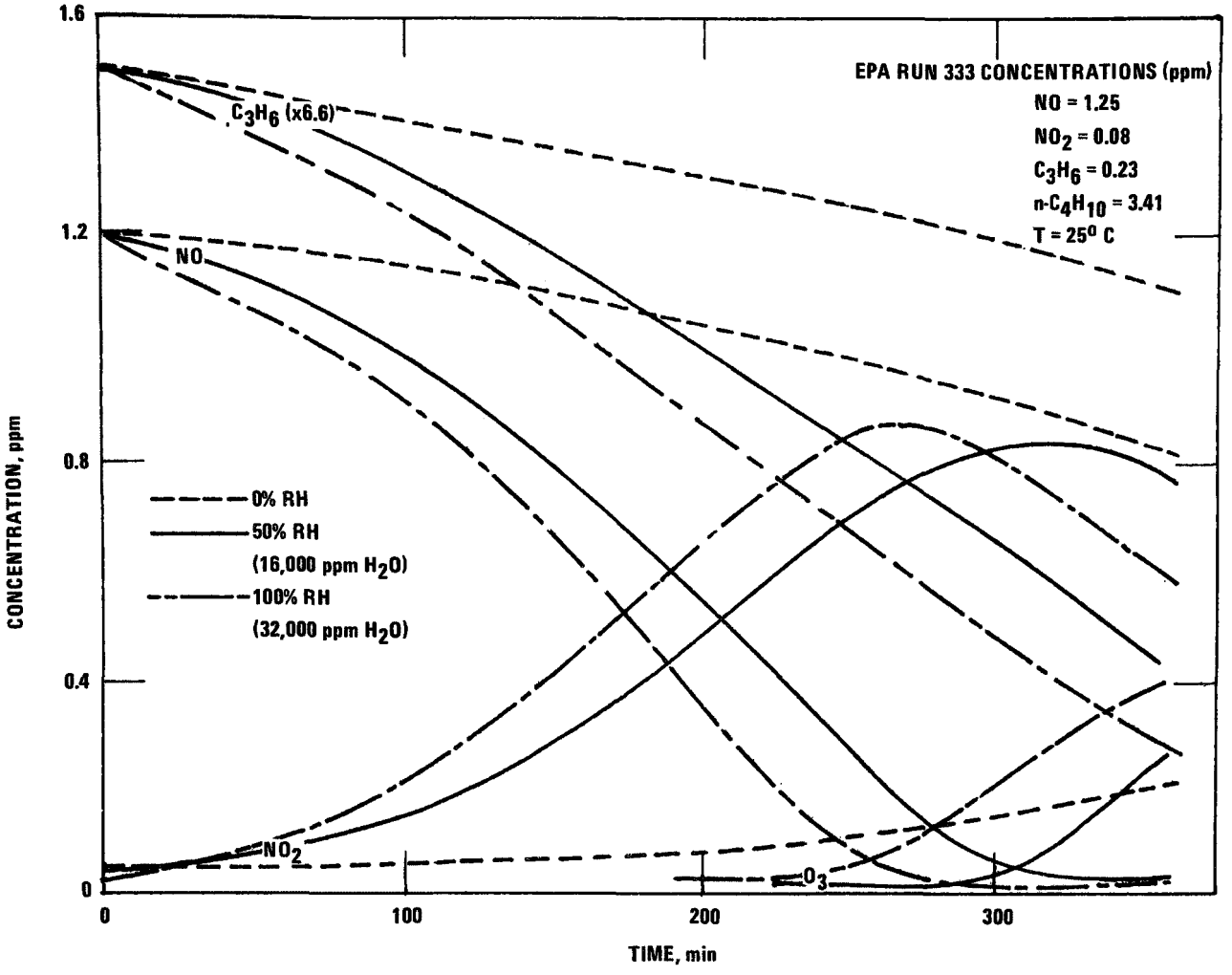

Figure 16. Predicted concentration-time profiles for NO, NO_2, O_3, and propylene at 0, 50, and 100 percent relative humidity.

3. Much evidence is accumulating to indicate that the interactions between trace gases and aerosols are very important in atmospheric chemical processes. The absence in smog chambers of aerosols typical of the atmosphere may render even more difficult the process of relating smog chamber results to atmospheric processes.

Dr. G. J. Doyle (University of California at Riverside) commented that short-lived intermediates [e.g., O(3P), OH.] are of no concern as far as wall quenching is concerned for a reasonable surface-to-volume ratio and for a reasonably convection-free chamber. The wall effects on concentrations of long-lived intermediates are of more concern, HNO_2 being a good example. One can use a simple model, in the case of wall losses, to generate a pseudounimolecular rate, le=sd/vS; s=surface, v=volume, d=diffusion constant and S= thickness of a "laminar layer," which can be roughly estimated from thermal convection relationships involving chamber size and temperature gradients. If this constant is comparable to the sum of all reactions leading to the disappearance of the intermediate, then

there can be an appreciable wall loss effect. This model can be extended to cover more complicated cases. Its chief drawback is that it requires a fairly good knowledge of the reaction mechanism.

Dr. T. Yang (Calspan) questioned whether efforts had been made to model the effect, if any, of surface-to-volume ratio on smog chamber results. According to Dr. Yang, it would seem possible that a modeling approach based on simultaneous assessment of diffusion to chamber wall and the relevant reaction rates may lead to a prediction of an abrupt increase in surface-to-volume effect after a certain breakoff point. This would be expected from a combination of incubation requirement for heterogeneous catalysis and adsorption-desorption equilibrium of a specific reaction intermediate governed in part by its probability of diffusion to the chamber wall surface.

In regard to the Lockheed observation that NO_x in the smog chamber increased during irradiation, Dr. Yang confirmed that small increases in NO_x were also observed in the Calspan chamber.

In response to Dr. C. W. Spicer's (Battelle) question, Dr. A. J. Jaffe (Lockheed) stated that O_3 interference in the NO_x measurement could not be the cause of the apparent NO_x increase during irradiation, because O_3 concentration during the early reaction stages is generally low, and because such interference should cause a negative, rather than positive, effect on NO_x.

Dr. Dimitriades concluded the discussion with the comment that a large chamber (e.g., 1000 ft^3) made of Teflon film and operated outdoors or indoors but under varying light intensity conditions may have advantages over other smog chamber designs, at least insofar as studies of the oxidant-precursor relationships are concerned. Dr. Dimitriades also suggested that more attention should be given by the modelers to the need for inclusion of heterogeneous reaction steps in the oxidant formation mechanism.

REFERENCES FOR CHAPTER 2

1. Jaffe, R.J., F.C. Smith, and K.W. Last. Study of Factors Affecting Reactions in Environmental Chambers; Final Report on Phase III. Lockheed Missiles and Space Co., Inc., Sunnyvale, Ca. 1975.

2. Dimitriades, B. Use of Smog Chamber Data in Formulating Oxidant Control Strategies. U.S. Environmental Protection Agency, Research Triangle Park, N.C. (Presented at Conference on Technical and Medical Bases for Control Strategies of Photochemical Oxidants: Current Status and Priorities in Research. Riverside, Ca. December 16-17, 1974.)

3. Whitten, G.Z. Rate Constant Evaluations Using a New Computer Modelling Scheme. Lawrence Laboratory, Berkeley, Ca. (Presented at 167th American Chemical Society National Meeting. Los Angeles. 1974.)

4. Hindmarsh, A.C. Gear: Ordinary Differential Equation System Solver. Lawrence Laboratory, Livermore, Ca. Report UCID-30001, Rev. 2. 1972.

5. Gear, C.W. Numerical Initial Value Problem in Ordinary Differential Equations. Englewood Cliffs, N.J., Prentice-Hall, 1971.

6. Demerjian, K.L., J.A. Kerr, and J.G. Calvert. The Mechanism of Photochemical Smog Formation. In: Advances in Environmental Science and Technology (Vol. 4). J.N. Pitts and R.L. Metcalf (ed.). New York, John Wiley and Sons, 1974. p. 1-262.

7. Niki, H., E.E. Daby, and B. Weinstock. Mechanisms of Smog Reactions. Adv. Chem. 113: 16, 1972.

8. Chemical Kinetics Data Survey VII; Tables of Rate and Photochemical Data for Modelling the Stratosphere. D. Garvin and R.F. Hampson (ed.). National Bureau of Standards. Washington, D.C. Report NBSIR 74-430. January 1974.

9. Hecht, T.A., J.H. Seinfeld, and M.C. Dodge. Further Development of Generalized Kinetic Mechanism for Photochemical Smog. Environ. Sci. Technol. 8(4): 327, 1974.

10. Johnston, H.S. et al. Atmospheric Chemistry and Physics (Vol. 4). Project Clean Air, Task Force Assessments. University of California. 1970.

3. ANALYTICAL TECHNIQUES IN SMOG CHAMBER STUDIES

MEASUREMENT OF NITROGEN OXIDES -- *D. Miller, Battelle*

This discussion is limited to two methods of measuring nitrogen oxides (NO and NO_2): the automated Saltzman and the chemiluminescence techniques. Of the instruments available for continuous nitrogen oxide measurements, these two are the most familiar to the author and probably the most widely used in other smog chamber laboratories. Hopefully, spectroscopic methods for NO_2 measurement, as well as other methods, will be reviewed in subsequent discussions.

Colorimetric Analyzers

The classic colorimetric method of Saltzman for measuring NO_2 is based on absorption of NO_2 in sulfanilic acid solution in which a specific reaction occurs between nitrite ions and diazotizing-coupling reagents to form a pink color.[1] Most commercial instruments incorporating this principle provide dual photocells such that the NO_2 concentration is read in one cell and the NO concentration is read in the second cell after oxidizing NO to NO_2. As oxidizer, we routinely use flutted filter paper impregnated with dichromate solution.[2] The dichromate oxidizer is at least 95 percent efficient when the papers are just slightly moist and dark red in color. Generally, a new scrubber is prepared daily.

Chemiluminescence Analyzers

The chemiluminescence method[3] is based on the reaction of NO with excess O_3 to form an excited NO_2 specie that emits light in a continuum extending from 600 to 900 nm. A cutoff filter at 600 nm is generally employed to absorb shorter wavelength emissions generated by other O_3 reactions. To use the chemilumenescence instruments to monitor NO_2 in addition to NO, the NO_2 must first be reduced to NO. In the last few years, carbon-based converters have become most popular. The reaction occurring at 200 to 250° C is quite efficient

$$C + NO_2 \longrightarrow CO + NO$$

Because of the familiarity that most of you have with these instruments I do not intend to review the detection principles in any more detail, nor spend time discussing optimal operating conditions, or the advantages and disadvantages of the two methods, or the work that has been done on the converters. The most important consideration with respect to obtaining accurate smog chamber data lies with the problems of interference associated with the primary and/or secondary (conversion) principles of these instruments, and I would like to present some data on that subject. Before that, however, calibration methods should be mentioned.

Calibration

It is common knowledge that low concentrations of nitrogen oxide standards in commercial cylinders are unreliable. We redetermine the NO concentration of bottled standards by an O_3-NO titration procedure somewhat similar to that used in confirming O_3 determinations.[4] Generally, the concentration in the bottles remains fairly stable at constant temperature. To determine the correct NO_2 concentration in pressurized cylinders, the gas mixture is passed over a catalytic reducer, and the concentration is read with a chemiluminescence analyzer previously spanned by the titration technique. The known NO_2 standard is then used to calibrate the automated Saltzman analyzer. Alternatively, a permeation tube can be used to calibrate the colorimetric analyzer and, upon reduction, the chemiluminescence analyzer. If one is careful to exclude water from the permeation systems, the NO_2 permeation technique is quite reliable.

Interferences

Chemiluminescence Analyzers--No notable interferences have been reported for the chemiluminescence detection of NO. Positive interferences are known to occur when the catalytic or carbon converters are used to reduce NO_2 to NO. We have found that the efficiency of some of these converters is near 100 percent for ethyl nitrate and, although inconsistent, sometimes 100 percent for nitric acid. PAN is also known to interfere, but we are not certain of the response factor. The high-temperature (600 to 700° C) catalytic converters are also efficient in oxidizing basic nitrogen species such as ammonia to NO.

Colorimetric Analyzers--There has been some controversy lately about negative interferences with the Saltzman method. At the time when the method was introduced, investigation was made of the effect of potential interfering gases, and no serious problems were evident.[5] About a year ago, however, Stevens[6] and his associates at EPA reported that ozone seriously interfered with the measurement of NO_2. Some of their data are shown in Table 6. As noted, interference becomes quite severe at O_3/NO_2 ratios near 2--a condition that often occurs in the later part of smog-chamber experiments. Unfortunately, we have not had the opportunity to conduct similar interference testing with our Saltzman-type analyzer, and I have no direct evidence to confirm or refute EPA's findings. However, I will present some data that cast doubt as to the probable extent of the interference reported.

Table 6. COLORIMETRIC NO_2 ANALYZER: OZONE INTERFERENCE, $[NO_2]$ = 0.23 ppm

$[O_3]/[NO_2]$	Percent reduction in $[NO_2]$
0	0
1.0	5
2.0	21
3.0	40
4.0	48

Comparison of Methods

Figure 17 compares the results of measuring NO and NO_2 by the Saltzman and chemiluminescence methods. There are some slight differences in the initial readings, but these are no doubt associated with calibrating and zeroing. There is nearly perfect agreement between the

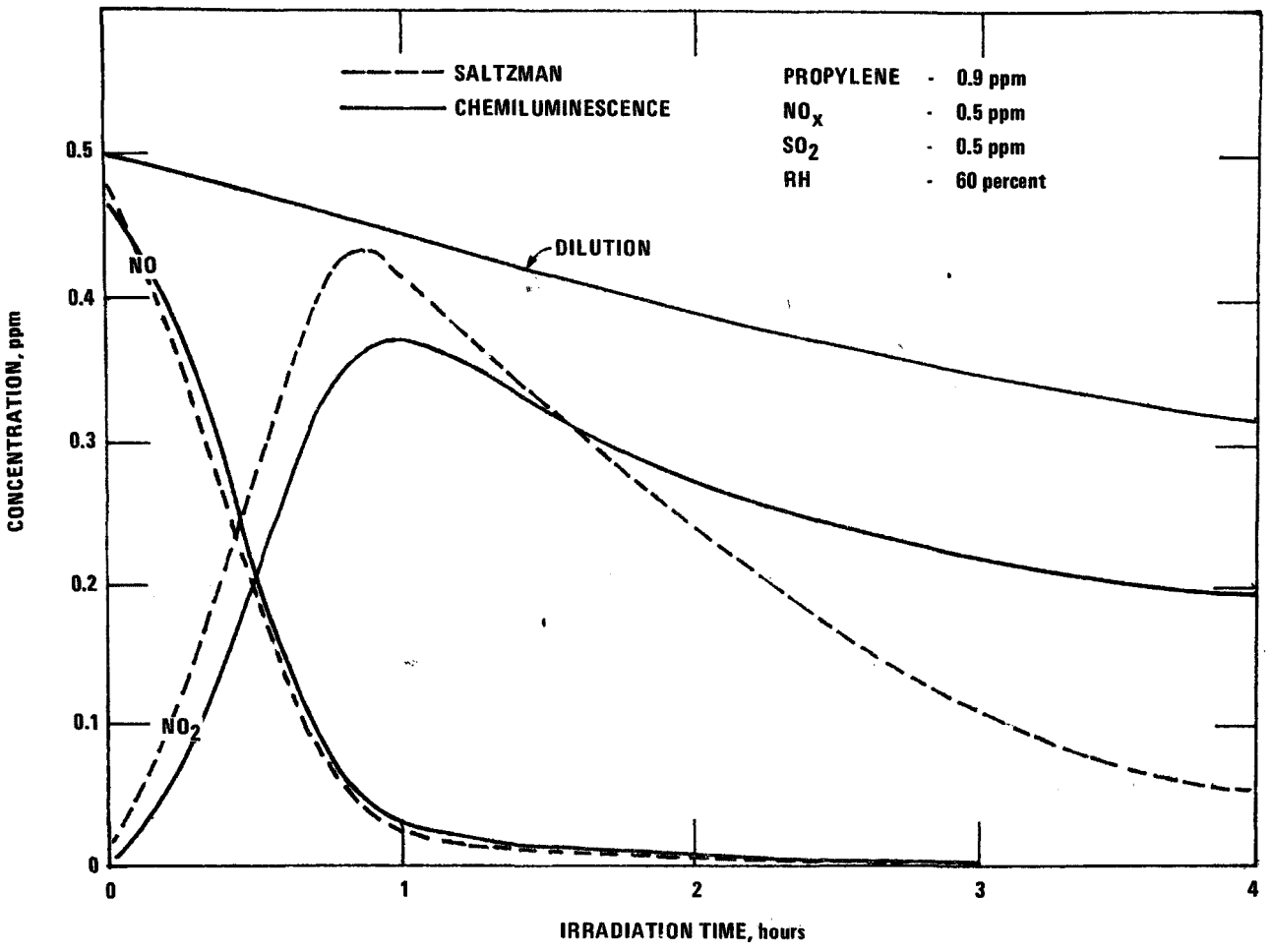

Figure 17. Comparison of methods for monitoring NO and NO_2 during a smog-chamber experiment.

two methods for NO analysis. There is also fairly good agreement between the NO_2 readings up until the time of maximum NO_2, the small difference between the two NO_2 curves being largely that occurring initially. After the time of maximum NO_2, however, there is a serious (nearly twofold) difference in the NO_2 concentrations and the slopes of the NO_2 removal rates. During the last hour of irradiation where the O_3/NO_2 ratio is >2, it might be argued that the factor of 2 difference in NO_2 is due to O_3 interference with the colorimetric analyzer, in accord with the findings of Stevens et al. Alternatively, it might be argued that the chemiluminescence analyzer is responding to nitrogen-containing products other than NO_2. Most of the data from our work, particularly that where we have attempted to make a nitrogen balance,[7] would support the latter contention.

Figure 18, for example, is a profile of a propylene-NO_x irradiation experiment where most of the initial NO_x was NO_2. As noted PAN and nitric acid were monitored here (as well as alkyl nitrates, which turned out to be of insignificant concentrations), and I have plotted total accountable nitrogen as the sum of NO, NO_2, PAN, and $HONO_2$. The dilution rate of the chamber is not precisely known in this case, but should be close to 4 percent/hour. The increase in total nitrogen occurring during the first hour is thought to be due to the lag time associated with the colorimetric analyzer. The instrumentation for

PAN and nitric acid yields concentration data in real time, while the NO_2 values at any given instant actually represent concentrations some 10 minutes earlier. Thus, where NO_2 is rapidly being converted to other nitrogen products, the sum of nitrogen species will be too high since the gain in products has been registered ahead of the loss of reactants. After most of the NO_2 is converted, the total nitrogen curve appears to parallel a typical dilution rate.

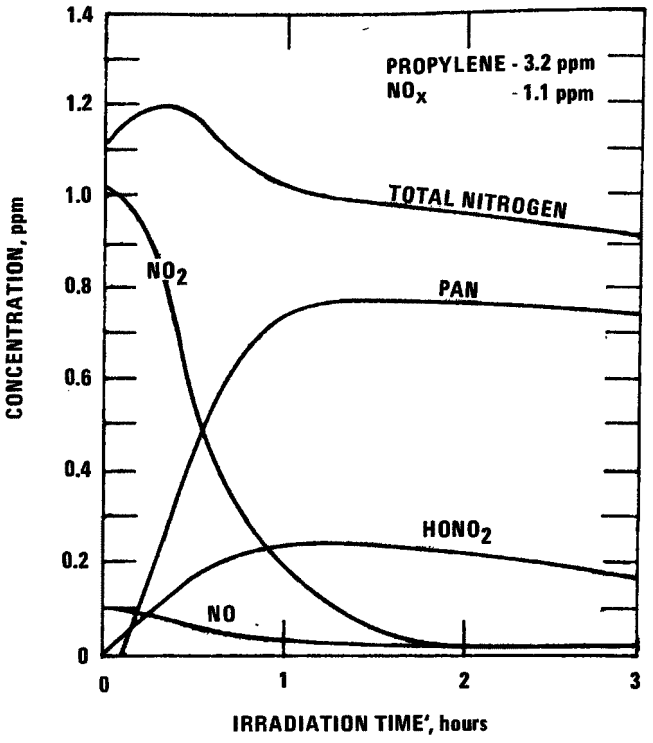

Figure 18. Nitrogen balance during irradiation of propylene-NO_x.

Figure 19 shows similar types of nitrogen analyses where synthetic auto exhaust is irradiated. In this case where NO is converted to NO_2 early in the irradiation, the excess in the total nitrogen curve is less severe than in the previous experiment because the error due to lag time tends to be self-cancelling when both product and reactant are read by the same analyzer. The reason for the increase in total calculated nitrogen occurring near the end of the irradiation is not apparent. Quite likely, it is due to slight inaccuracies in either the PAN and/or HNO_3 calibrations.

After 90 minutes of irradiation, the O_3/NO_2 ratio is >2 and at 3 hours it is >4. If during this time the colorimetric measurement for NO_2 was low by a factor of 2 due to O_3, interference, as suggested by the results in Table 6, it is obvious that the true account of total nitrogen would be seriously out of balance. Thus, on the basis of the smog chamber data presented here where NO_2 was measured by the Saltzman method and where a good material balance in nitrogen is indicated, we conclude that any interference to the Saltzman method by O_3 is not likely substantive. Furthermore, it is recommended that chemiluminescence analyzers not be used for NO_2 determinations in smog chamber studies until converters have been developed that are specific in reducing NO_2 to NO.

Discussion

Dr. A. Winer (University of California, Riverside) reported on recent Statewide Air Pollution Research Center (SAPRC) findings regarding the response of commercial chemiluminescent NO_x analyzers to nitrogeneous smog constituents. Specifically, SAPRC investigated instrument response to PAN, ethyl nitrate, ethyl nitrite, and nitroethane for a commercial NO_x analyzer equipped with a molybdenum converter and operated in the "NO_x" and "NO, NO_2" modes, and response to PAN and n-propylnitrate for an instrument equipped

with a carbon converter. Within experimental uncertainty, an essentially 100 percent response--that is, a response equal to that by NO--was observed in all cases except for the thermodynamically more stable nitroethane, which gave a 6 to 7 percent response. A response to nitric acid was observed but was not characterized quantitatively. Although the problem of nitrogen-containing compounds being reduced on the converters of commercial chemiluminescent NO-NO_x instruments has been known to most smog chamber groups for some time, the vast majority of users who are involved in ambient air measurement applications are unaware that these instruments are not specific for NO. For this reason, SAPRC has given a more detailed report of its studies.[8]

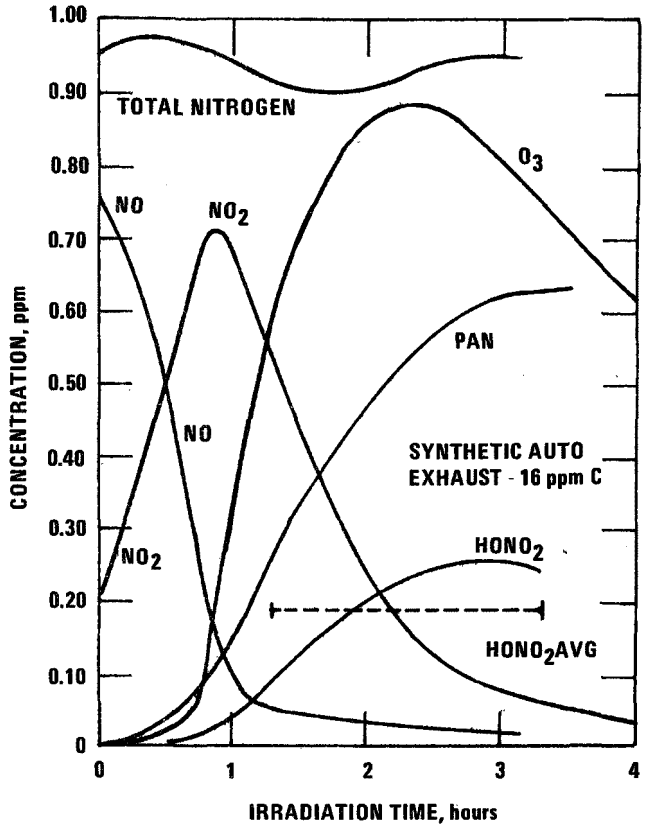

Figure 19. Nitrogen balance during irradiation of synthetic auto exhaust.

Dr. C. W. Spicer (Battelle) offered the observation that the Battelle smog chamber has been demonstrated to yield good nitrogen balances based on PAN and HNO_3 in the gas phase (not on the walls). He believes that HNO_3 is formed at the surface and then desorbs into the gas phase to a degree depending on the nature of the surface.

IN SITU MEASUREMENTS -- *P. Hanst, EPA*

Optical measurements have been made in smog chambers for twenty years. The chambers used for these measurements have generally been in the form of a long tube surrounded by ultraviolet lights. Such a configuration has the advantage of a high ratio of optical path to chamber volume but the disadvantage of a high ratio of surface to volume. In spite of this disadvantage, many of the fundamental discoveries of atmospheric photochemistry have been made in such chambers.

The first application of long path infrared spectroscopy to the study of smog chemistry was carried out at the Franklin Institute Laboratories in Philadelphia between 1953 and 1956. That program of study established an analytical technique that has been highly productive. Among the contributions from that first program were the discovery of the peroxyacyl nitrate family of pollutants, proof of ozone formation in smog, insights into the reaction mechanism that causes ozone to accumulate in smog, demonstration of the formation of aldehydes in the course of the oxidation, and establishment of mechanisms to explain the varying degrees of reactivity among the hydrocarbon poilutants.[9-12]

The analytical method has not been as fully used since that time as it deserved, but at present its application is being expanded.

For detection of molecules, six portions of the electromagnetic spectrum are generally recognized: ultraviolet, visible, near infrared, fundamental infrared, far infrared, and microwave. Molecules have both emission and absorption spectra in all these regions, but in smog chamber studies only absorption spectra have had wide use.

The ultraviolet is the region of absorption by electronic transitions in molecules. Vibrational and rotational transitions also occur and can produce a characteristic structure in the bands. Although the ultraviolet band systems of different molecules are likely to overlap, the structure sometimes permits distinguishing one molecule in the presence of others. Pollutant species that are measurable by ultraviolet absorption include sulfur dioxide, nitric oxide, ammonia, and ozone. At atmospheric pressure, however, many pollutant molecules do not show structure in their ultraviolet bands.

The visible region of the spectrum has very few molecular absorption bands. If this were not the case, the sunlight would not penetrate the atmosphere. Nitrogen dioxide is the only pollutant of significance that absorbs in the visible.

The near infrared, 0.70 to 2.50 microns in wavelength, is the spectral region where the overtones of the molecular vibration-rotation bands appear. These overtones are about 100 times weaker than the fundamentals; thus, the region is not generally useful for molecular detection and analysis. A notable exception is the study of the atmospheres of the planets, where large concentrations of absorbing gas are viewed over extremely long paths. The overtone region has been the principal source of information on the composition of the atmospheres of Mars, Venus, and Jupiter.

The fundamental infrared, 2.50 to 25 microns in wavelength, is the spectral region that has been widely used for chemical analysis for many years. In this region, nearly every air pollutant has a characteristic absorption band. Generally, these bands show many variations in shape, location, and intensity. This spectral region is the one that has been found the most useful for in situ analysis in smog chambers.

The far infrared shows rotational lines as well as some vibration-rotation bands. Unfortunately, the very intense absorption by water vapor will blank out the far infrared in smog chamber studies, even under the driest of conditions.

The microwave region of the spectrum has no application in smog chamber studies because at atmospheric pressure the microwave absorption lines are so broad that distinguishing between different types of molecules is impractical.

It would be desirable to analyze real atmospheres and smog chamber atmospheres by examining both the ultraviolet and infrared spectra. Unfortunately, the two spectral regions require different kinds of spectrometers and detectors. Ultraviolet absorption bands are usually stronger than infrared bands, so that a shorter path suffices, but the number of molecules that can be measured by ultraviolet is limited. If only one optical

system is to be used, the infrared is preferred in spite of the requirement for a long path. It has been found practical to achieve the long path by folding the infrared beam between mirrors.[13,14]

Among the institutions that are using in situ infrared measurements are the General Motors Laboratories, the Ohio State University, the University of California, Riverside, the University of North Carolina, and the EPA's National Environmental Research Center, Research Triangle Park, N. C. In Table 7 there are listed some of the pollutants observed in recent work at the National Environmental Research Center.

In the past, the instruments for measuring infrared spectra in smog chambers have exclusively been dispersive spectrometers employing prisms and gratings. Spectra were recorded periodically across a single long path in the chamber, and changes in the composition of the air were noted by visually comparing a spectrum to an earlier spectrum. The sensitivity of detection in such work has been much increased in recent years by the use of nitrogen-cooled photodetectors. Replacing a thermocouple by a mercury cadmium telluride detector, for example, can raise the signal-to-noise level in a spectrum by a factor of 10 or even 100. Dispersive spectrometry is, therefore, still an effective mode of operation. It is being used at the National Environmental Research Center as well as in other laboratories.

The most notable new instrument for application to in situ smog chamber studies is the Fourier transform spectrometer.[15] In this instrument a scanning interferometer modulates the infrared energy before transmission through the long path cell, and a digital computer transforms the resulting interferogram to a spectrum. The on-line computer is also used to calculate and plot ratios of successive spectra. Such an instrument is obviously much more convenient to work with than a dispersive spectrometer that does not have computational capabilities. However, cost considerations remain as an equalizing factor. A high performance dispersive spectroscopy system can be assembled for a price much lower than the price of a Fourier transform spectrometer.

Sample spectra obtained with Fourier transform spectrometer system are shown in Figures 20 through 25. These are representative of the large number of spectra recorded in the past 2 years at the National Environmental Research Center. The reactants were 0.1 part per million (ppm) molecular chlorine and 5 ppm 1,1 dichloroethylene in 1 atmosphere of tank air. They were contained in a Pyrex long path cell 1 foot in diameter and 30 feet long. Fifty-six passes of infrared radiation through the tube gave a total absorption path of 500 meters. The reactants were irradiated with the light of 96 black-light 40-watt fluorescent lamps. According to the rate of photolysis of nitrogen dioxide, the lamps gave an ultraviolet light intensity within the chamber about 50 percent higher than the intensity of normal sunlight. Spectra were recorded at a resolution of 1 reciprocal centimeter (cm^{-1}). The resultant large number of data points in the fundamental infrared region cannot conveniently be displayed in a single figure.

Table 7. INFRARED DETECTION OF POLLUTANTS

Pollutant	Frequency of most useful band, cm^{-1}	Where seen recently
Acetylene	735	Seen in ambient air at concentrations ranging between 0.10 and 0.001 ppm.
Ammonia	965	Seen in the air at Houston, Texas, at concentrations up to 0.050 ppm.
Carbon monoxide	2180	Seen as product of NO_x-hydrocarbon reactions and as product of chlorine attack on organic compounds.
Carbonyl fluoride	960	Seen as product of the attack of chlorine atoms on difluoro monochloro methane in air.
Chloro acetyl chloride	720	Seen as product of the attack of chlorine atoms on 1,1 dichloroethylene.
Difluoro dichloro methane	921	Seen in air at the background level of 0.0001 ppm, using a cryogenic concentration step.
Difluoro monochloro methane (Freon 22)	1110	Seen in air at Research Triangle Park at 0.005 ppm, using a cryogenic concentration step.
Ethylene	950	Studied in laboratory and measured in ambient air.
Formic acid	1105	Observed in laboratory as product of hydrocarbon photooxidation. Also seen as product of formyl chloride hydrolysis. Measured in California smog at concentrations up to 0.070 ppm.
Formaldehyde	2765	Observed in laboratory as product of hydrocarbon photooxidation. Also seen in ambient air polluted by auto exhaust in Houston, Texas, and Raleigh, N. C.
Hydrogen chloride	2820	Observed in laboratory as product of chlorine attack on organic materials.
Hydrogen peroxide	1250	Seen in the laboratory chamber as product of chlorine attack on formaldehyde in air.
Ketene	2150	Seen in laboratory reactions as product of ozone attack on propylene and 2-butene.
Methane	3020	Measured in clean and polluted atmospheres.

Table 7 (continued). INFRARED DETECTION OF POLLUTANTS

Pollutant	Frequency of most useful band, cm^{-1}	Where seen recently
Methanol	1035	Seen in air at Pasadena, Calif., at concentrations up to 0.100 ppm.
Monofluoro trichloro methane (Freon)	845	Seen in air at the background level of 0.0001 ppm, using a cryogenic concentration step.
Nitric acid	880	Seen as product of N_2O_5 hydrolysis in laboratory chambers.
Nitric oxide	1900	Measured in ambient air.
Nitrogen dioxide	1615 (2900 in humidity)	Routinely monitored in laboratory chamber studies.
Nitrogen pentoxide	1250	Seen as product of ozone-nitrogen dioxide reaction in laboratory chamber.
Nitrous acid	850	Seen in auto exhaust and in chambers as product of the H_2O-NO-NO_2 interaction.
Ozone	1060	Measured in laboratory chamber as product of hydrocarbon-NO_2 reaction. Seen in ambient air.
Peroxy acetyl nitrate	1160	Seen in laboratory photooxidations. Also measured in California smog at concentrations up to 0.050 ppm.
Peroxy benzoyl nitrate	990	Seen as product of photooxidation of styrene in laboratory chamber.
Phosgene	815	Seen as product of oxidation of chlorinated hydrocarbons in the laboratory chamber.
Propylene	915	Followed in laboratory reactions; seen in air polluted by auto exhaust.
Sulfur dioxide	1360	Measured in auto exhaust.
Vinyl chloride	920	Seen in the air at Houston, Texas, at a concentration of 0.37 ppm.

Figure 20 shows the spectral region between 2700 and 3100 cm^{-1} in single beam mode, before irradiation. The detailed structure in the spectrum is mainly due to an impurity of approximately 2 ppm of methane in the tank air. There are also absorption lines of water. In this region the absorption by 1,1 dichloroethylene is insignificant. Chlorine, being a homonuclear diatomic molecule with no permanent dipole moment, shows no infrared absorption. Actually, chlorine is about the only possible air pollutant that does not have an infrared spectrum. Figure 21 shows the same spectral region as Figure 20 after 15 minutes of irradiation. Bands of the products hydrogen chloride, formaldehyde and chloro acetyl chloride have appeared. Figure 22 is a ratio plot of the spectrum of Figure 20 over the spectrum of Figure 21. Figure 23 shows a ratio plot of part of the spectrum of the initial reactants over the spectrum of tank air. The absorption in this

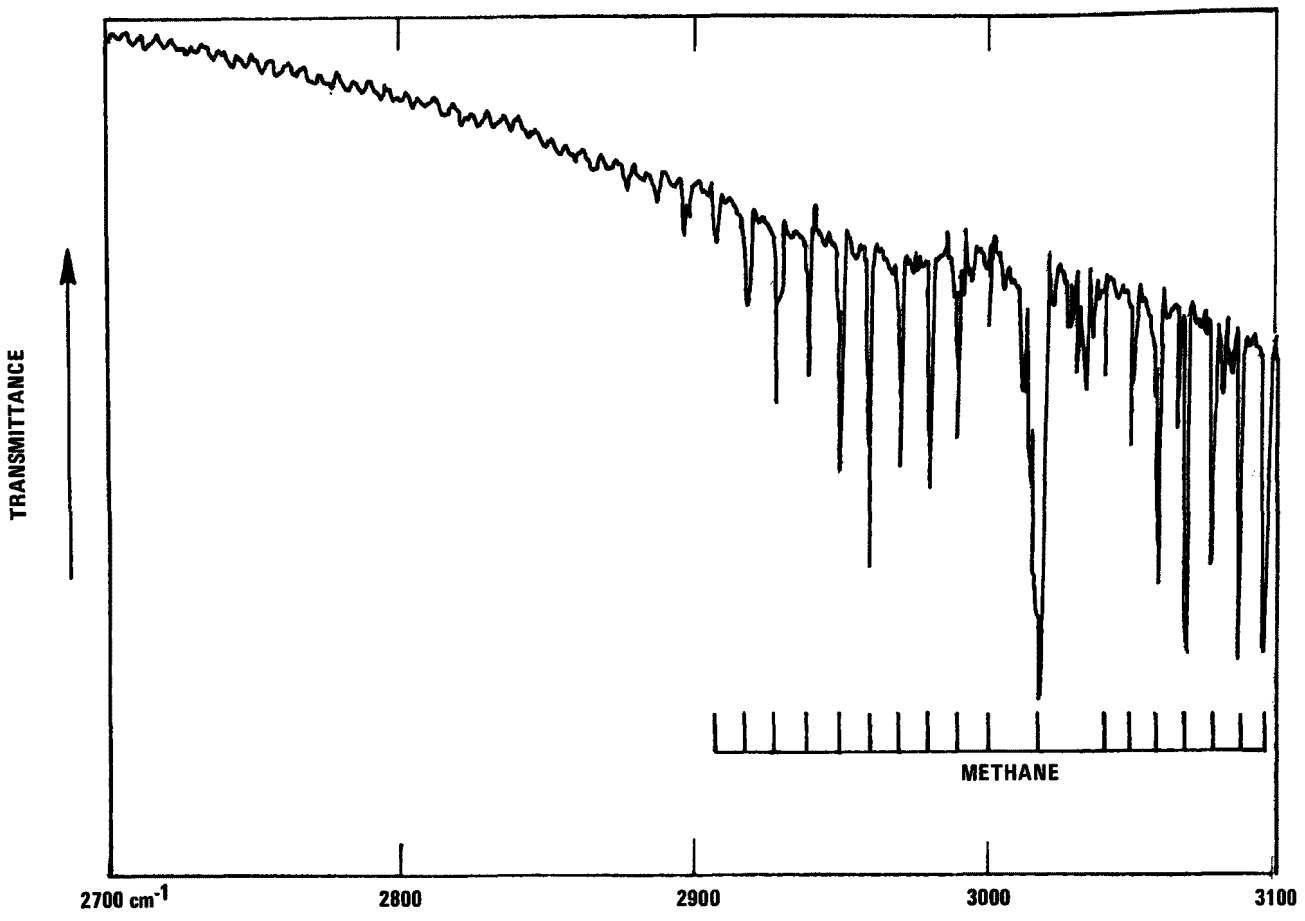

Figure 20. Single beam plot in CH absorption region for 1 atmosphere of tank air with addition of 5 ppm 1,1 dichlorethylene and 0.1 ppm molecular chlorine, before irradiation. Path length, 500 meters; resolution, 1 cm^{-1}.

spectrum is all due to the 1,1 dichloroethylene. Figure 24 shows a similar ratio plot, chamber contents over the tank air, after 10 minutes of irradiation. This figure shows that more than 80 percent of the 1,1 dichloroethylene was consumed and converted mainly to chloro acetyl chloride. This is an impressive result, indicating a chain reaction, as will be discussed in a separate publication. Figure 24 also shows a band due to phosgene. Figure 25 is a partial ratio plot of the spectrum of the reaction products after 10 minutes over the spectrum of the starting material. The 1,1 dichloroethylene band at 1620 cm^{-1} was removed by the reaction and, therefore, appears upside down and cut off at the top. The band at 1830 cm^{-1} is the carbonyl band of the product chloro acetyl chloride.

These sample spectra have shown the capability of in situ spectroscopy to reveal a variety of reaction products with unequivocal identification and with a high degree of detection sensitivity. It should also be noted that successive recordings of the spectrum yield time versus concentration plots for both reactants and products. It is clear, therefore, that the in situ spectroscopic technique that was first productive twenty years ago is still highly productive and deserves to have its application expanded.

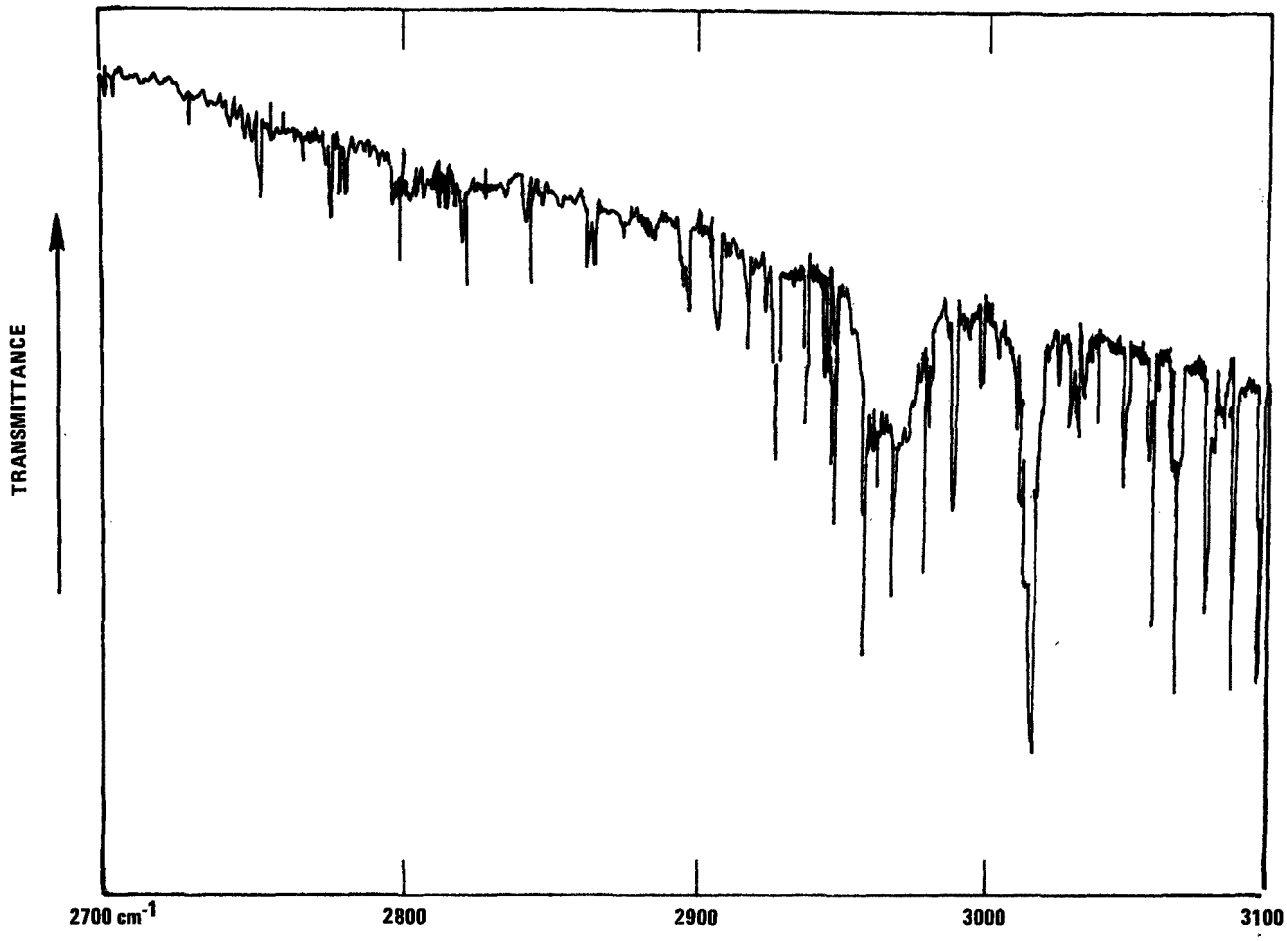

Figure 21. Single beam plot in CH absorption region for 1 atmosphere of tank air with addition of 5 ppm 1,1 dichlorethylene and 0.1 ppm molecular chlorine, after 15 minutes of irradiation. Path length, 500 meters; resolution, 1 cm^{-1}.

DISCUSSION

Dr. Winer (UCR, SAPRC) reported on the SAPRC experiments with an in situ multipass infrared system attached to a smog chamber. Dr. Winer's report was as follows:

The evacuable chamber at SAPRC contains an insitu multipass optical system with a 1.3-meter base length capable of producing pathlengths of 100 meters or more for use with either a 1-meter scanning monochromator or a Fourier infrared interferometer. During the past year, a variety of studies have been conducted in the evacuable chamber with this long-path infrared system (LPIR) including both photolysis and dark experiments. For example, the good time resolution (as well as spectral resolution) afforded by the interferometer has made it possible to obtain concentration-time data from the in situ measurement of a large number of species resulting from the photolysis of HC/NO_x systems, including some species not easily detected by other means, i.e., HONO, HNO_3, $C_2H_5ONO_2$ and HCOOH. A second application of the Fourier interferometer LPIR system was a detailed product analysis for the reaction of ozone with ethene, propene and cis-2-butene in the evacuable chamber at both one atmosphere and reduced pressures. In addition

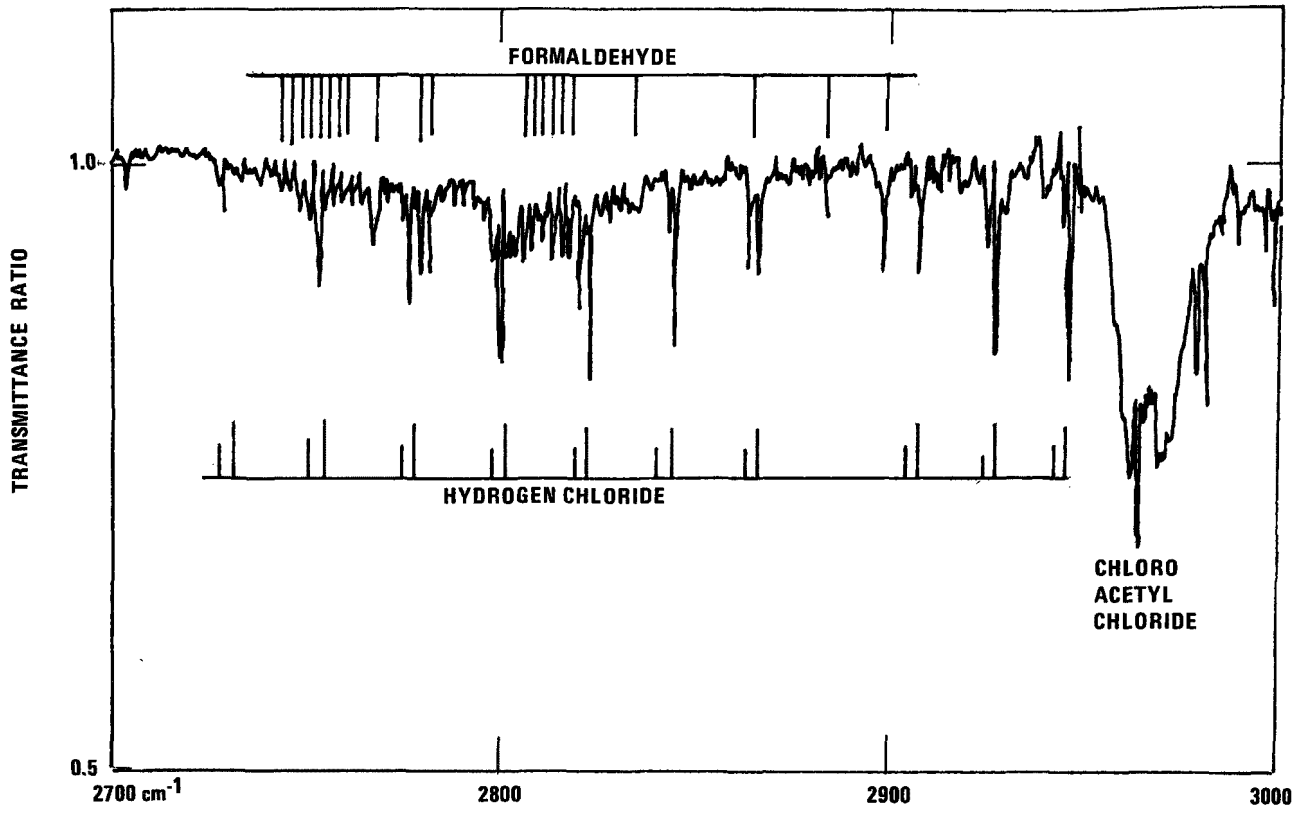

Figure 22. Ratio plot, spectrum of products over spectrum of reactants; 5 ppm 1,1 dichlorethylene and 0.1 ppm molecular chlorine in air, after 15 minutes of irradiation. Path length, 500 meters; resolution, 1 cm^{-1}.

to species identified in previous studies, preliminary assignments have been made to several α-carbonly hydroperoxides and peroxyformic acid. A third recent application was the use of the dispersive LPIR system to investigate the stoichiometry of the 2 percent neutral buffered potassium iodide (2 percent NBKI) method employed by the California Air Resources Board (ARB) for the measurement of ozone, following disclosure of a discrepancy between this method and the 2 percent unbuffered KI method employed by the Los Angeles Air Pollution Control District (LAAPCD). Using the 5500-liter evacuable chamber as a convenient reservoir for ozone and with a 70-meter pathlength and a liquid nitrogen cooled HgCdTe detector, quantitative infrared data were obtained simultaneously with 2 percent NBKI impinger samples (ARB method) for ozone concentrations ranging from 0.1 to 1.2 ppm. Comparison of the resulting KI and IR ozone concentrations established, within uncertainties of 3 to 5 percent, a 1:1 stoichiometry for the reaction of ozone with iodide in a 2 percent buffered solution. In contrast, we found that the 2 percent unbuffered KI (LAAPCD) method yields values of ozone systematically lower by more than 30 percent. (A complete report of this work has been submitted for publication in Environmental Science and Technology.)

In summary, we have found the in situ long-path infrared capability to be invaluable in a variety of our environmental chamber studies, largely because of its capacity

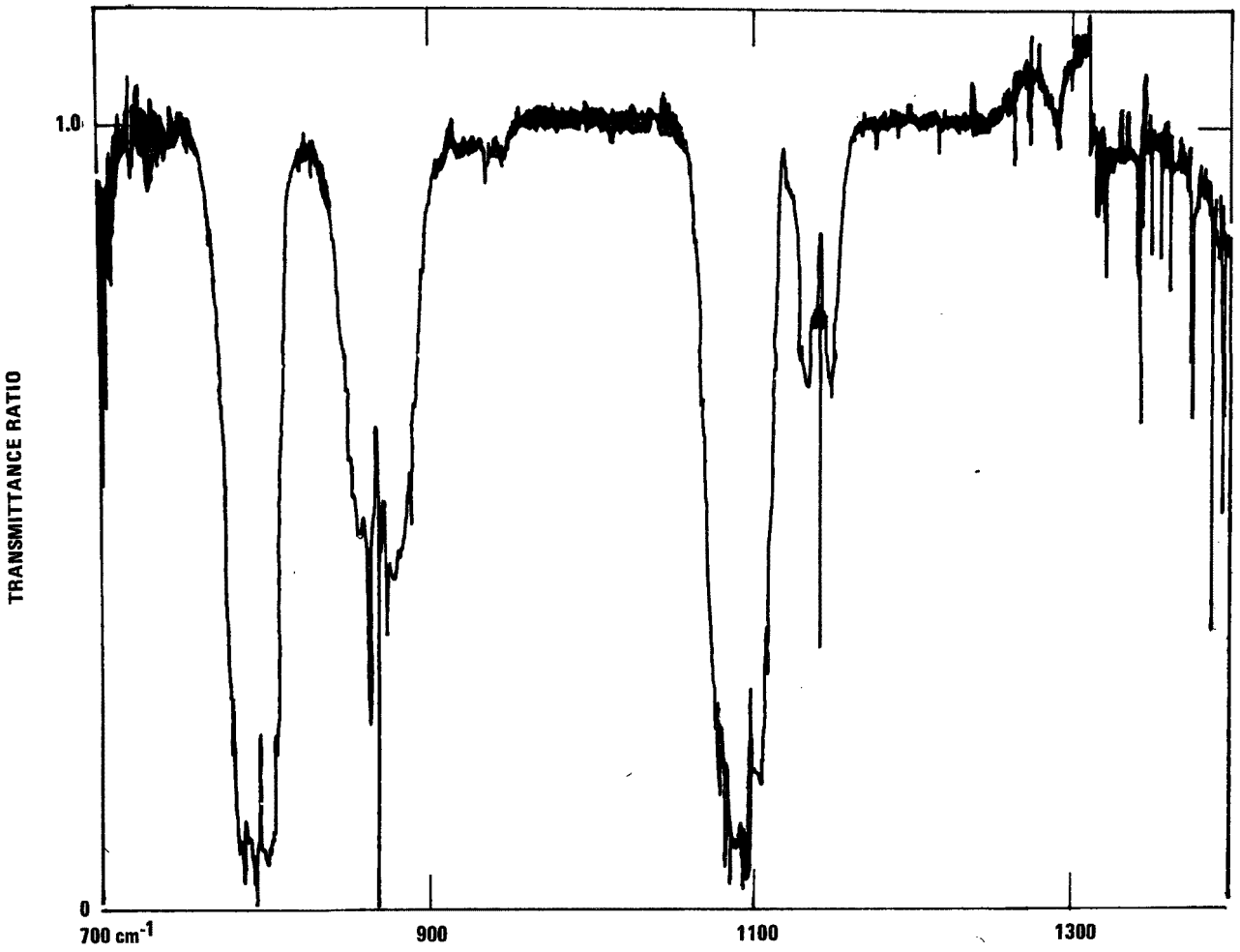

Figure 23. Ratio plot, spectrum of reactants over spectrum of tank air; 5 ppm 1,1 dichlorethylene and 0.1 ppm molecular chlorine in air, before irradiation. Path length, 500 meters; resolution, 1 cm^{-1}.

to validate, by in situ measurement, the data being obtained by external sampling and determination methods for species such as PAN, HCHO, O_3, and organic nitrates.

AEROSOL MEASUREMENT -- *P. Reist, UNC*

Small particles can be formed from reactions involving two gases, a gas and water vapor, a gas and energy in the form of radiation, or a combination of these factors. They can also arise through the condensation of a gas onto its own molecules or onto a particle or molecules of some other material. Particles can be either solid or liquid. They range in size from about 0.005 micrometer for fresh reaction products up to about 1 micrometer in diameter for droplets formed by condensation.

Particle concentrations of 10^6 particles per milliliter or greater are not uncommon in some chamber studies, and concentrations may be as low as several hundred per milliliter. Mass concentrations can be as high as several hundred micrograms of aerosol per cubic meter. When number concentrations are greatly in excess of 10^6 particles/ml,

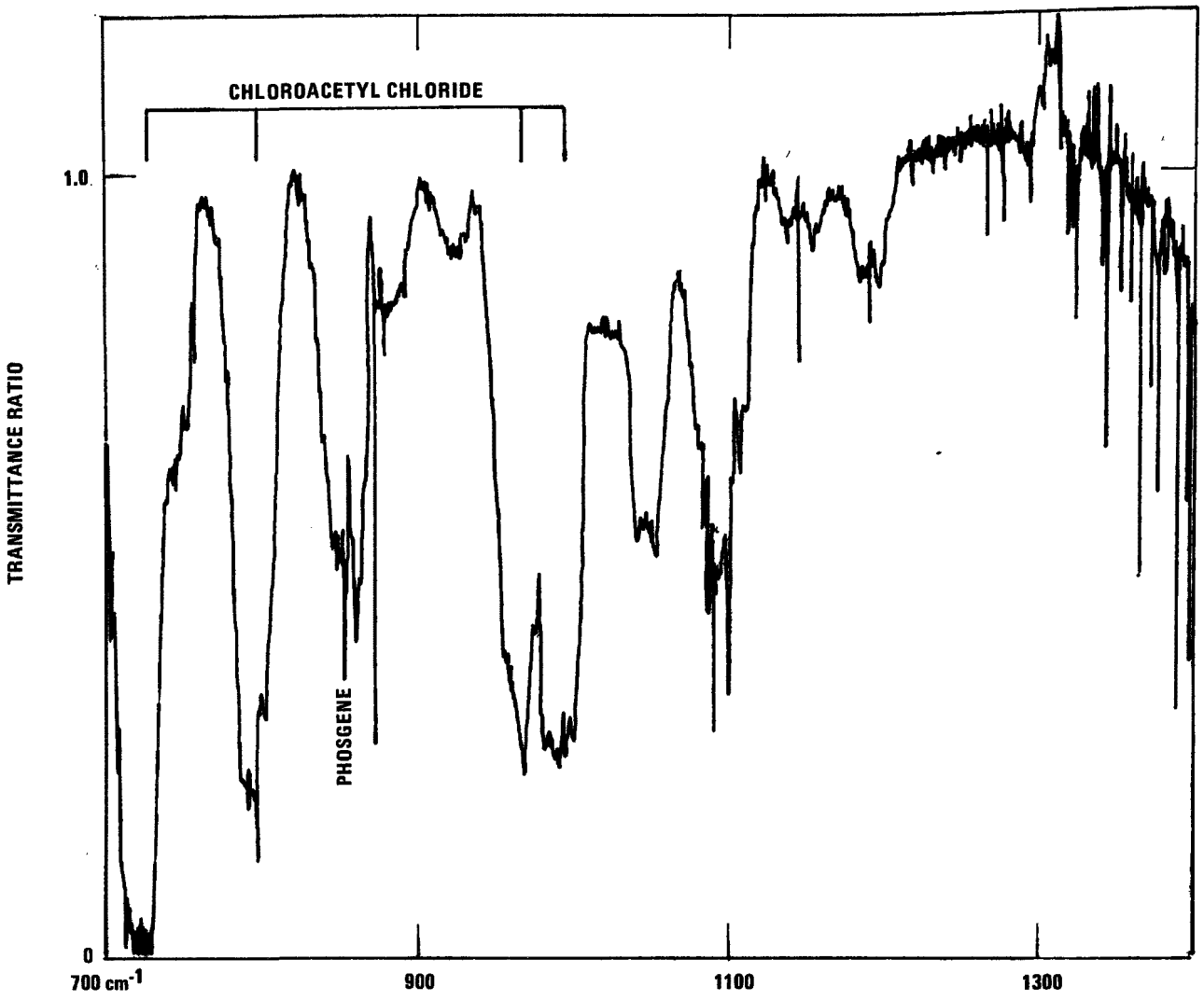

Figure 24. Ratio plot, spectrum of products over spectrum of tank air; 5 ppm 1,1 dichlorethylene and 0.1 ppm molecular chlorine in air, after 10 minutes irradiation. Path length, 500 meters; resolution, 1 cm^{-1}.

particle size and concentration will change rapidly through the process of coagulation, particles growing to larger sizes with a resulting decrease in aerosol concentration. Particles can also be lost to the walls of a chamber, and such losses can be particularly important with long experiments or small chambers.

Particles act as sites for condensation of water vapor, producing clouds or haze, and can also in themselves significantly alter visibility. By providing increased surface area per unit mass of material, small particles can enhance reactions between atmospheric gases. They can be transported great distances by air currents, and represent a potentially significant inhalation hazard since they can penetrate deep into the lower portions of the lung where lung clearance mechanisms are least effective.

Particle concentration, size, and chemical composition interplay to determine whether aerosol particles produce a dramatic effect or remain unnoticed. Toxic materials in very

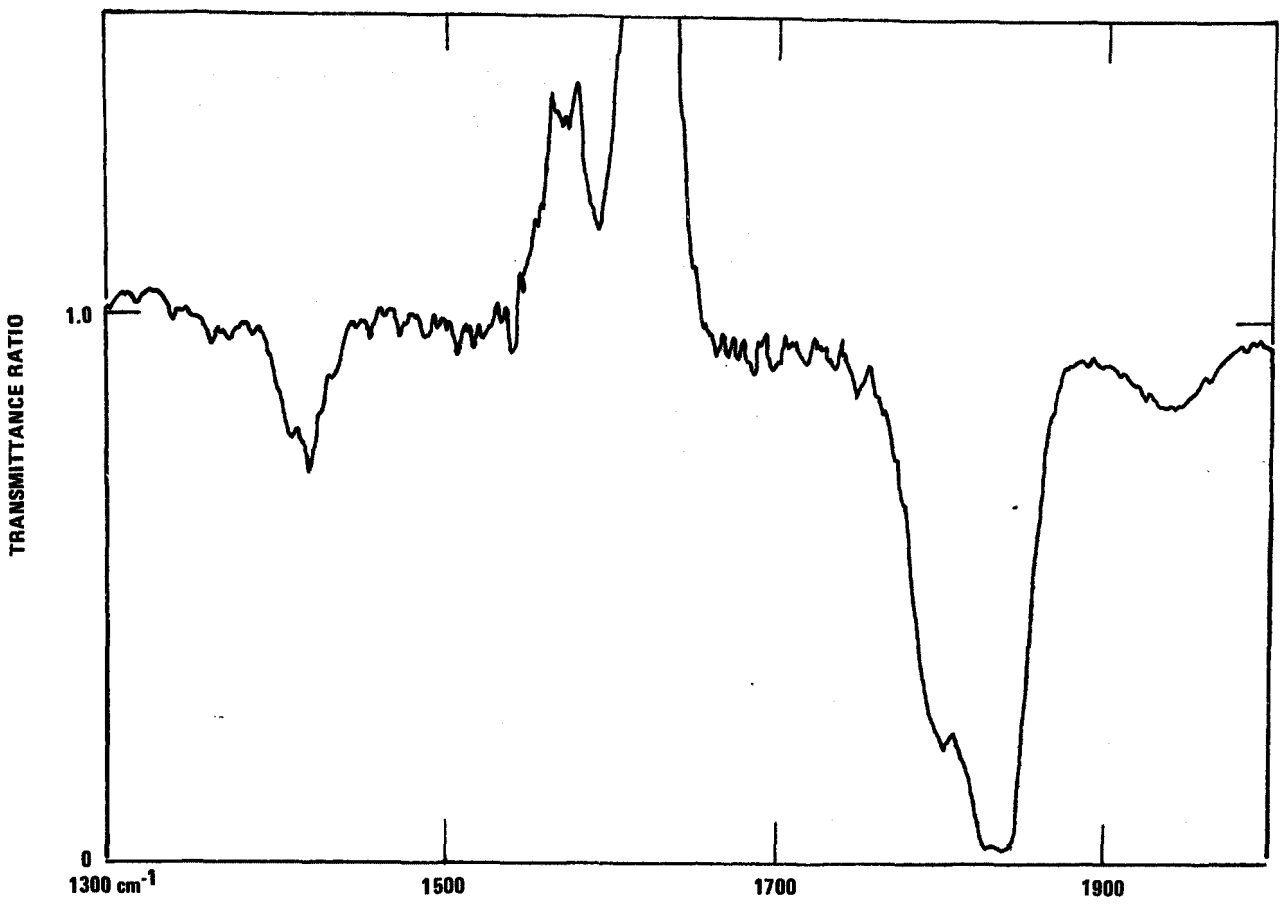

Figure 25. Ratio plot, spectrum of products over spectrum of reactants; 5 ppm 1,1 dichlorethylene and 0.1 ppm molecular chlorine in air, after 10 minutes irradiation. Path length, 500 meters; resolution, 4 cm^{-1}.

low number and mass concentration are benign. Large numbers of very small particles produce little interference with visibility; fewer numbers of larger particles have a much more pronounced effect.

There are gaps in determining the proper aerosol measurement techniques for chamber studies. The tradeoff is between ease of data collection and accuracy or completeness of data. Condensation nuclei counts provide only the barest of information about the aerosol in a chamber, the number concentration, but provide it in a continuous manner so that aerosol trends can at least be observed. Intergrating nepholometers also fall into this category. Since these two devices give indications of number and mass concentrations, respectively, they represent the minimum aerosol instrumentation that should be included in chamber studies.

The electric mobility analyzer has been used frequently to determine atmospheric particle size distribution data. It has the distinct advantage of speed over more accurate methods; a particle size distribution can be determined in 10 minutes. This permits the dynamic properties of the aerosol to be followed during the course of a chamber experiment.

Single particle optical counters have been used in some previous chamber studies but appear to be of much less value than the instruments listed above. Single particle optical counters have a limited effective size range and a very low effective concentration range. The data from them, although easy to collect, is difficult to interpret. Similar to the mobility analyzer, single particle optical counters are useful in showing trends in aerosol size, particularly in the size range approaching 1 micrometer in diameter.

Filters are useful for total mass samples or for chemical analysis of the total aerosol. Since mass concentrations are relatively low (10 to 100 micrograms per cubic meter) sampling times must be long enough for a sufficient amount of sample to be collected. Glass fiber filters are generally used for sampling for chemical analysis since they are considered to be the least reactive, and membrane filters are used for total mass concentration measurements because of their high collection efficiencies, even for very small particles.

Impactors will continue to be used for chamber studies since they provide a means of getting chemical composition data on various particle size fractions. The data from these samplers is at best crude, and they are severely limited in the smallest sizes of particles that can be collected. Nevertheless, they do provide useful information that at present would otherwise be impossible to get.

The other techniques mentioned as possibilities for chamber studies, although proved out in the laboratory, have not been applied as working tools for chamber experiments. As becomes apparent with the application of any instrument to chamber work, there is a large gap separating the successful performance of an instrument in the laboratory and its useful application in the field. Future research and development should provide the chamber scientist with improved aerosol instrumentation; at present, existing equipment must be used, recognizing the limitations of the equipment while appreciating the value of the data developed.

A listing of aerosol sampling procedures and characteristics of selected aerosol instruments is given in Tables 8 and 9.

Discussion

Referring to Dr. Reist's presentation, Dr. G. J. Doyle (UCR, SAPRC) commented that, in general, the optical particle counter is indeed inextricably complicated. However, for spherical particles, which are likely to be frequently encountered in smog chamber experiments, the response to particle size dependence can and often has been calculated. The chief drawback is that one must know the refractive index, both the real and imaginary parts. Dr. Doyle further stated that recent counter designs are directed towards minimizing sensitivity to refractive index so that the data obtained should be at least as good as the data from the Whitby analyzer within the appropriate size region.

MEASUREMENT OF OXYGENATED SULFUR COMPOUNDS -- *D. Miller, Battelle*

The problem concerning the measurement of SO_2 and its oxidation products in smog chamber experiments is exemplified in Figure 26. Under typical smog chamber conditions,

Table 8. AEROSOL SAMPLING PROCEDURES

I. Aerosols studied in the suspended state
   1. Techniques applicable to particles greater than 0.1 micrometer diameter
      A. Nephelometry
      B. Single particle optical counter
   2. Techniques applicable to particles less than 0.1 micrometer diameter
      A. Mobility analyzer
      B. Laser doppler spectroscopy
      C. Condensation nuclei counter
      D. Vapor phase enlargement
      E. Particle size magnifier
      F. Flame photometry

II. Particles removed before studying
   1. Particles examined
      A. Impaction
      B. Centrifugation
      C. Filtration
      D. Electrostatic precipitation
      E. Thermal precipitation
   2. Effluent examined
      A. Diffusion
      B. Impaction

the change in SO_2 concentration due to oxidation is often quite small, and sometimes smaller than other SO_2 loss processes, such as dilution and wall losses. If one attempts to conduct experiments at ambient conditions, say <0.1 ppm SO_2, and the oxidation rate is 2 percent/hour, one is faced with trying to measure <2-ppb/hour change in SO_2 concentration. Such a requirement exceeds the sensitivity of commercially available SO_2 analyzers. At the present, we are having to study SO_2 oxidation at higher than ambient concentrations (~0.5 ppm), and the instrumentation is still required to measure changes in concentration of <2 percent; a determination of questionable accuracy.

The measurement of SO_2 oxidation products is not much easier. Under many experimental situations, the H_2SO_4 aerosol concentration may not exceed 10 ppb, even after 4 or 5 hours of irradiation. In this case, at least, one is trying to measure only a small concentration rather than a small change in a relatively large concentration.

My objective in this discussion is to review and compare some of the analytical methods we are employing in our SO_2 studies. The number of methods I will discuss is quite limited, and it is hoped that other participants of the conference will discuss other techniques that they have found to be successful.

Table 9. CHARACTERISTICS OF SELECTED SAMPLERS

Type	Sampling rate, liters/min	Sampling time	Type of sample collected	Sample analysis	Remarks
TSI mobility analyzer	30-50	10 minutes	Size distribution from electrical mobility	Internal	Direct reading
MRI integrating nephelometer	140	Continuous	Light scattering coefficient	Internal	Direct reading, mass concentration implied
Royco single particle optical counter	30	Variable	Size distribution from light scattering	Internal	Direct reading
Environment One condensation nuclei counter	3	Continuous (5-sec response)	Particle number concentration only	Internal	Direct reading
Lundgren impactor	113	Variable	Four stages plus filter, ECD_A, 4th stage = 0.4	External	Gravimetric or chemical analysis
Aerosol centrifuge	20[a]	Variable	Continuous aerodynamic size separation	External	Gravimetric or chemical analysis
Point-plane electrostatic precipitator	0.2	Variable	Random fraction of aerosol	External	Size distribution by electron microscopy

[a]Variable.

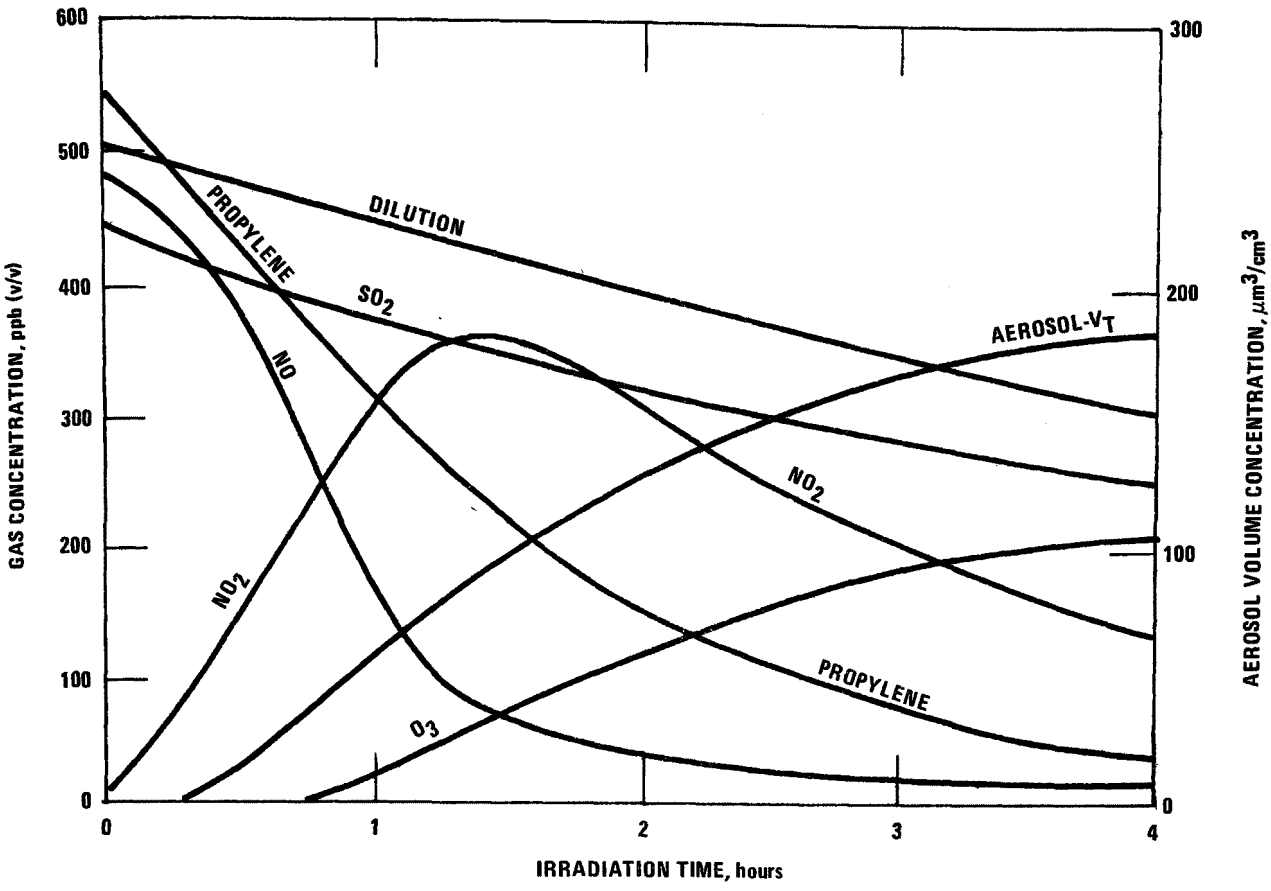

Figure 26. Sulfur dioxide removal during irradiation of propylene-NO_x.

Sulfur Dioxide

The continuous SO_2 monitors commonly used in our work are hydrogen flame photometers and coulometric-titration analyzers. The coulometric analyzers operate on the principle of oxidizing SO_2 with iodine or bromine. Iodine is the charge carrier, and any change in iodine concentration due to reduction by SO_2 is detected as a flow of current through a reference electrode. The instruments are generally equipped with scrubbers for removing oxidants, which cause negative interferences. The sensitivity of these analyzers is about 10 ppb.

Flame photometric analyzers are based on the chemiluminescence principle. When sulfur-bearing gases are burned in a hydrogen flame, excited sulfur molecules ($S + S \rightarrow S_2^*$), which emit light in returning to the ground state, are formed. The emission is generally read at 394 nm. Such instruments have a wide range of linearity, with the response being proportional to the square of the sulfur concentration. Gas chromatographic techniques can be incorporated to permit separation of various sulfur gases. In most smog chamber applications, the instruments can be used to specifically monitor SO_2 by merely placing a particulate filter in the sample line. The filter removes the aerosol products of SO_2 oxidation. The sensitivity of the flame photometers is also near 10 ppb.

In Figure 27 simultaneous measurements of SO_2 are shown for coulometric and flame photometric instruments. Figure 27a represents results of irradiating 0.5 ppm SO_2 in unpolluted air. The change in SO_2 concentration with time is largely due to chamber dilution. The important observation here is the nearly identical measurement of SO_2 by the two different instruments.

Figure 27b shows SO_2 loss where 1.3 ppm propylene and 0.5 ppm NO_x were irradiated with 0.5 ppm SO_2. In this case, the agreement between the two SO_2 monitors was good until about the last hour of irradiation. This pattern during the latter period of irradiations with olefins is quite consistent; the flame photometer indicating a higher concentration than the coulometric analyzer. Figure 27c shows greater disparity between the two methods. In this case, 1-butene was irradiated with NO_x at a HC/NO_x ratio of about 4 in a dynamic 200-liter smog chamber.

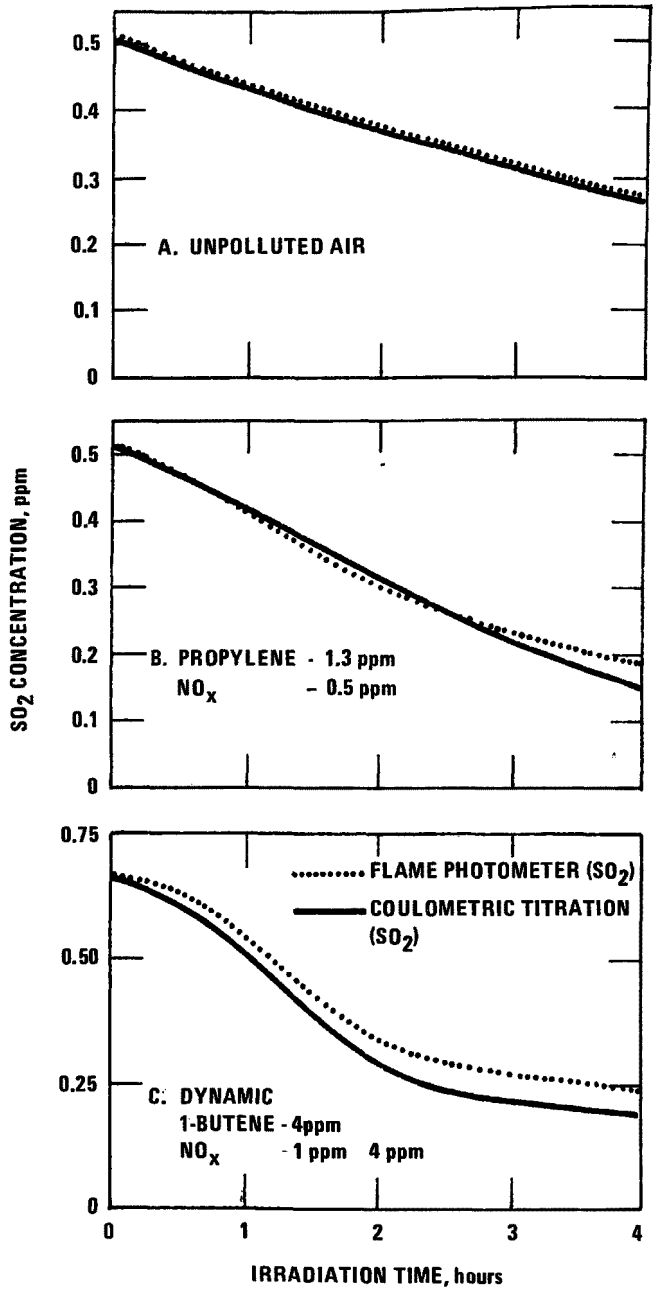

Figure 27. Comparison of methods for sulfur dioxide analyses during smog-chamber irradiations.

In general, we find that the difference in SO_2 concentrations determined by these two methods increases as the photochemical reactivity of the system increases. The disagreement is most pronounced after the maximum O_3 concentration is reached. It is not clear which analyzer might be suffering interference problems at this point in the irradiation, nor what the interfering specie(s) may be. We do know that in experiments where a considerable amount of nonsulfate aerosol is produced, the coulometric analyzer suffers a positive-type interference. Also, during relatively fast photochemical reactions, we have noticed anomalous behavior of the coulometric SO_2 analyzer, often showing an increase in the SO_2 concentration during the early stages of irradiation. In conclusion, it seems that the flame photometric technique is the more reliable method for smog chamber work except in instances where one is confident that interference is not occurring with coulometric analyzers.

Sulfate Aerosols

We are currently using two methods for determining sulfate concentrations. The barium chloranilate method[16,17] is used for intermittant analyses during the course of the irradiations, and the barium perchlorate method[18] is used on a much larger aerosol collection made at the conclusion of irradiation.

For intermittant SO_4^{2-} analyses, about 60 liters of sample are withdrawn through 25-mm glass fiber filters that were previously washed by refluxing with water and methanol. The aerosol is extracted from the filters with 80 percent isopropanol. Excess barium chloranilate is added, followed by thorough mixing and centrifuging. The sulfate ions are precipitated with barium, and the acid chloranilate ion yields a pink color read at 310 nm. The reaction is

$$Ba\,C_6Cl_2O_4 + H^+ + SO_4^{2-} \longrightarrow BaSO_4 + HC_6Cl_2O_4^-$$

The sensitivity of the method is about 2 μg H_2SO_4.

Aerosols analyzed by the barium perchlorate method are collected on 10-cm quartz fiber filters. In this analysis, barium perchlorate is added from a microburet to the sulfate solution. Barium sulfate percipitates, and as soon as excess barium ions appear, a complex forms with thorin indicater. The titration is also carried out in 80 percent isopropanol to minimize the solubility of barium sulfate. The end point of the titration is marked by a yellow-to-pink color change.

A third method I want to mention is a technique applied to determine the dissociated proton concentration of the aerosol extract, presumably protons of sulfuric acid. In this case, aerosol is collected and extracted in the same manner as with the barium chloranilate method. One drop of neutral iodate-iodide solution is added to the extract, which is then centrifuged, and the liberated iodine is read at 352 nm. The intensity of the iodine solution is directly proportional to the proton concentration. The reaction occurring is

$$6H_3O^+ + IO_3^- + 5I^- \longrightarrow 3I_2 + 9H_2O$$

The sensitivity of the method is about 5 μg H_2SO_4 and could probably be improved with the addition of starch indicator.

A similar proton-determining method has recently been reported in which a bromate-bromide mixture is used to liberate bromine by protons.[19] Subsequent bromination of fluorescein solution yields a distinctive color.

In smog chamber experiments conducted earlier this year at Battelle, analyses for sulfuric acid aerosol were limited to the barium chloranilate method. In many cases, the sulfate concentration agreed fairly well with the concentration expected from the consumption of SO_2. However, under some conditions, the agreement was not good. Thus, in more

recent experiments we have employed all three of the methods described above. It is regretable, however, that at this time our analytical work has not been completed, and I am not in a position to comment on the comparability of the methods, nor the significance of the analytical methods.

Discussion

In response to a question from Mr. R. Stevens (EPA), Dr. C. W. Spicer (Battelle) explained that HNO_3 interference is avoided in the H_2SO_4 filter analysis since HNO_3 passes quantitatively through Teflon and neutral quartz filters. HNO_3 can be scrubbed by glass and several other types of filters.

QUALITY CONTROL -- *C.E. Feigley, UNC*

Two major problems in controlling data quality are (1) establishing reliable calibration techniques and (2) placing some quantitative measure of quality on the resulting data.

Calibration

Chemiluminescent NO_x and O_3--At the University of North Carolina, we have found that the use of multiple calibration methods was necessary to assure correct calibration. Figure 28 illustrates the calibration techniques employed. Bottled NO has been a stable source for calibration, but we have had to use tanks from two different supplies. Differences between tanks we have received have been as much as 5 percent, not including occasional mislabeling. Bottled NO_2 has not proven to be as reliable as bottled NO; it sometimes required running gas out of the bottle for 5 or 6 hours before reaching a stable concentration that agreed with other techniques. Also, when a stainless capillary was used as a flow restrictor, some NO appeared in the gas. Use of Teflon instead reduced this problem. NO_2 permeation tubes using a Warburg compensation syringe gave high readings compared with

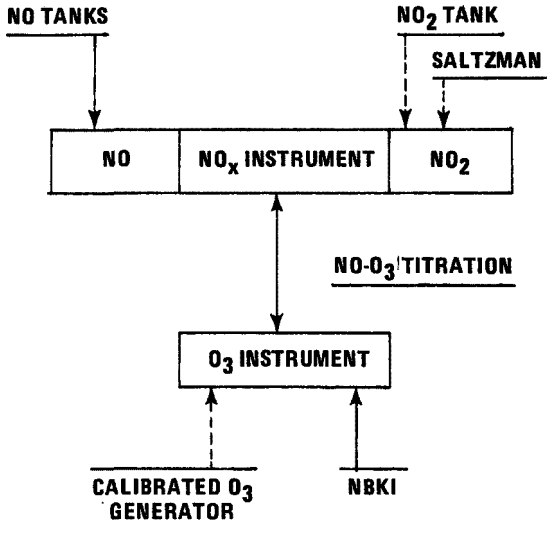

Figure 28. Calibration methods used for chemiluminescent NO_x and O_3 instruments.

other techniques, and thus their use was discontinued. No great effort has been made to determine why the NO_2 permeation tubes failed to agree with other methods. Saltzman has occasionally been used to calibrate the NO_x instrument, usually when there is difficulty obtaining agreement between other methods.

The ozone instrument is primarily calibrated with NBKI bubblers. A detailed statistical analysis of ozone instrument calibration identified the major sources of error.[20] In the preparation of the standard I_2 curve, the major sources of error were the titration and the subsequent two dilutions of standard I_2 solutions, not the serial dilutions on measurement of absorbances. Thus, we at UNC recommend a standard I_2 curve resulting from six separate titration and dilution series. The slope of the line is determined by least-square regression with points weighted by the inverse of the absorbances. The major errors in NBKI bubbler determinations are in measuring volumes, times, and flowrates. The bubbler technique is very accurate, but rather imprecise. Thus, five or six bubbler samples should be run for each calibration performed.

Methane and Nonmethane Hydrocarbons with an Environmental Chromatograph--For measuring methane and nonmethane hydrocarbons, the UNC group's experience is mostly with the environmental chromatograph. The Federal Register states that total hydrocarbon and methane modes of an environmental chromatograph shall be calibrated with methane. In the first calibration of our instrument, bottled methane from two sources was compared with a propane permeation tube. The permeation tube gave low results. This was at first thought to be an error in calculating permeation rates. After checking the instrument on two tanks of n-butane, two of n-hexane, one of toluene, and one of mixed hydrocarbons (from 4 to 12 ppmC), it was concluded that the instrument did not respond 100 percent to nonmethane hydrocarbons and that the permeation tube values were in good agreement with bottled gas.

It was felt that the efficiency of measurement of NMHC should be calculated using known concentrations of the hydrocarbons to be measured. Data collected after this are then corrected for this efficiency.

Recommendation--The calibration of instrumental methods for smog chamber research still raises many questions. The problem of NMHC efficiency is still far from resolved. The effect of frequency of calibration is not known quantitatively. There is no standardization of procedures.

Since good calibration is an indispensible prerequisite to data accuracy, I would like to recommend that EPA sponsor a committee, drawing on the experience and talents of many of the groups represented at this meeting, to establish standard calibration procedures. Applications of such procedures would help assure uniformly high data quality.

Statistical Approach

Recently, questions have been raised concerning the quality of data from various third generation air monitoring instruments. For instance, modelers of atmospheric reactions

often express the concern that measurement errors may be of such a magnitude as to have adverse effects on the validation of their models.

Accuracy and Precision--Initial efforts have been made to quantitate data quality by specifying statistically interpretable confidence intervals for measurements.[20] When such confidence intervals are placed on measurements, there can be little question as to the quality of data. In addition, the analysis required to determine these intervals can point out the steps in the calibration procedure to which data quality is most sensitive. Both accuracy and precision can affect the width of the confidence interval.

Air monitoring instrument inaccuracy (bias) results from three factors: (1) uncertainties in knowing the concentrations of gas used for calibration, (2) long-term time drift, or (3) interferences. On the other hand, precision is an inherent instrument characteristic, unaffected by these factors.

The variation of instrument readings due to imprecision can be estimated by letting an instrument read a stable source for some time. The variation due to bias can be estimated by analyzing the sources of errors, especially calibration.

Ozone Instrument Calibration--An analysis of O_3 instrument calibration led to the following formula for the confidence interval on the concentration measured by NBKI with a weighted regression I_2 standard curve:

$$[L,U] = \bar{y}_p \pm t_{(1-\alpha/2)\,(n-1)} \left[\frac{\mathrm{var}(\bar{y}_p)}{k} + S_e^2 \, \frac{\bar{x}_a^2}{\sum_{i=1}^{n} x_i} \right]^{1/2}$$

where

$$S_e^2 = \frac{1}{n-1} \sum_{i=1}^{n} \frac{(y_i - y_{pi})^2}{x_i};$$

$\bar{y}_p$ is the amount of ozone collected (pphm-liters) corresponding to an absorbance reading $\bar{x}$; $\bar{x}_a$ is the mean of absorbances from k NBKI bubbler samples at some ozone generation setting (absorbance units); var (y_p) is the variance associated with absorbing ozone from a constant source $(\text{pphm-liters})^2$; x_i is an absorbance measurement from the standard I_2 curve determination; y_i is an equivalent ozone-absorbed value from standard curve determination corresponding to x_i; n is the number of (x_i, y_i) points from the standard curve determination; t is Student's t statistic; y_{pi} is the estimated equivalent ozone collected from the standard I_2 curve corresponding to x_i.

If simple linear regression has been used to obtain a standard I_2 curve, the following equation should be used in lieu of the preceding equation.

$$[L,U] = \bar{y}_p \pm t_{(1-\alpha/2)\,(n-2)} \left\{ \frac{\mathrm{var}(\bar{y}_p)}{k} + S_e^2 \left[\frac{1}{n} + \frac{(\bar{x}_a - \bar{x})^2}{\sum_{i=1}^{n} (x_i - \bar{x})^2} \right] \right\}^{1/2}$$

where

$$S_e^2 = \frac{1}{n-2} \sum_{i=1}^{n} (y_i \; y_{pi})^2$$

and $\bar{x}$ is the mean of all the absorbances used to determine the standard I_2 curve.

These equations reflect uncertainties in knowing the concentration of ozone to which an instrument is calibrated. Thus, these equations can serve as a confidence interval on measurements made with an ozone instrument at the concentration to which it was calibrated. Table 10 shows 95 percent confidence intervals on measurements made at an ozone concentration of 8 pphm (the Federal air quality standard) after calibrating at that concentration. The best case and worst case values are presented since $var(y_p)$ was not known exactly. In the worst case, it equaled 6.75 (pphm-liters)^2, and in the best case, 0.69 (pphm-liters)^2. The tightening of the confidence interval with increased replication of NBKI bubbler samples is obvious.

Table 10. CONFIDENCE INTERVAL ON BIAS IN MEASURING OZONE AT THE FEDERAL AIR QUALITY STANDARD WITH A CHEMILUMINESCENT INSTRUMENT CALIBRATED BY REPLICATED NBKI MEASUREMENTS

Number of replicates	Confidence intervals, pphm	
	Best case	Worst case
1	8 ± 1.4	8 ± 4.4
2	8 ± 1.1	8 ± 3.1
4	8 ± 0.83	8 ± 2.2
6	8 ± 0.73	8 ± 1.8
8	8 ± 0.68	8 ± 1.6

After calibration, the relative error due to bias is constant throughout the linear range of the instrument. If an instrument is calibrated so that the output, O_c, corresponds to the estimated concentration C_c, then the confidence interval on a new concentration measurement with an output O_n is given by the expression

$$[U,L] = \left[\frac{U_c}{O_c} O_n, \frac{L_c}{O_c} O_n\right]$$

where U_c and L_c define the confidence interval on C_c.

The effect of instrument noise on the confidence interval was neglected in this case since the instrument's precision was quite good.

Recommendations--The manner in which precision and accuracy affect the statistical properties of the measurement is rather complex and more work is needed in this area before a confidence interval can be specified for all instrumental measurements. Also, the problem of measuring concentrations in the part-per-billion range plunges measurement further into the realm of statistics.

The nature of this work is such that a group effort is not appropriate. I do suggest, however, that EPA encourage individual researchers with interests in instrumentation and statistics to pursue this problem.

Measures of Reactivity

In addition to assuring and quantitating data quality from smog chambers, we are concerned that data from different smog chambers be comparable, or at least, that differences between chambers be known explicity. The effects of chamber design have already been discussed. Consideration of these effects, as well as routine data analysis, makes use of measures of reactivity which require mathematical definition. Perhaps the most important measure is that of light intensity.

Light Intensity--The pseudo-first-order rate constant of NO_2 disappearance, k_d, has been used in the past as a measure of light intensity. Even now there is some disagreement as to just what is meant by k_d:

$$k_d = \frac{1}{t} \ln \frac{(NO_2)i}{(NO_2)f} \qquad \text{Reference 21}$$

$$k_d = \frac{d \ln [NO_2]}{dt} \qquad \text{Reference 22}$$

$$k_d = \lim_{t \to 0} -\frac{d \ln [NO_2]}{dt} \qquad \text{References 23,24}$$

There are several similar definitions. It has been pointed out by several investigators that k_d is a function of irradiation time; and it is possiblly a function of initial NO_2, NO, and O_2.

Thus, the measure that should be used is ϕk_a, also called k_1, the true rate constant of NO_2 photolysis. Several techniques have appeared in the literature in the past 2 years for measuring k_1, both in an inert gas and in air.

The following equation was presented by Holmes et al.[23] for calculating k_1 from photolysis in N_2 at very low levels of O_2, say less than 1000 ppm, and low initial NO. Rate constants refer to reactions in Table 11.

$$k_1 = \frac{1}{2\Delta t}\left[\left(1.0 + \frac{k_{21}}{k_9} - \frac{k_{20}}{k_9}\right)\ln\frac{[NO_2]_o}{[NO_2]} + \frac{k_{20}}{k_9}\left(\frac{[NO_2]_o}{[NO_2]} - 1\right) + \left(\frac{k_{20}}{k_9}[NO] + \frac{k_2}{k_9}[O_2]\right)\left(\frac{[NO_2]_o - [NO_2]}{[NO_2]_o [NO_2]}\right)\right]$$

Table 11. INORGANIC REACTIONS OF PHOTOCHEMICAL SMOG FORMATION

1.	$NO_2 + h\nu$	→	$NO + O$
2.	$O + O_2(+M)$	→	$O_3(+M)$
3.	$O_3 + NO$	→	$NO_2 + O_2$
4.	$O_3 + NO_2$	→	$NO_3 + O_2$
5.	$NO_2 + NO_3$	→	N_2O_5
6.	N_2O_5	→	$NO_2 + NO_3$
7.	$N_2O_5 + H_2O$	→	$2HNO_3$
8.	$NO_2 + NO_3$	→	$NO + NO_2 + O_2$
9.	$O + NO_2$	→	$NO + O_2$
10.	$NO + NO_3$	→	$2NO_2$
11.	$NO + NO_2 + H_2O$	→	$2HNO_2$
12.	$HNO_2 + h\nu$	→	$NO + OH\cdot$
13.	$CO + OH\cdot$	→	$CO_2 + H\cdot$
14.	$H\cdot + O_2(+M)$	→	$HO_2\cdot(+M)$
15.	$HO_2\cdot + NO$	→	$NO_2 + OH\cdot$
16.	$HO_2\cdot + NO_2$	→	$HNO_2 + O_2$
17.	$OH\cdot + NO_2(+M)$	→	$HNO_3(+M)$
18.	$OH\cdot + NO$	→	$HONO$
19.	$HO_2\cdot + HO_2\cdot$	→	$H_2O_2 + O_2$
20.	$O + NO(+M)$	→	$NO_2(+M)$
21.	$O + NO_2(+M)$	→	$NO_3(+M)$
22.	$2NO + O_2$	→	$2NO_2$
23.	$2HNO_2$	→	$NO + NO_2 + H_2O$
24.	$H_2O_2 + h\nu$	→	$2OH$
25.	$NO + HNO_3$	→	$HNO_2 + NO_2$
26.	$HNO_2 + HNO_3$	→	$2NO_2 + H_2O$

Simulations at UNC by Joe Sickles suggest that the assumptions of this approach are valid between 1 minute and 10 minutes after the start of irradiation.

The equation, presented by Stedman and Niki[22]

$$k_d = 2K_1 k_9/(k_9 + k_{21})$$

makes the assumptions of photostationary state (PSS) for O, O_3, NO_3, and N_2O_5, and also that no NO or O_2 is present. These assumptions appear to be somewhat contradictory. Sickles' simulation results indicate that PSS is not established until about 30 seconds after the beginning of irradiation, but after this time some reactions of NO and O_2 cannot be neglected.

The problems of k_1 determinations in N_2 are that (1) it may be difficult or extremely expensive to get such low O_2 concentrations in some chambers, or in bags, and (2) it is hard to measure these low O_2 concentrations.

The following two equations were used by Stedman and Niki[22] for determining k_1 in air.

$$-\frac{d[NO_2]}{dt} = \frac{d[NO]}{dt} = \frac{d[O_3]}{dt} = k_1 [NO_2]$$

$$k_1 = \frac{k_3 [NO] [O_3]}{[NO_2]}$$

The upper equation is termed the direct measurement approach and is assumed to be valid up to 30 seconds. Sickles' results indicate this period may be considerably shorter, perhaps less than 5 seconds. An extremely fast instrument response is required for this determination.

The lower equation assumes PSS for ozone. A major problem here, as pointed out by Seinfeld et al.,[24] is that rather small changes in NO_2 levels must be measured. Also, errors in the concentrations of all three species in the equation contribute to errors in k_1.

Seinfeld et al.[24] suggest an alternative way of getting around this. Given a number of NO or NO_2 concentrations measured during the first minute or so, they solve their 11-reaction mechanism for k_1 by quasilinearization. This requires computerized calculations for each measurement.

An alternative that avoids many of the problems of the above approaches is described in a soon-to-be-published paper by Sickles and Jeffries[25] of UNC.

It was found that the mass-balance on NO_2 in a continuous-flow stirred-tank reactor could be solved analytically to yield the following equation for k_1 at steady-state:

$$k_1 = \frac{x}{2\tau}\left[\frac{1 + (k_{21}/k_9)}{1 - x} + \frac{k_{20}x}{k_9(1-x)^2}\right]$$

where τ is reactor residence time and x is the fractional conversion of NO_2

$$x = \frac{[NO_2]_{in} - [NO_2]_{out}}{[NO_2]_{in}}$$

Thus, one must know only the inlet and outlet NO_2 concentrations. In addition, this approach provides a continuous measure of k_1 whereas other techniques work on a batch principle.

Other Measures--Some other measures of reactivity, in addition to k_d, were defined by the CAPI-6 committee.[26] Many of these definitions are not applicable to all smog chamber data nor to the ambient air. Thus, they should be reevaluated so that all workers in the field use measures that facilitate interchamber comparisons.

An example of an ambiguous definition is that of NO_2 formation rate. CAPI-6[26] defines NO_2 formation rate as half the initial NO divided by the time to form an amount of NO_2 equal to one-half the initial NO. The broken line in Figure 29a shows such a rate on data from a typical indoor chamber. The slope of the NO_2 concentration line is quite close to the straight-line slope at any instant. Examining the data from a hypothetical run in a hypothetical outdoor smog chamber in Figure 29b, it will be noted that the instantaneous rate of NO_2 formation differs markedly from the straight-line slope. This is mainly a result of constantly increasing light intensity in the morning. The length of the initial period with zero light intensity is a function of injection time and sunrise--not a characteristic of system reactivity as we would like.

One means of avoiding this is to consider the maximum instantaneous rate instead of some average rate. The maximum rate is uniquely defined from nearly all NO_2 curves. It may be calculated by hand, or a computer can easily calculate and output the maximum rates.

Recommendations--This is one example, but it seems that the area of defining measures of reactivity needs more thought to assure the applicability of these measures to all situations. Smog chamber technology and applications have changed considerably since CAPI-6.[26] I would like to recommend that EPA sponsor a group whose task would be to arrive at a new standard set of reactivity measures. The use of standard definitions of these measures would greatly improve communications between those who collect data and those who use the data.

REFERENCES FOR CHAPTER 3

1. Saltzman, B.E. Modified Nitrogen Dioxide Reagent for Recording Air Analyzers. Anal. Chem. 32(1): 135, January 1960.

2. Wilson, D. and S. Kopczynski. J. Air Pollut. Contr. Ass. 18: 160, March 1968.

3. Fontijn, A., A.J. Sabadell, and R.J. Ronco. Homogeneous Chemiluminescent Measurement of Nitric Acid with Ozone. Anal. Chem. 42(6): 525, May 1970.

4. Hodgeson, J.A., R.E. Baumgardner, B.E. Martin, and K.A. Rehme. Stoichiometry in the Neutral Iodometric Procedure for Ozone by Gas-phase Titration with Nitric Oxide. Anal. Chem. 43(8): 1123, July 1971.

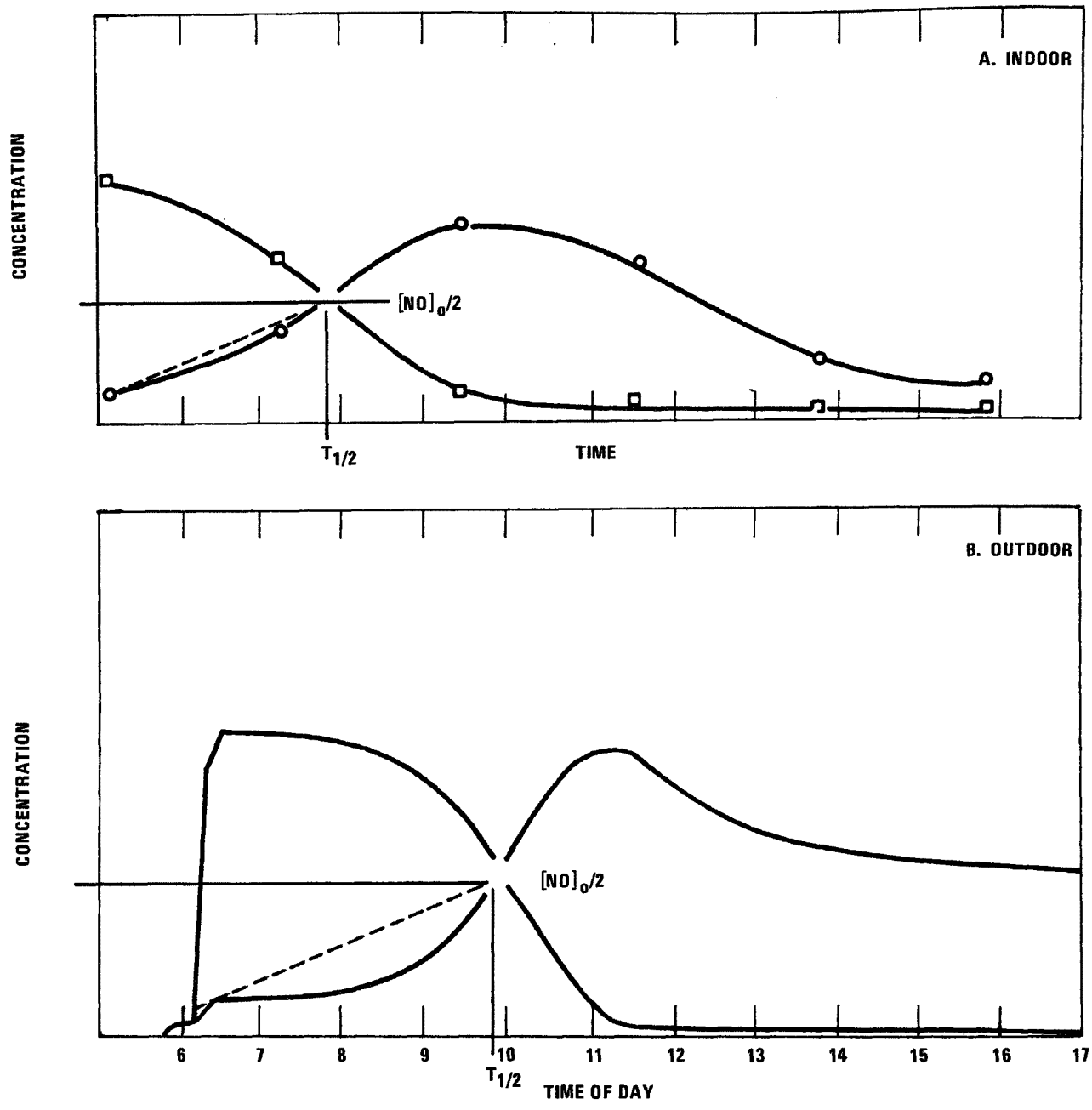

Figure 29. Comparison of typical reaction data for indoor and outdoor smog chambers.

5. Saltzman, B.E. Colorimetric Microdetermination of Nitrogen Dioxide in the Atmosphere. Anal. Chem. 26: 1949. December 1954.

6. Stevens, R.K., T. Clark, R. Baumgardner, and J.A. Hodgeson. Instrumentation for the Measurement of Nitrogen Dioxide. U.S. Environmental Protection Agency, Research Triangle Park, N. C. (Presented at American Society for Testing and Materials Symposium on Instrumentation for Monitoring Air Quality. Boulder. August 1973.)

7. Spincer, C.W. and D.F. Miller. Nitrogen Balance in Smog Chamber Studies. Battelle, Columbus, Ohio. (Presented at Annual Meeting of Air Pollution Control Association. Denver. June 1974.)

8. Environ. Sci. Technol. 8: 1118, December 1974.

9. Hanst, P.L., E.R. Stephens, and W.E. Scott. Reactions Involving Ozone, Nitrogen Dioxide, and Organic Compounds at Low Concentrations in Air. Proc. Air Pollut. Inst. 35(III): 175, 1955.

10. Stephens, E.R., P.L. Hanst, R.C. Doerr, and W.E. Scott. Reactions of Nitrogen Dioxide and Organic Compounds in Air. Ind. Eng. Chem. 48: 1498, 1956.

11. Stephens, E.R., W.E. Scott, P.L. Hanst, and R.C. Doerr. Recent Developments in the Study of the Organic Chemistry of the Atmosphere. J. Air Pollut. Contr. Ass. 6: 159, 1956.

12. Scott, W.E., E.R. Stephens, P.L. Hanst, and R.C. Doerr. Further Developments in the Chemistry of the Atmosphere. Proc. Air Pollut. Inst. 37(III): 171, 1957.

13. White, J.U. Long Optical Paths of Large Aperture. J. Opt. Soc. Amer. 32: 285, 1942.

14. Hanst, P.L. Spectroscopic Methods for Air Pollution Measurement. In: Advances in Environmental Science and Technology. J.N. Pitts and R.L. Metcalf (ed.). New York, John Wiley and Sons, Inc., 1971.

15. Hanst, P.L., A.S. Lejohn, and B.W. Gay, Jr. Detection of Atmospheric Pollutants at Parts-per-billion Levels by Infared Spectroscopy. Appl. Spectrosc. 27: 188, 1973.

16. Bertolacini, R.J. and J.E. Barney. Anal. Chem. 29: 281, February 1957.

17. Schafer, H.N.S. Anal. Chem. 39: 1719, December 1967.

18. Leithe, W. The Analysis of Air Pollutants. Ann Arbor, Humphrey Science Publisher, 1970.

19. West, P.W., A.D. Shendrikar, and N. Herrara. Determination of Sulfuric Acid Aerosols. Anal. Chem. Acta. 69: 11, 1974.

20. Feigley, C.E. Some Statistical Aspects of Air Monitoring Instrument Calibration. University of North Carolina, Chapel Hill, N. C. (Presented at Air Pollution Control Association National Meeting. Denver. June 1974. APCA No. 74-14.)

21. Tuesday, C.S. Chemical Reactions in the Lower and Upper Atmosphere. R.D. Cadle (ed.). New York, Interscience, 1961. p. 15-49.

22. Stedman, D.H. and H. Niki. Photolysis of NO_2 in Air as Measurement Method for Light Intensity. Environ. Sci. Technol. 7(8): 735-740, August 1973.

23. Holmes, J.R. et al. Measurement of Ultraviolet Radiation Intensity in Photochemical Smog Studies. Environ. Sci. Technol. 7(6): 519-523, June 1973.

24. Seinfeld, J.H., T.A. Hecht, and P.M. Roth. Existing Needs in the Experimental and Observational Study of Atmospheric Chemical Reaction. U.S. Environmental Protection Agency. Research Triangle Park, N. C. Publication No. EPA-R4-73-031. June 1973.

25. Sickles, J. and H.E. Jeffries. Continuous Chemical Actinometer Using NO_2. University of North Carolina, Chapel Hill, N. C. (In press.)

26. Jaffe, R.J., F.C. Smith, and K.W. Last. Study of Factors Affecting Reactions in Environmental Chambers; Final Report on Phase III. Lockheed Missiles and Space Co., Inc., Sunnyvale, Ca. 1975.

4. BACKGROUND REACTIVITY

INTERPRETATION OF BACKGROUND REACTIVITY DATA

– B. Dimitriades, EPA

Traditionally background reactivity was determined and expressed based on the following tests:

1. Ozone Formation Test: Background air is irradiated and O_3 formation is measured and followed.
2. R_{NO_2}-Test: Background air and added NO are irradiated and rate of NO_2 formation (R_{NO_2}) is measured.
3. Aerosol Formation Test: Background air is irradiated and aerosol formation is measured and followed.
4. SO_2 Oxidation Test: Background air and added SO_2 are irradiated and loss of SO_2 (and formation of SO_4^{2-}) is measured and followed.

In addition to these commonly used tests, some chamber operators have also been conducting the following relevant tests:

1. Ozone Loss Test: Ozone loss in the chamber is measured in the dark and under irradiation.
2. NO_2 Loss Test: NO_2 loss in the chamber is measured in the dark and under irradiation.
3. Propylene Loss Test: Background air and added propylene are irradiated and loss of propylene and formation of products are measured and followed.

Experiences from such tests with existing chambers and some interpretations and use of resultant data are as follows:

Ozone formation tests have shown that all large chambers, regardless of degree of cleanness, form up to 0.2 ppm of "oxidant" (as measured by KI). Chambers with barely detectable levels of HC and NO_x contaminants also form 0.03 to 0.05 ppm oxidant. It is submitted here that such oxidant is a result of photochemical reactions of HC and NO_x, and its concentration depends mainly on the HC and NO_x concentrations and their ratio, however small these concentrations may be. Because of the ratio effect, this test has little value as an index of chamber contamination. Nevertheless, if contaminants are removed completely, to the point of no detection, then O_3 formation does not exceed 0.035 ppm. This has been demonstrated repeatedly in EPA tests using a 400-liter Pyrex glass chamber.

R_{NO_2}-tests have given results ranging form 2 to 12 times the thermal rate of NO oxidation in air. It is submitted here that such accelerated oxidation of the NO is caused mainly by photochemical reactions involving organic contaminants (surface may also have a role). This test, therefore, is a more valid index of organic contamination in chamber and/or background air.

Aerosol formation tests have shown that condensation nuclei form at levels depending on contamination level. It is not clear as to what the relative contributions of the organic, NO_x, and SO_2 contaminants are to the measured total. In the absence of measurable levels of contaminants, virtually no aerosol can be measured in the chamber. In general, no light scattering aerosol forms from irradiation of reasonably cleaned air and chamber.

SO_2 oxidation tests have given results ranging from 0.05 to 5 percent per hour--a serious inconsistency. While contaminants have been shown to accelerate SO_2 oxidation, there is also evidence that heterogeneous reactions or "third body" effects of surface have a role. Thus, the lowest SO_2 oxidation rate values were obtained with chamber walls that had been preconditioned. The question of what causes the variation in SO_2 photooxidation rate in "clean" air is still an open one.

Ozone loss, in the dark, has been found to be negligibly small in all chambers of 100 ft^3 or greater size. Generally, with an initial concentration of 1 ppm, half life of O_3 ranges from 10 to 40 hours. Under irradiation, ozone loss in the chamber is accelerated considerably. Many investigators have attributed the accelerative effect of radiation to enhanced contact of O_3 with the chamber walls. It is submitted here that the radiation effect upon O_3 loss is the result of photochemical reactions involving chamber contaminants. The questions to be asked here are whether this explanation is correct, and whether these reactions have a role in the mechanism of the O_3 formation and O_3 decay processes (these reactions, for example, may account for the O_3 decline following the O_3 peak in irradiated HC-NO_x systems).

The NO_2 loss tests have not yielded any revealing information. Under irradiation, NO_2 disappears slowly, presumably as a result of oxidation into nitric acid.

The propylene loss tests have shown that propylene disappears suprisingly fast when irradiated in "pure" air (in the absency of injected NO_x). Thus, in 6 hours of irradiation, propylene consumption ranged from 30 to 80 percent. The consumption reaction is probably initiated by the same chamber contaminant reactions that cause O_3 formation in "pure" air; aldehyde products could instigate additional photochemical activity resulting in propylene comsumption.

Overall conclusions and implications arising form this background reactivity evidence are as follows:

Background contaminants, that is, organic and inorganic vapors at subtrace levels, can cause reactivity manifestations of appreciable intensity. This obviously is

important from a control standpoint. The evidence suggests that O_3 levels comparable to the O_3 standard can be caused by precursor concentrations lower than those of the present precursor (air quality) standards. Further, the evidence suggests that for such extremely low concentration systems, the role of NO_x may be much more important -- relative to the role of HC--than in the higher concentration systems. Such evidence is not inconsistent with real atmospheric observations. Ozone levels are low in source-free rural areas perhaps because the NO_x level is extremely low. With higher NO_x levels (as, for example, in mixtures of natural and anthropogenic emissions) that optimize the HC/NO_x ratio, O_3 could form at significant levels. This is one of the possible mechanisms explaining, partly at least, the high levels of O_3 formed in some nonurban atmospheres. This mechanism is being explored now by EPA. Limited initial data show that injection of NO_x in rural air can, indeed, result in increased O_3 yield upon irradiation.

Certain reactivity manifestations appear to be strongly affected by the surface factor. This is important in that it introduces a bias to the experimental study. Conditioning of the surface is acceptable as a solution to the problem, provided, however, that such conditioning does not create contamination problems. Since the surface to volume ratio in any one of the existing smog chambers is 2 to 3 orders of magnitide greater than the surface to volume ratio, for example, in Los Angeles air during the smog season (including porosity-related area of aerosol particles), it follows that increasing the size of the chamber beyond, say, 1000 ft^3 will not solve the surface effect problem. Note, however, that this is a problem only when the chamber is used to study atmospheric photochemistry. For study of $O_x/HC/NO_x$ relationships at ground level, the surface to volume ratios in chamber and real atmosphere may be comparable.

DISCUSSION

Dr. E. R. Stephens (UCR, SAPRC) suggested that PAN formation be used as an index of chamber background contamination. The advantages of this index over "ozone formation" are that PAN can be detected at concentrations as low as 0.1 ppb, and that presence of PAN is an unequivocal proof of presence of both HC and NO_x contaminants.

Dr. T. A. Hecht (SAI) reported on some recent modeling efforts to investigate the causes of O_3 decay in a smog chamber, in the dark and under irradiation. Dr. Hecht's report was as follows:

Scientists have shown that the surface-to-volume ratio and surface materials of a smog chamber influence the overall chemical process observed.[1] The detailed nature and magnitude of the effects of surfaces on the kinetics, however, are poorly understood. The only wall reaction that has been considered extensively is the heterogeneous decomposition of O_3 (see references in Seinfeld et al.),[1] which can be represented as

$$O_3 \xrightarrow{k_{O_3}} \text{Wall}$$

Scientists at UCR have carried out several ozone decay experiments to determine k_{O_3} in their evacuable cylindrical chamber. The chamber was prepared for a "k_{O_3} experiment"

in the following manner. First, the reactor was pumped to a few microns of mercury pressure. Air containing about 1 ppm of O_3 was then rapidly introduced into the chamber, and a total pressure of 1 atmosphere was achieved through the addition of pure air. Subsequently, the time required for one half of the ozone to be consumed in the dark was determined. The half-life was found to be about 8.35 hours.

If we assume that the loss of O_3 during a decay experiment is attributable entirely to the reaction on the walls, the rate of O_3 decay is given by

$$\frac{dO_3}{dt} = -k_{O_3}[O_3]$$

The half-life of O_3 is related to the O_3 decay constant as

$$k_{O_3} = \frac{0.693}{\gamma_{1/2}}$$

from which we calculate that $k_{O_3} = 0.0014\ min^{-1}$. This value indicates, for example, that the rate of O_3 loss to the walls will exceed the rate of loss due to reaction with propylene, should the concentration of C_3H_6 in the reactor be less than 0.08 ppm. (Two of the eight experiments in the propylene experimental block recently conducted under EPA sponsorship had an initial C_3H_6 concentration of 0.1 ppm.) Thus, the rate of O_3 decay in the UCR chamber is significant, and the O_3 wall loss reaction must be included in our simulations.

Ozone decay experiments were also performed under irradiated, rather than dark, conditions, and the O_3 half-life was found to be about 4.25 hours. We believe that this decrease in the O_3 half-life from that observed in a dark chamber may be due to a series of chemical reactions involving O_3, $O(^1D)$, H_2O, free radicals, and light, rather than any intrinsic change in the activity of the walls when the solar simulator (light source) is in operation. (The solar simulator is focused so that it does not shine directly on the cylindrical surfaces.)

We carried out a mathematical simulation of the August 15, 1973, light decay experiment, which was similar in all ways, except for the presence of light, to the dark decay experiments used to calculate k_{O_3} above. We assumed that the 13 reactions in Table 12--in addition to the wall reaction--participated in the total O_3 decay process.

The O_3 photolysis rates were based on the results of Demerjian et al.,[2] who calculated the photolysis rates of NO_2, O_3, and many other species for sunlight with $z = 45^o$. Under those conditions, they calculated that the photolysis constant for NO_2 was $0.48\ min^{-1}$. Since the rate of that reaction in the UCR chamber is $0.223\ min^{-1}$, we scaled Demerjian's O_3 photolysis constants by 0.223/0.48. We further assumed that the rate of H_2O_2 photolysis was 1/250 of the rate of NO_2 photolysis. This rate constant is quite uncertain; we found that this reaction can be eliminated from the mechanism without seriously affecting the reactions, and so the choice of this rate constant is not critical. The rate constants of the other reactions are based on the recommended values of Garvin and Hampson[3] and Demerjian et al.[2]

Table 12. REACTIONS PARTICIPATING IN THE TOTAL OZONE DECAY PROCESS

Number	Reaction	Rate constant[a]
1	$O_3 \rightarrow$ Wall	1.38×10^{-3} min^{-1}
2	$O_3 + h\nu \rightarrow O(^1D) + O_2$	1.58×10^{-3} min^{-1}
3	$O_3 + h\nu \rightarrow O(^3P) + O_2$	9.76×10^{-3} min^{-1}
4	$O(^1D) + M \rightarrow O(^3P) + M$	8.70×10^{4}
5	$O(^3P) + O_2 + M \rightarrow O_3 + M$	2.00×10^{-5} ppm^{-2} min^{-1}
6	$O(^1D) + O_3 \rightarrow 2O_2$	9.80×10^{4}
7	$O(^1D) + H_2O \rightarrow 2OH$	5.25×10^{5}
8	$OH + O_3 \rightarrow HO_2 + O_2$	8.60×10^{1}
9	$HO_2 + O_3 \rightarrow OH + 2O_2$	2.40
10	$HO_2 + HO_2 \rightarrow H_2O_2 + O_2$	8.40×10^{3}
11	$H_2O_2 + h\nu \rightarrow 2OH$	8.90×10^{-4} min^{-1}
12	$OH + OH + H_2O \rightarrow H_2O_2 + H_2O$	3.25×10^{-1} ppm^{-2} min^{-1}
13	$OH + OH + M \rightarrow H_2O_2 + M$	6.50×10^{-2} ppm^{-2} min^{-1}

[a] In units of ppm^{-1} min^{-1} unless otherwise indicated.

Integrating the mechanism in Table 12 and using the initial conditions for the experiment ($[O_3]_o = 1.15$ ppm, $[H_2] = 2.0 \times 10^4$ ppm, $[O_2] = 2.0 \times 10^5$ ppm, and $[M] = 1.0 \times 10^6$ ppm) resulted in a predicted O_3 half-life of 4.48 hours. The observed half-life for this particular experiment was 4.35 + 0.09 hours.

The results of this exercise are consistent with two tentative conclusions. First, the "true" O_3 wall decay constant appears to be that measured in the dark, rather than in the illuminated decay experiments. Second, the O_3 photolysis reactions, which initiate reactions such as $O(^1D) + H_2O$, are an important sink for O_3 and should be considered in future smog chamber simulations.

REFERENCES FOR CHAPTER 4

1. Seinfeld, J.H., T.A. Hecht, and P.M. Roth. Existing Needs in the Experimental and Observational Study of Atmospheric Chemical Reactions: A Recommendations Report. U.S. Environmental Protection Agency. Research Triangle Park, N.C. Report No. EPA-R4-73-031. 1973.

2. Demerjian, K.L., J.A. Kerr, and J.G. Calvert. The Mechanism of Photochemical Smog Formation. In: Advances in Environmental Science and Technology (Vol. 4). J.N. Pitts and R.L. Metcalf (ed.). New York, John Wiley and Sons, 1974. p. 1-262.

3. Chemical Kinetics Data Survey VII; Tables of Rate and Photochemical Data for Modelling the Stratosphere. D. Garvin and R.F. Hampson (ed.). National Bureau of Standards. Washington, D.C. Report No. NBSIR 74-430. January 1974.

5. COMPARABILITY OF SMOG CHAMBER ATMOSPHERE AND REAL ATMOSPHERE

A METHOD FOR COMPARING SMOG CHAMBER DATA WITH ATMOSPHERIC DATA-- *E.R. Stephens, SAPC, URC*

Ozone is considered to be the major health hazard in photochemical smog, and so control strategies have been directed toward reducing ozone exposures to acceptable levels. This toxic compound is a product of a very complex reaction of primary pollutants (hydrocarbons and nitrogen oxides), which are not themselves highly toxic. A new project has been initiated at UCR to develop, demonstrate, and use methods for the study of polluted air that will help clarify this complex relationship between oxidant and oxidant precursors. Understanding of this relationship is vital to sound development of control strategy, air quality standards, and emission standards.

Emission standards for hydrocarbons and nitrogen oxides cannot be independent because of the complex atmospheric interaction to produce ozone, which is affected by sunlight intensity and time available for reaction. Laboratory irradiation chamber data (for example, Reference 1) have been used to estimate emission standards[2] needed to meet air quality standards. On the other hand, ambient air data form the basis of the EPA recommended oxidant abatement strategy.[3] Both approaches have been subject to criticism. Anyone who has tried to use either approach will recognize that much of the criticism is valid. The proposed project has as its primary objective the development of new approaches to the use of ambient air quality data for the study of oxidant/precursor relationships. This is proposed as an adjunct to the study of oxidant/precursor relationships in smog chambers or with computer models rather than a substitute--a kind of "ground truth." If these three approaches can be reconciled with each other so that one control strategy emerges, we will be in a far stronger position than if only one or two of these methods are used. The various procedures used to estimate the degree of control required for auto emissions give answers varying between 90 and 97 percent or even more.[2] While this may seem to be an acceptably narrow range, when translated into emission standards, it gives a variation in allowable emission of more than 3 to 1. This is far from trivial to the automotive engineer.

One of the principal weaknesses of the oxidant/precursor relationship as derived from ambient air data in the Air Quality document[3] is that oxidant and precursor are measured on two different parcels of air. Precursors are at a maximum in the 6 to 9 a.m. hours, while oxidant maximum occurs at noon or later and often in a different place.

The assumption that the measured oxidant is produced by the measured early morning HC/NO_x is especially serious when you think of the use to which these curves (scatter patterns) have been put. One draws a boundary around the scatter pattern and extrapolates to the oxidant air quality standard. The position of the boundary is determined by those few points at the lowest values of HC/NO_x and oxidant. These are also the points most subject to error because of their small values. The nonmethane hydrocarbon (NMHC)

is especially vulnerable if it is estimated by subtracting methane from total hydrocarbon. What is needed is a way to estimate the NMHC and NO_x that correspond to the oxidant measured at some particular time and place. A method for back extrapolation in time for an air parcel that has had a chance to react and develop maximum oxidant is also required. This involves estimation of the amount of hydrocarbons that have reacted to provide a better comparison with chamber data then the data so far used. For back extrapolation of hydrocarbon values, we proposed to extend the procedures first used and described in Reference 4.

In that paper the relative amounts of three hydrocarbons of widely differing reactivity (acetylene, ethene, and propene) were used to estimate that a Riverside smog has been photoreacted for about 6 to 8 hours. This estimate was then combined with data on photolysis of ambient air to estimate that about one-third of the NMHC had reacted.

To back extrapolate the NO_x to zero time, the use of a chemiluminescent analyzer is proposed. This can be done by taking advantage of one weakness of this method. This weakness is the fact that the catalysts reduce not only NO_2 but PAN and probably nitrate to NO. The instrument, therefore, probably in the NO_x mode, gives a good measure of the initial oxides of nitrogen. Catalytic reduction then constitutes back extrapolation.

Sampling and Data Collection

The hydrocarbon analysis reported in the previously cited reference[4] was carried out opportunistically, sporadically, and manually. No paraffins higher than C_6 nor olefins higher than C_5 were measured. It was, therefore, necessary to estimate the higher molecular weight hydrocarbons. It is proposed in the new project to monitor methane, the three C_2 hydrocarbons, and nonmethane hydrocarbons by a gas chromatographic procedure using direct sample injection followed by back flush. This will also permit unattended operation. A considerable part of this method has already been demonstrated. A recent report from this laboratory[5] describes a flame ionization chromatograph that will give about 0.5 mm/ppb peak height for the C_2 hydrocarbons with direct injection of 3.2 ml of air sample. Less than 5 ppb would be detectable and 20 ppb of each C_2 would be readily measurable.

Another instrument has been automated for this same procedure. To keep the methane peak on scale, this instrument was operated at high attenuation. Even under these conditions the C_2s in ambient air were readily visible. There is such a large disparity between the concentrations of methane and the C_2s that measurement of these on the same attenuation is not practical. This procedure is now being extended by back-flushing the remainder of the hydrocarbons after elution of methane and the C_2s. An important advantage is that C^{3+} hydrocarbons are measured directly and not by difference between total hydrocarbon and methane. This chromatograph will give five pieces of data: methane, ethane, ethene, acetylene, and C^{3+} hydrocarbons. An early chromatogram is shown in Figure 30. The ethene/acetylene ratio will be used as an index of degree of reaction.

The fourth measurement will be ultraviolet intensity. For this project, no attempt will be made to make quantitative, calibrated measurements of ultraviolet intensity. Both

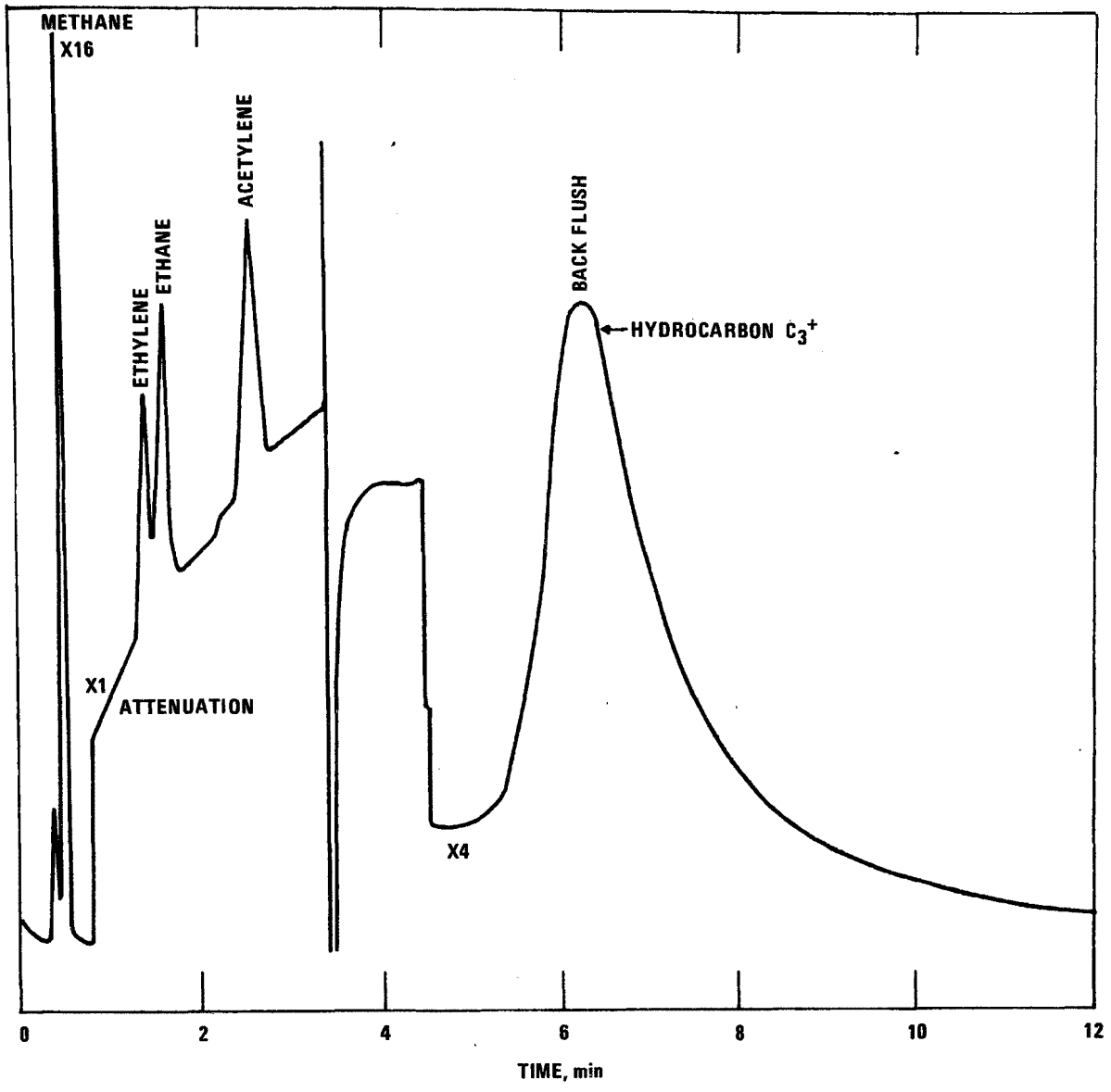

Figure 30. Injection and back flush of ambient air sample.

integrated and instantaneous values of relative intensities will be used to judge whether lack of ultraviolet radiation can, in any given case, explain a low oxidant value.

Data from these four monitoring instruments (see Table 13), which will be set up on the UCR campus, will be reviewed for degree of reaction (as judged by ethylene/acetylene ratio) and adequacy of sunlight. For those cases that show a substantial degree of reaction and substantial sunlight, the oxidant will be plotted as a contour against NMHC and NO_x (back extrapolated as described).

Several "bonus" benefits may well be derived from the present project. It will be possible to study the variation in NMHC/NO_x with time, degree of reaction, and atmospheric conditions. It can be argued that the ratio in a community inventory should be roughly constant from day to day and that major social changes would be required to change this ratio.

Table 13. SUMMARY OF MEASUREMENTS TO BE MADE AT UNIVERSITY OF CALIFORNIA, RIVERSIDE (All on a Continuous or Automatic Basis)

Measurement	Measurement method
Hydrocarbon	Gas chromatography with flame ionization. Direct injection measurement of methane, ethane, ethene, acetylene, and C_3^+ hydrocarbons (by back flush).
Nitrogen oxides	Ozone chemiluminescence. This will measure NO and NO_x and the latter will be taken to be total oxidized nitrogen.
Oxidant	Coulometric KI method.
UV intensity	Recording of UV meter.

It would be helpful to know if control strategies should take into account large random fluctuations in this ratio. It could make a substantial difference in standards. Comparisons of the average ratio in reacted and unreacted mixtures will be a useful corroboration of our back extrapolation procedures. The data will permit comparison of methane with higher hydrocarbons to see if the former constitute a constant fraction of the total. Methane may form a useful index of effective trapping of pollutants, since it is inert, emitted in large quantities, and easy to measure. It will be interesting to see if photochemical smog itself significantly reduces ground level ultraviolet radiation.

Discussion

In response to several questions from the audience, Dr. Stephens explained further his method for estimating the HC concentrations responsible for the oxidant observed in ambient air. The method is based on the diagrams of Figure 31, depicting expected changes in the relative levels of ethylene, propylene, and acetylene in an air sample as the sample is irradiated by sunlight. The diagrams of Figure 31 were based on experimental measurements as well as on certain assumptions. Thus, analyses of morning air were used to establish the relative levels of ethylene, propylene, and acetylene in the unreacted air sample (point at 0 hours in Figure 31). Changes in the three-component mixture with irradiation time were calculated assuming "batch reactor" and "stirred flow reactor" kinetics, and using first-order reaction rate constants determined experimentally by irradiation of morning air. For application of the method, an afternoon sample of air is analyzed for hydrocarbons. The relative levels of ethylene, propylene, and acetylene are compared with Figure 31 to estimate extent of reaction in terms of hours of irradiation. Using then the first order rate constant for acetylene and assuming stirred flow reactor kinetics, the concentration of acetylene at zero reaction time is estimated by back extrapolation. The zero-time concentrations of the other hydrocarbons are then estimated using first order rate constants derived from ambient air irradiation experiments to back extrapolate to zero time.

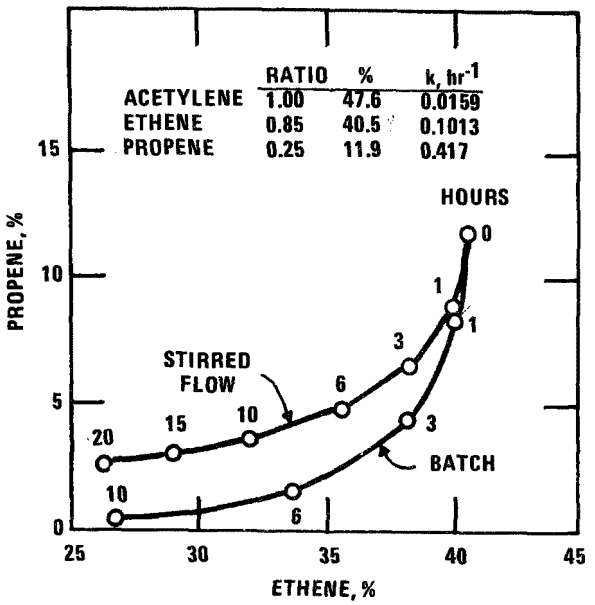

Figure 31. Ambient air photolysis. (Ethane + propene + acetylene = 100%.)

STATIC AND DYNAMIC SMOG CHAMBER TESTS -- *L. Ripperton, RTI*

The ultimate or prime purpose of air pollution studies is to provide information that will aid in protecting the health and welfare of the breathing public, present and future--presumably the nonbreathing public has lost interest in the problem.

The purpose of the smog chamber studies is to characterize the behavior of polluted air and to obtain information that is of value in suggesting air pollution control tactics and strategy.

This presentation considers studies dealing with the atmospheric generation of ozone (O_3). These studies can be classified in several ways; one such classification system could contain two general components:

1. Characterization descriptive studies of chemical models of the existing atmosphere by variation of reactants, etc.
2. Studies designed to test the effects of possible control measures upon the O_3 dosage of the atmosphere, including studies to determine the worst possible conditions (i.e., maximum O_3) derivable from various concentrations and ratios of initial reactants.

The topic here is the dynamic operation of smog chambers. Nondynamic static studies are batch reaction systems with no more mass transfer in and out of the chamber than is necessary to sample and replace sample volume. "Dynamic" means moving or changing, not static.

In a dynamic chamber study the factors that are subjectable to the manipulation of the operator, once a general set of conditions has been initiated and a run started, are:

1. Temperature
2. Pressure
3. Light intensity
4. Dilution
   a. Timing (e.g., dilution starting at time = t proceeding at a rate of X % per unit time)
   b. Composition of diluent air
   c. Addition of more reactant without withdrawing chamber volume
   d. Pressure (only use is to simulate upward movement of air to strata aloft)

Temperature has an effect, but apparently this effect is caused by the maximum temperature. Figure 32 presents field data showing this effect. Dynamic temperature progression apparently has little effect. This is apparent in the data to be presented by Dr. Jeffries.

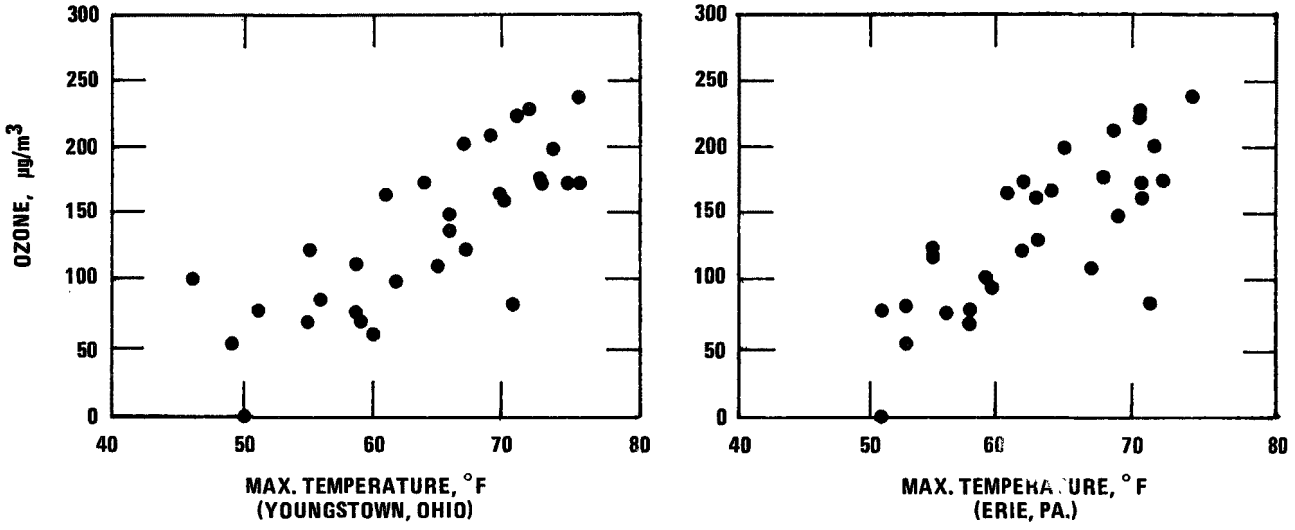

Figure 32. Maximum 4-hour-average ozone, Kane, Pennsylvania, versus maximum temperature at nearest reporting stations, October 1974.

Natural changes in light intensity, however, do have a significant effect on rates, peaks, concentrations, and time of occurrence of various events in the course of a chamber run. Again, this is evident in the data and simulations of Dr. Jeffries. This effect is to be expected on purely theoretical grounds. The actinic activity of light for CH_3CHO and NO_2 below 4000 Å varies by almost 14-fold from zenith angle Z = 40 to Z = 80 for acetaldehyde and about 5-fold for NO_2 from Z = 40 to Z = 80. The use of a single high intensity of light compresses the time span between events in the smog chamber and the use of a single low intensity can make these unrealistically drawn out.

Static studies have been used to understand the chemical relationship involved. In a sense, they are simpler because they are all chemistry. Meteorology and fluid dynamics have been removed from experimental conditions.

In order to get studies started and to gain an appreciation of the overall effect of the kinetic processes involved in photochemical air pollution systems, the batch study was the order of the day. In these studies, once initial concentrations of reactants were set, O_3 concentration was a function of photochemical primary and secondary reactions of fixed initial amounts and ratios of NO_x, organic vapors, etc. In the real atmosphere, the O_3 concentration in air following a trajectory is a function of photochemical primary and secondary reactions and thermal reactions involving precursors whose concentrations are affected not only by chemical reactions but by dilution and the behavior of primary sources. Even under "completely stagnant" conditions, the sources have a generally cyclic behavior and the effective volume is changed by the varying depth of the mixing layer.

For characterizing the real atmosphere, the operation of the chamber should follow a physical model. That model should provide simulation of a real set of circumstances. Ideally, it should approximate the content of the real atmosphere both as to kinds of pollutants and their concentrations and ratios and it should approximate the injection rate of new material and the dilution of the original volume. The part of the physical model describing the dilution should be worked out with or developed by a meteorologist. That dilution has an effect on absolute O_3 concentration achieved is shown by the UNC chamber data shown in Figures 33 and 34.

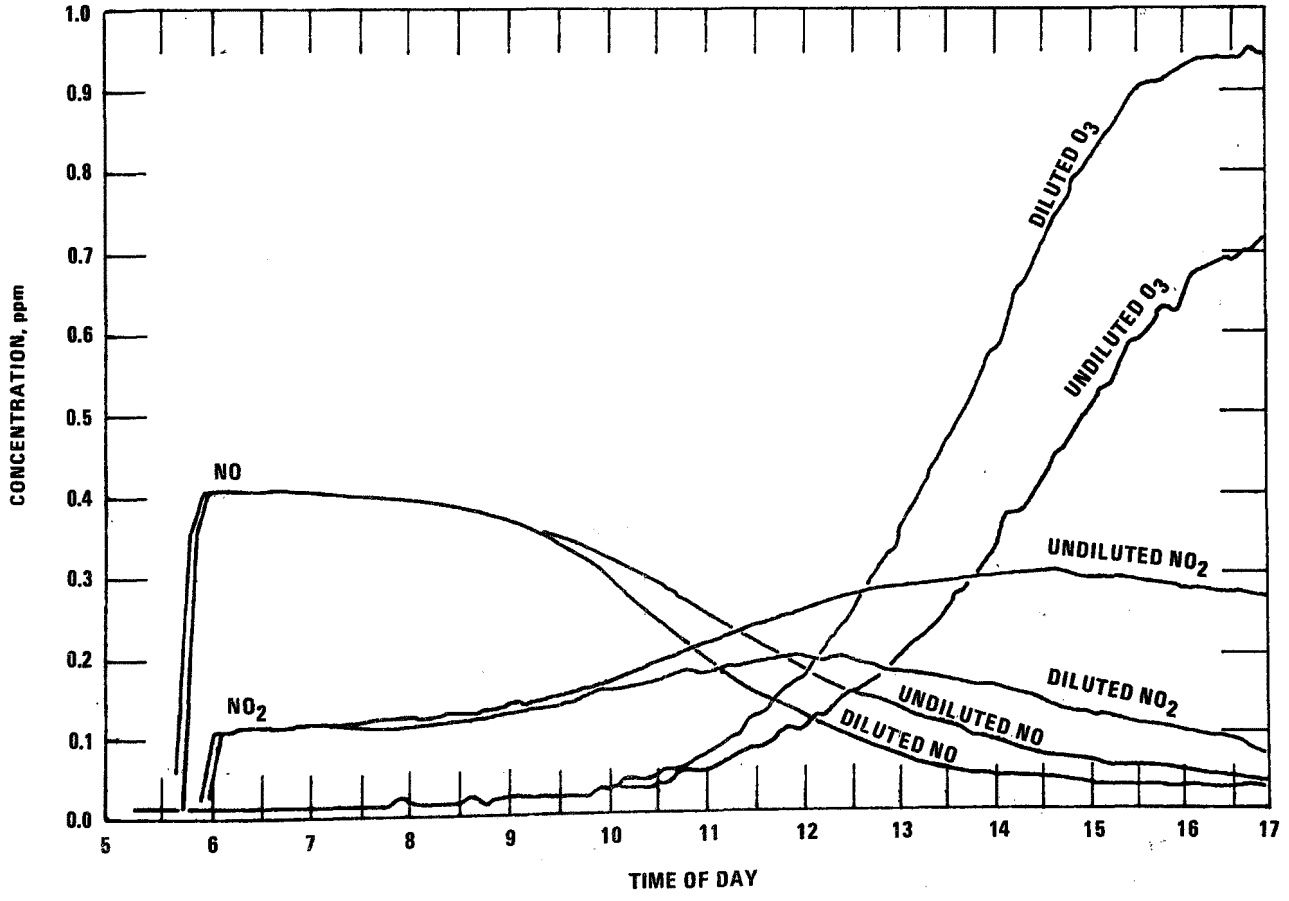

Figure 33. Effect on ozone generation by dilution of reactants: NO, NO_2, and O_3, October 7, 1974.

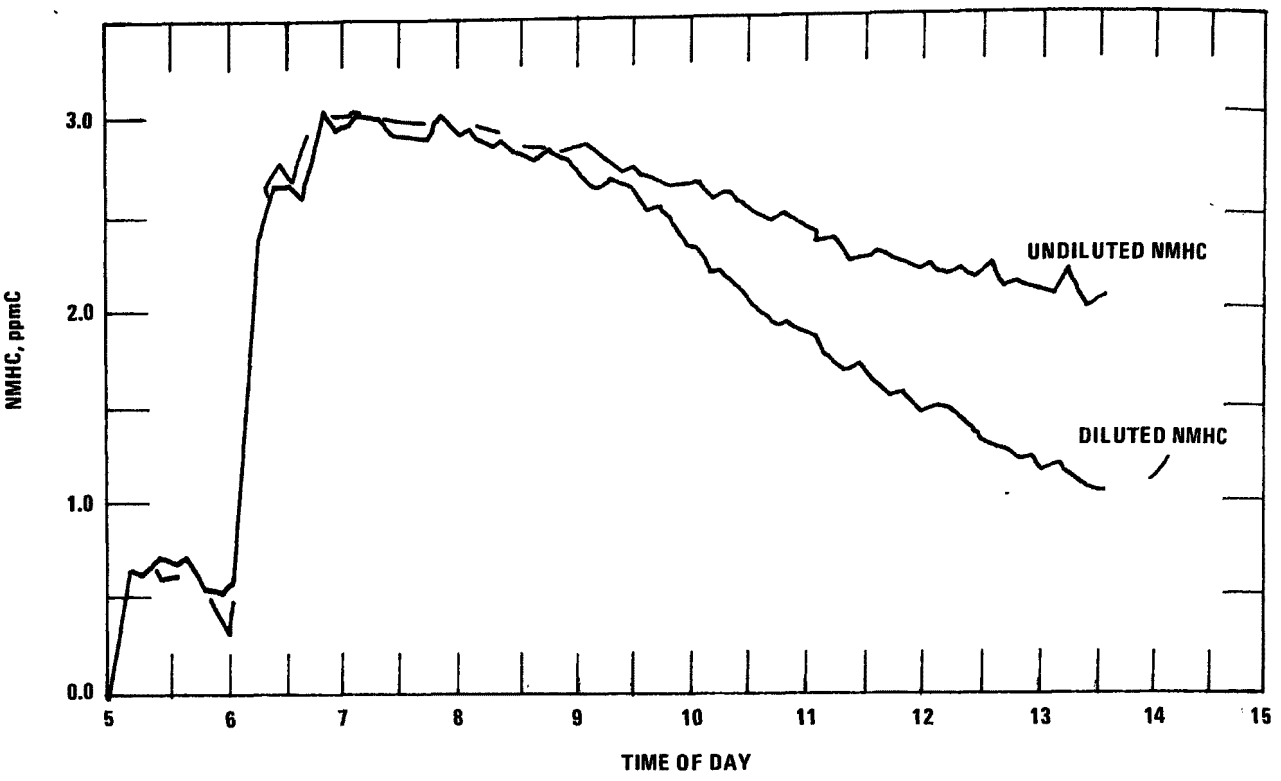

Figure 34. Effect of reaction and dilution on a simulated urban mix of hydrocarbons, October 7, 1974.

Let us look at three kinds of dynamic situations and suggest ways of dynamic simulations:

1. A stagnant situation where there is virtually no dilution but that due to increased mixing height. Here then could be a programmed injection of new reactants with minimum carrier air. (Here it should be noted that all dilution or injection in a dynamic program should be accompanied by good mixing.) The rate and time of injection should be correlated with the operating cycles of the local sources.

2. (Somewhat similar.) The drift of urban air over suburbs (e.g., Los Angeles to Riverside or to Azuza). The kind and rate of reactant injection should simulate the behavior of the sources enroute and the degree and kind of dilution may be different or similar to simulation 1--certainly one would expect the L.A.-Riverside model to be different from a N.Y.-Jersey City model.

3. Drift from city to country (Figure 35). Start a simulated urban mix and at time t begin diluting. Here a meteorologist should be able to help in estimating at what rate the city system is diluted by country air. (previous acetylene sampling in a trajectory from the city to some place downwind could help also.) What is in the simulated country air used for a diluent: "natural" air, "eastern rural" air or "clean" air? (Clean air: air from a clean air source such as a catalytic oxidizer with subsequent NO_x scrubbing. Simulated natural air: NO_x at 6 ppb, O_3 at 0.02 ppm, hydrocarbon at 0.10 ppm C. Simulated eastern "high-O_3" air: NO_x at 10 ppm, O_3 at 0.10 ppm, and hydrocarbon at 0.25 ppm C.)

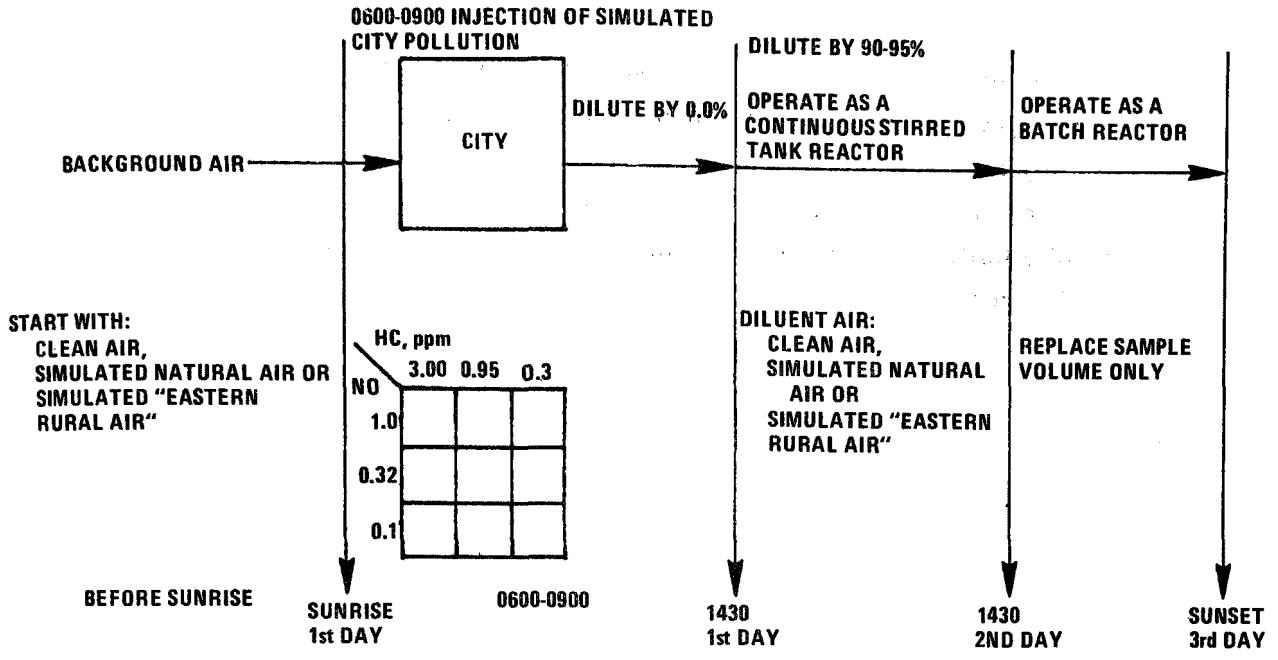

Figure 35. Chamber simulation of extended urban influence on surface ozone concentration.

Although much can and will be done with smog chambers operating in the batch mode, dynamic manipulation of the operating variables can aid in closer simulation of ambient conditions. It can possibly produce better data than batch studies for setting standards and determining control strategy.

SIMULATION OF NATURAL SUNLIGHT -- *E. Stahel, NCSU*

The outdoor smog chamber's basic problem as it relates to sunlight is to extract from an arbitrarily real (daily atypical) diurnal variation a baseline case devoid of local artifacts. The indoor smog chamber routinely operated today has to interpret an unrealistic baseline case, i.e., reactions under steady illumination. The acceptance of the latter as a real atmosphere simulation is tenuous.

What characteristics of natural sunlight can be identified as relevant, of what level of significance are they, and under real constraints, what impact do they have on chamber design? Light intensity, spectral distribution, and their respective diurnal variations appear to be basic, with the mode of the radiation, whether direct, scattered, reflected, etc., of some interest.

At the outset, it is enlightening to reflect on the physical constraints of the indoor smog chambers to be illuminated as their fundamental design parameters affect the light simulation. The following concepts are open to discussion but form, I believe, the basics of chamber design from a reaction engineering point of view. We are trying to ensure a spatially uniform concentration field and a spatially uniform light intensity, with minimum thermal gradients and heterogeneous effects. Some of the consequences of these in terms of the

state of the art are the following: Experimental chambers must be mixed at the outset and throughout the reaction cycle. Mixing must effect both macro- and microuniformity. Chambers must be relatively large, 500 to 1000 ft^3. The wall effects as interrelated to mixing are complex and unresolved, but sampling flexibility and surface to volume ratio dictate this range. Light intensity uniformity for large chambers of approximately 1000 ft^3 can be achieved at reasonable cost in only limited ways. The most desirable geometric arrangement appears to be the halo-lighted right circular cylinder. The intensity decrease with the square of the distance from the cylindrical outer surface is balanced geometrically by the compensating decrease in illuminated area. Uniformity is achieved, barring end effects that require some augmentation. The common array of predominately blue with black and sunlight flourescents lends itself to this application at low cost. Discharge lamps, while undoubtedly more spectrally similar to sunlight, have severe limitations in meeting the two levels of uniformity outlined above.

Diurnal changes in frequency and spectral distribution deficiencies of illumination systems are secondary effects, compared to diurnal intensity variations. These effects, while tentatively observed, have not been documented experimentally and are kinetically very complex. John Nader's volumetric intensity measurements compare favorably with Leighton's theoretical prediction of diurnal intensity variation and form the basis for a pragmatically programmed diurnal cycle monitored by k_1 evaluation techniques to assure the absolute level as well. Returning to the candidate chamber--1000 ft^3 in volume illuminated by a surrounding array of flourescent lamps--it is of incremental cost to program the large number of lamps in, say, decades controlled to approximate the given diurnal light intensity cycle.

Recent data tend to indicate major effects of diurnal intensity variation compared to constant illumination, and this appears to be the single greatest weakness of existing indoor chamber data in simulating stagnant air mass kinetics. Dynamic considerations only reinforce the criticality of the reactor engineering concepts enumerated.

OUTDOOR SMOG CHAMBERS -- *H.Jeffries, UNC*

The "theoretical" advantages of an outdoor smog chamber are no longer theoretical--they are real. The UNC dual outdoor smog chamber was finished in May 1973 and it has been operated almost continually since that time, except for the winter months of December-March.

Figure 36 gives details of the chamber shape and construction. The chamber volume is 12,000 ft^3, divided into two 6000-ft^3 compartments. The walls and floor are 5-mil FEP Teflon film secured to an exterior wooden frame by aluminum u-channels. The design and performance of the chamber have been highly satisfactory. It is a durable structure. It has withstood rain, ice, snow, storm winds, and temperatures ranging from 20 to 95° F without any signs of stress. The cover system is only used during the winter months. The chamber is not a greenhouse, that is, the air temperature rise above ambient is less than 8° F during intense irradiation. It has excellent light characteristics: approximately 85 percent trans-

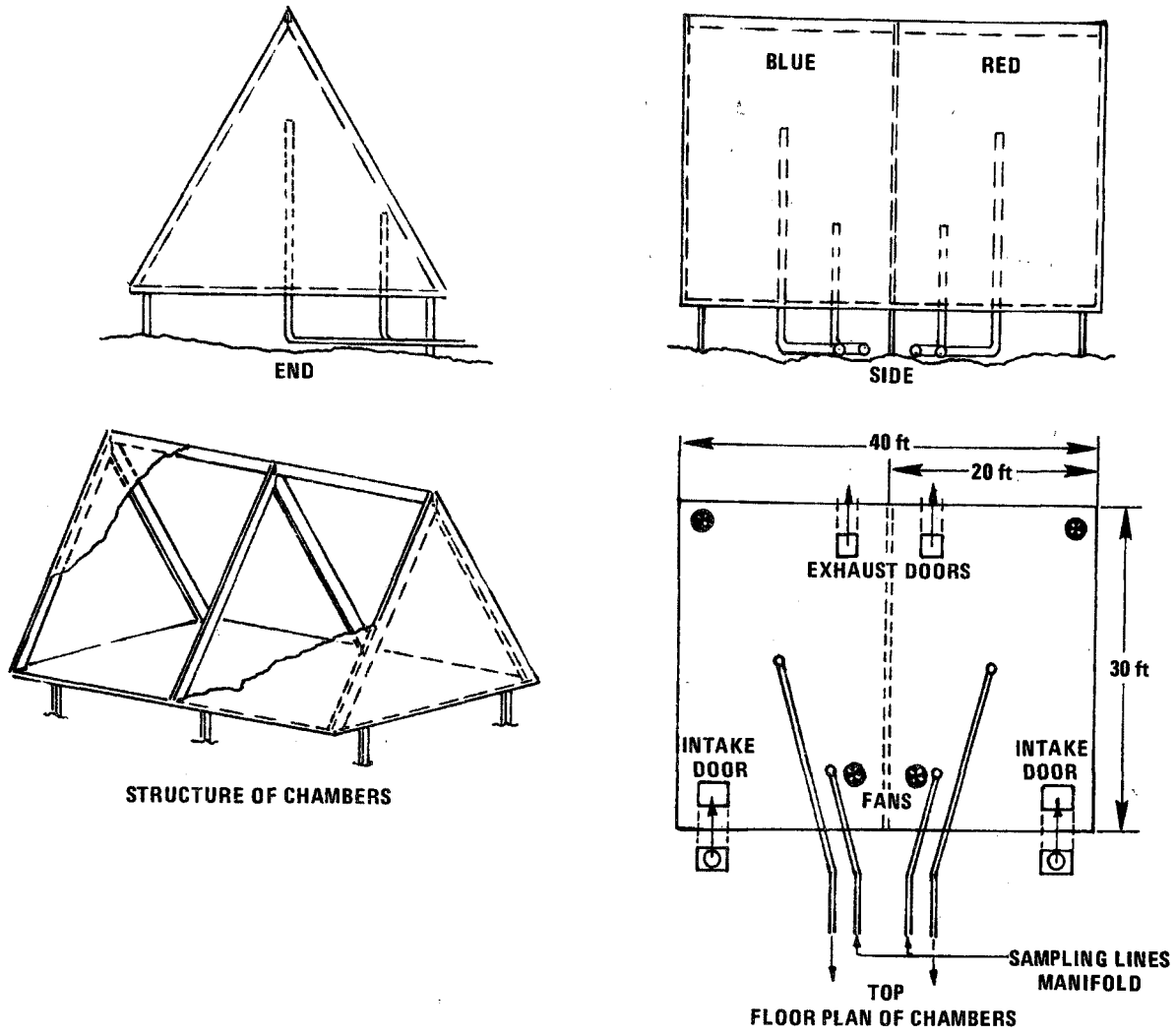

Figure 36. The University of North Carolina smog chamber.

mission of total solar radiation (TSR) and approximately 93 percent transmission for ultraviolet solar radiation (UV) less than 4000 Å. The transmission losses are largely compensated for by a reflective floor for heat and radiation. This results in a ϕKa for $NO_2 + h\nu$ of 0.37 min^{-1} when TSR = 1.0 cal cm^{-2} min^{-1}. It is well mixed. Thermal mixing occurs, in addition to that from the two 1000 ft^3/min mixing fans in each chamber half. Samples from "corner" locations are the same as those from the middle of the chamber, and concentrations of materials in the chamber follow an exponential dilution curve during exhausting very well. The chamber exhibits a low background reactivity: the ozone (O_3) half life is greater than 20 hours in the light and greater than 45 hours in the dark at an initial concentration of 0.85 ppm; the nitric oxide (NO) oxidation rate for background air is 0.2 ppb/min at $[NO]_o$ = 0.45 ppm and 0.1 ppb/min at $[NO]_o$ = 0.24 ppm; the O_3 formation in blank runs varies with ambient air and is 0.05 to 0.08 ppm O_3 when ambient air concentrations rise to 0.03 to 0.04 ppm. The compartment to compartment replication is excellent; this is partly due to the use of a fully computerized data acquisition and control system that operates the chamber and to instruments that are time shared between each chamber half.

More than 63 propylene/NO_x and 68 simulated hydrocarbon mix/NO_x (mix/NO_x) dual 12-hour runs (that is, 262 individual experiments) have been conducted in the chamber in the last 15 months. Some of these will be presented below to indicate the effects of variations in natural sunlight and temperature on the chemical profiles.

The first order rate constant for the photolysis of NO_2, herein called K_1 ($=\phi Ka$), is one of the most sensitive parameters in a HC/NO_x photochemical system. The value of K_1 is usually measured by NO_2 photolysis in N_2 as either K_D, a pseudo-first-order rate, or better as ϕKa by using a kinetics derived relationship such as that developed by Holmes et al.[6] Sickles and Jeffries[7] at UNC have developed a continuous unit to measure K_1. The device is a 1-liter quartz flask operated as a continuous stirred flow reactor. The calculating equation for K_1 as a function of time in real sunlight is given in Table 14.. The advantages of this device over other techniques are numerous. It is nearly ideal as a three-dimensional sensor; it is continuous and rapid; it is based on a complete and well verified kinetics mechanism that includes all essential nitrogen chemistry; and the rate expression does not have to be integrated.

This continuous chemical actinometer for NO_x (CCANOX) has undergone extensive evaluation by computer simulation (using the EPA program with modification for variable light intensity) and by field testing. Figure 37 shows data taken on September 19, 1974, using the CCANOX and an Eppley total solar radiation sensor, which measures the direct and diffuse intensity on a horizontal surface. The K_1 data are presented as discrete points because a black bag was used to check the zero point between each reading. No explanation can be offered at this time for the fact that the volumetric (that is, the three dimensional) light intensity for wavelengths <4000 Å follows the same pattern as does the total intensity on a flat horizontal surface. The evidence, however, for this particular set of measurement conditions (there is a similar set for September 18), seems overwhelming The data strongly suggest that, at least at our site, the TSR readings from the Eepley sensor can be taken as a good approximation to K_1.

Figures 38 and 39 show the TSR and chamber air temperature for two selected run days in the outdoor chamber. The chemical system under study for each of these days was 2.0 ppmC NMHC, propylene, 0.50 ppm NO_x, and 10 percent NO_2. The concentration-time profiles for these days are presented in Figures 40 and 41. May 7, 1974, was a dual matched run and Figure 40 indicates the degree of side to side reproducibility of the UNC chamber. The NO_2 data in these runs were acquired with a chemiluminescent NO_x analyzer, which is subject to late-afternoon interference by HNO_3 and PAN, hence the dashed lines in the figures. Other work[8] has shown that the late afternoon NO_2 reading is [NO_2 = PAN] and the HNO_3 is probably lost in our sampling lines.

In all of the outdoor runs, the variation in the NO and NO_2 time profiles is not very much affected by what appears to be substantial variations in the TSR. Besides the slight adjustments to the time axis to match NO-NO_2 cross-over points, there are subtle differences among the NO and NO_2 profiles and much larger differences among the O_3 profiles. However,

Table 14. DERIVATION OF CONTINUOUS CHEMICAL ACTIONOMETER FOR NO_x (CCANOX)
(by Joe Sickles)

1. Accumulation = IN-OUT-RXN <Mass Balance>

$$\text{Accumulation} = \frac{d[NO_2]f}{df}$$ <computed from inst. readings>
<$[NO_2]f$ = outlet conc., $[NO_2]$ = inlet conc.>

$$IN = \frac{[NO_2]o}{\tau}$$ <where τ = volume/flow rate>

$$OUT = \frac{[NO_2]f}{\tau}$$ <from kinetics model>

$$RXN = -2K_1 \Big/ \left(\frac{1}{[NO_2]f} + \frac{R_1}{[NO_2]f} + \frac{R_2\,[NO]f}{[NO_2]_f^2} + \frac{R_3[O_2]f}{[NO_2]_f^2} \right)$$

where $R_1 = 0.272$ $R_2 = 0.261$ $R_3 = 1.59 \times 10^{-3}$

2. Let $X = \dfrac{[NO_2]o - [NO_2]f}{[NO_2]o}$, Drop R_3 Term <$[O_2] \approx 0$>

<X = conversion>

3. Solve first equation:

$$K_1(t) = \left(\frac{dx}{dt} + \frac{X}{\tau} \right) \left[\frac{1 + R_1}{1 - X} + \frac{R_2 X}{(1 - X)^2} \right] \left(\frac{1}{2} \right)$$ <Nonsteady State>

$$K_1(ss) = \frac{X}{2\tau} \left[\frac{1 + R_1}{1 - X} + \frac{R_2\,X}{(1 - X)^2} \right]$$ <Steady State>

4. Calculating Forms: Let $\Delta NO_2 = [NO_2]o - [NO_2]f$

$$K_1(f) = \left(\frac{\Delta NO_2}{\tau} - \frac{d[NO_2]f}{df} \right) \left(\frac{1}{[NO_2]f} \right) \left[1 + R_1 + \frac{R_2(\Delta NO_2 + [NO]o)}{[NO_2]f} \right] \left(\frac{1}{2} \right)$$

$$K_1(SS) = \left(\frac{\Delta NO_2}{2\tau} \right) \left(\frac{1}{[NO_2]f} \right) \left[1 + R_1 + \frac{R_2(\Delta NO_2 + [NO]o)}{[NO_2]f} \right]$$

5. Advantages: Spherical sensor, continuous, X independent of actual $[NO_2]o$ in range 1 to 50 ppm, response time limited by NO_2 sensor and steady state assumption for O, O_3, NO_3, N_2O_5 <fast relative to K_1 changes>, rate expression does not have to be integrated. Zero tested with black bag. Initial O_2 flushed from system in 7τ. Need only volume, flow rate, $[NO_2]o$, $[NO_2]f$.

May 19 (Figures 40 and 41) shows small changes in NO and NO_2 slopes that correlate well with changes in TSR.

It is difficult to discern these effects in the concentration time profiles, but much easier in the rate or first derivative-time profiles. Figure 42 shows the NO and NO_2 rate

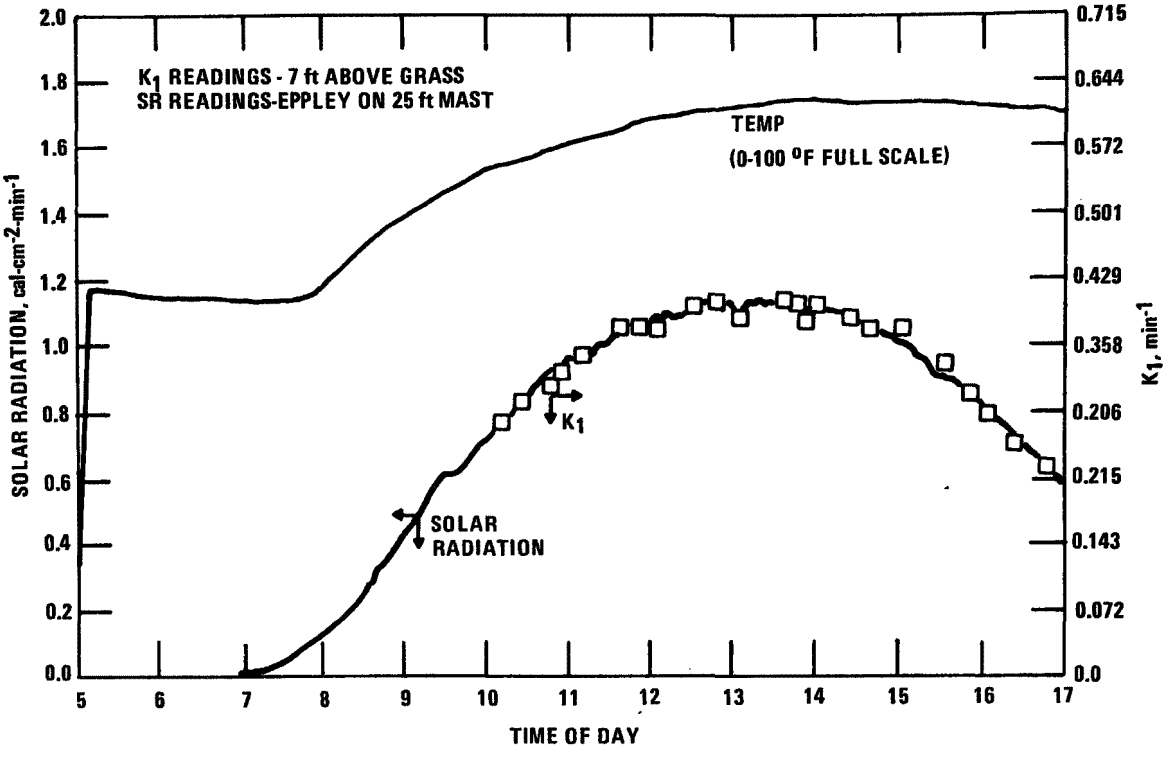

Figure 37. Comparison of total solar radiation on horizontal surface with rate of photolysis of NO_2 (K_1) (latitude 35.72°), September 19, 1974.

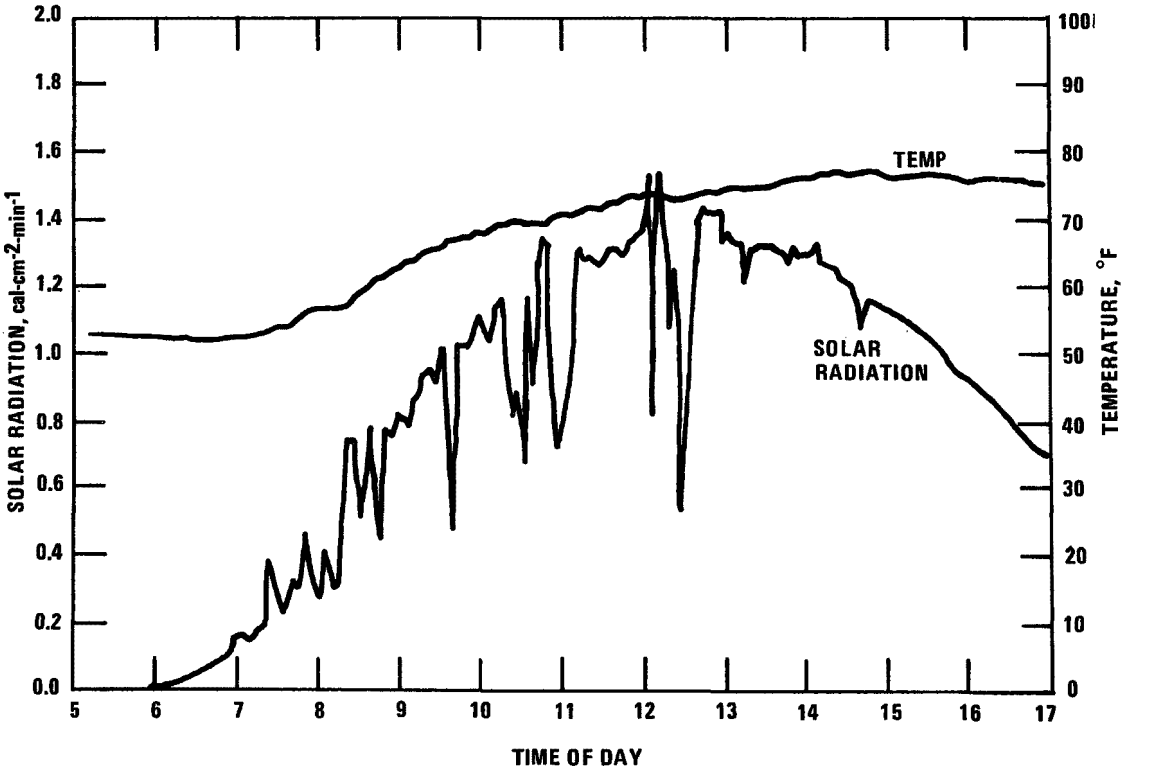

Figure 38. Diurnal variation of solar radiation and temperature, May 7, 1974.

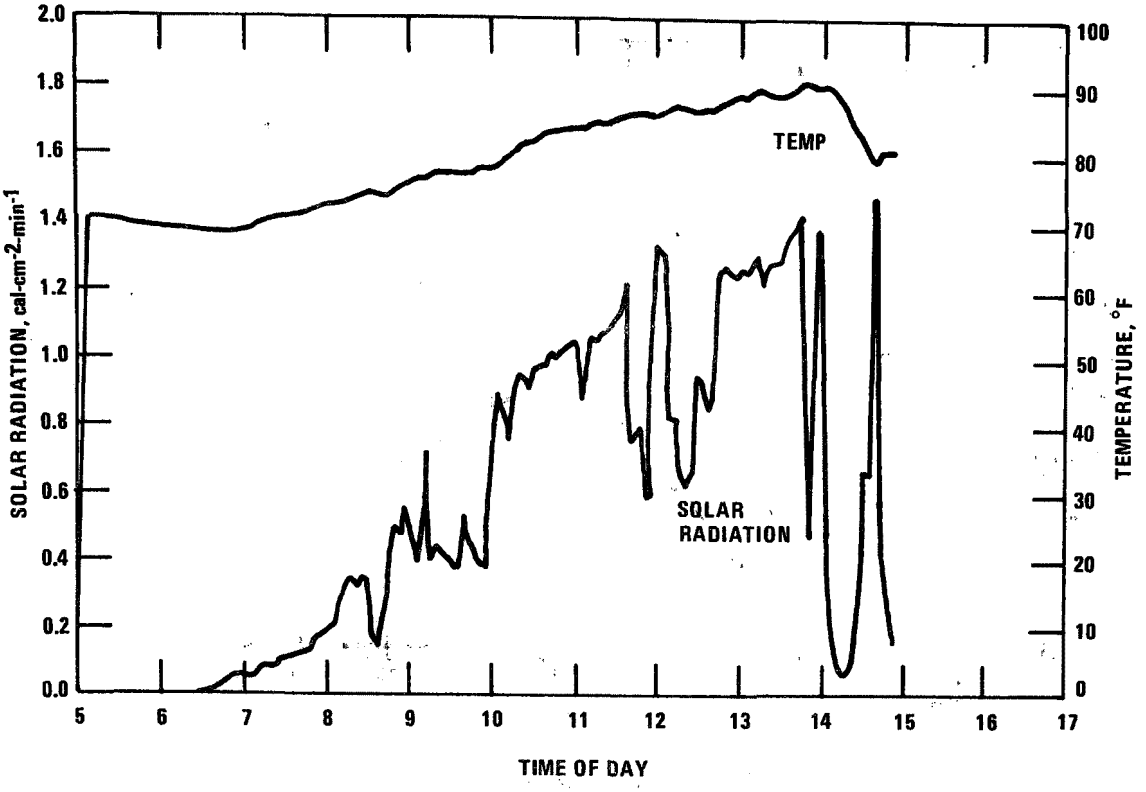

Figure 39. Diurnal variations of solar radiation and temperature, May 19, 1974.

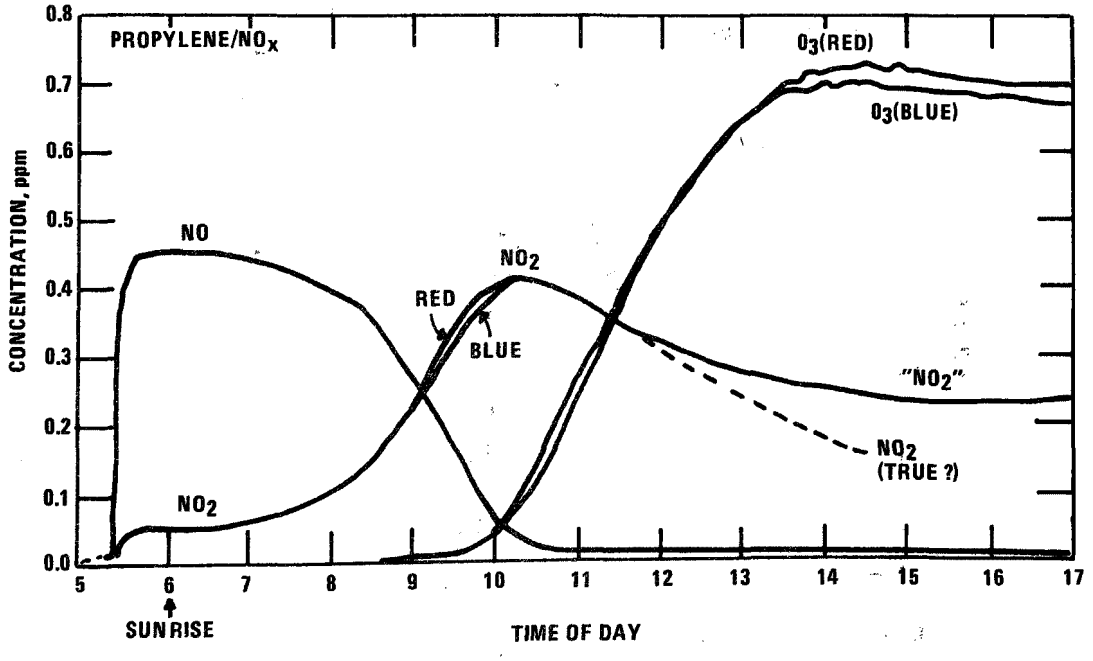

Figure 40. Comparison of concentration-time profiles from the two chamber compartments (red and blue), May 7, 1974.

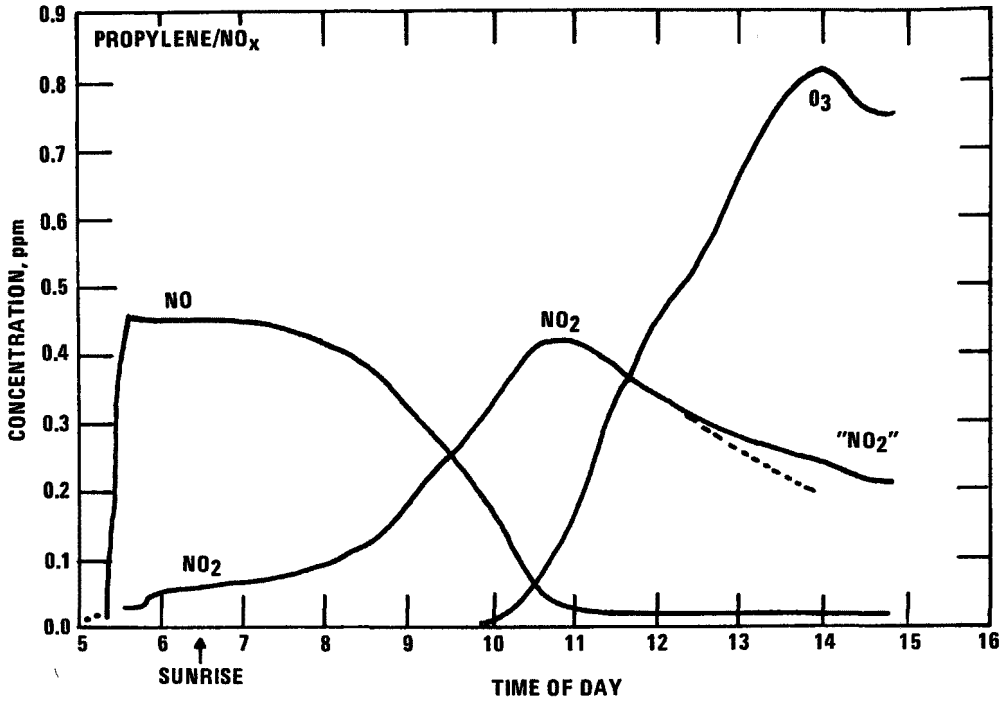

Figure 41. Concentration-time profiles, May 19, 1974.

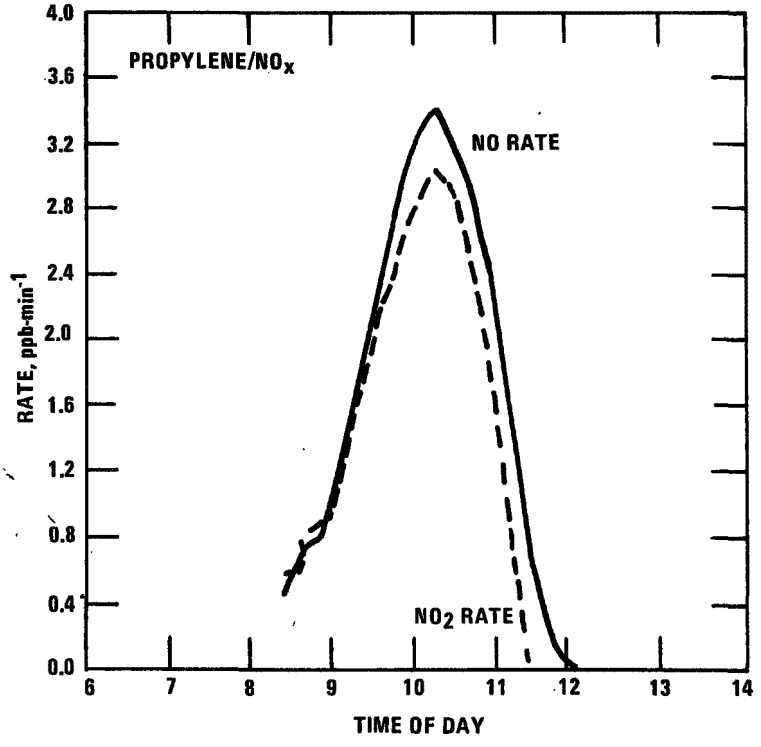

Figure 42. Rate of NO disappearance and NO_2 appearance for a clear day, October 13, 1973.

computed by a digital 5-point formula from the time profiles of October 13, 1973, a totally clear, full sunshine day. The rate changes are smooth and peak values are 3.5 and 3.0 ppb/min for NO and NO_2, respectively. The NO and NO_2 rate for May 19, 1974, are given in Figure 43. The deacceleration and acceleration with changes in TSR are evident; however, the system still achieved a peak rate equal to or slightly greater than the clear day of October 13, 1973. Note that the flat part of the rate curve lasted almost 1 hour.

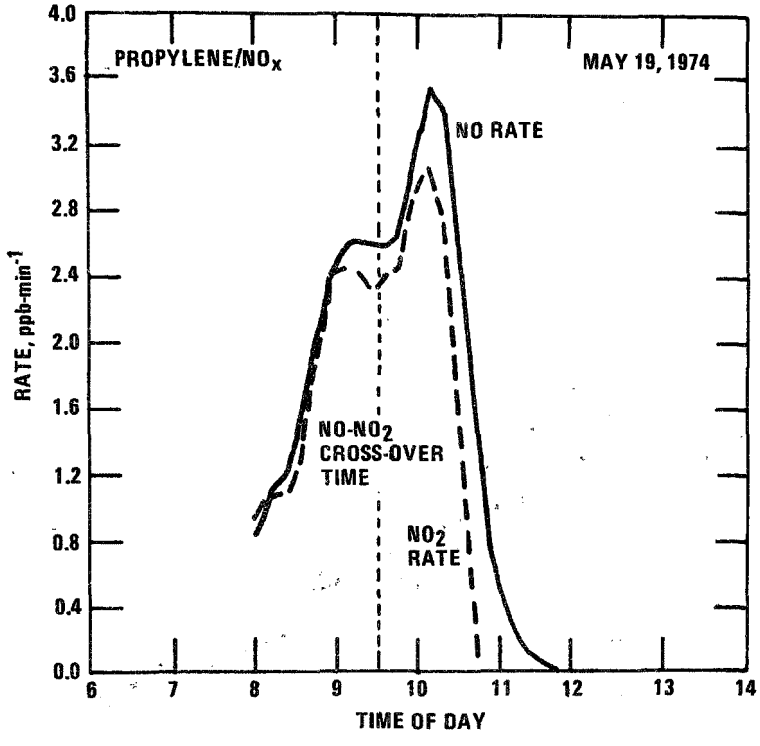

Figure 43. Rate of NO disappearance and NO_2 appearance for a partly cloudy day, May 19, 1974.

In Figure 44, the O_3 profiles from 7 days are displayed together with TSR profiles. The O_3 profiles are much more affected by TSR variations. The O_3 that accumulates in the system is the difference between that which is generated by NO_2 photolysis and that which is lost by reactions with NO and to a much lesser extent olefins. Free radicals from the degradation of hydrocarbons and aldehydes by O, O_3, OH, and photolysis compete with O_3 for the NO to regenerate NO_2. Thus, the buildup of O_3 is dynamic. A free radical NO oxidation chain, which is relatively short, can sustain itself for short periods without fresh initiation, by photolysis steps, but depending on the state of the system, the acceleration of O_3 accumulation may decrease or at the worst become negative. Thus, the effects of "choppiness" in the TSR profile on O_3 profiles depend upon the frequency and where in the chemical process it occurs.

Figures 45 to 48 show TSR, NO, NO_2, and O_3 profiles from two selected days of outdoor chamber runs in which the chemical system was a less reactive simulated urban hydrocarbon mix at 2.0 ppmC, 0.35 ppm NO_x, and 20 percent NO_2. The mix contains acetylene,

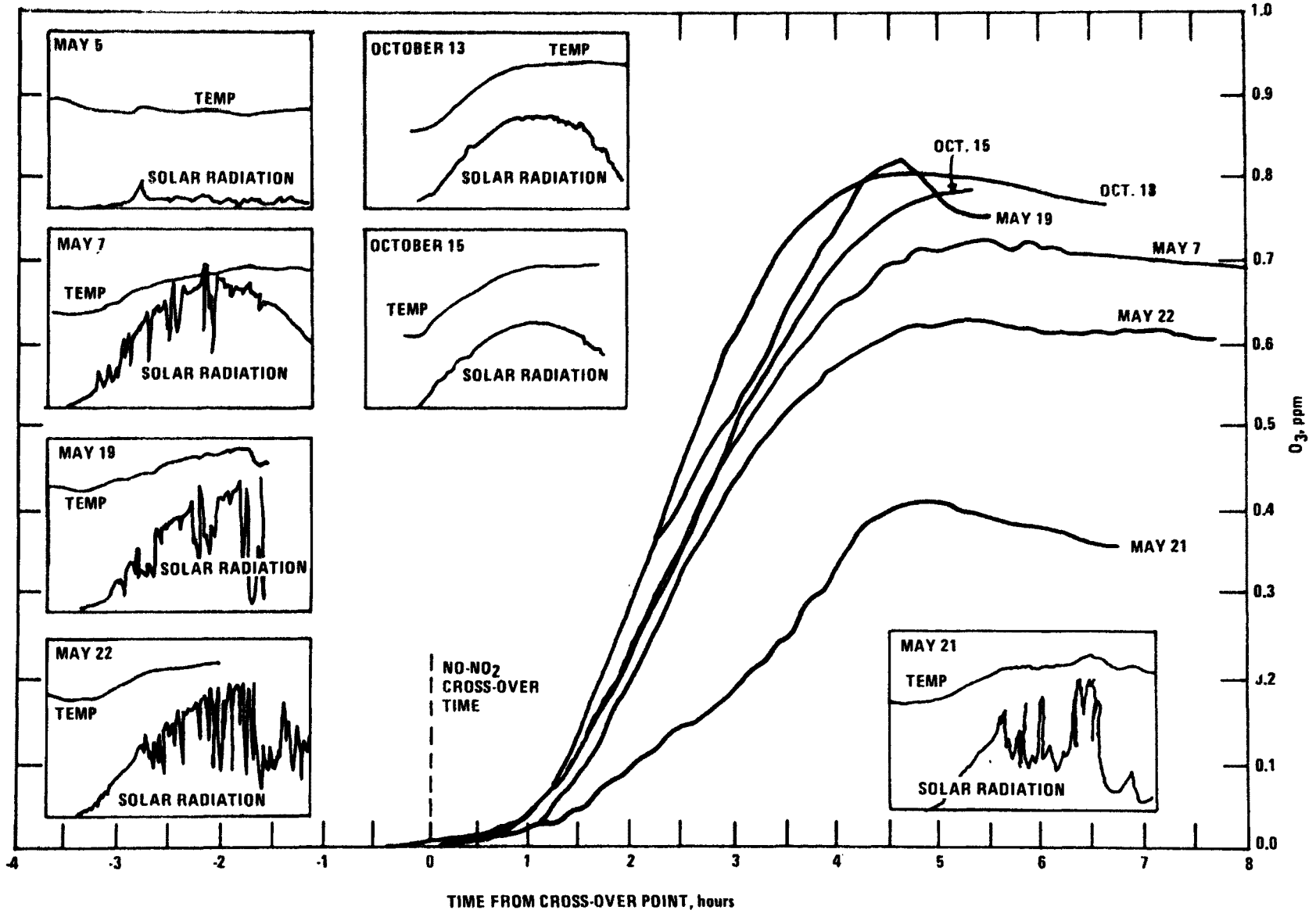

Figure 44. Comparison of ozone profiles and solar radiation profiles for propylene runs.

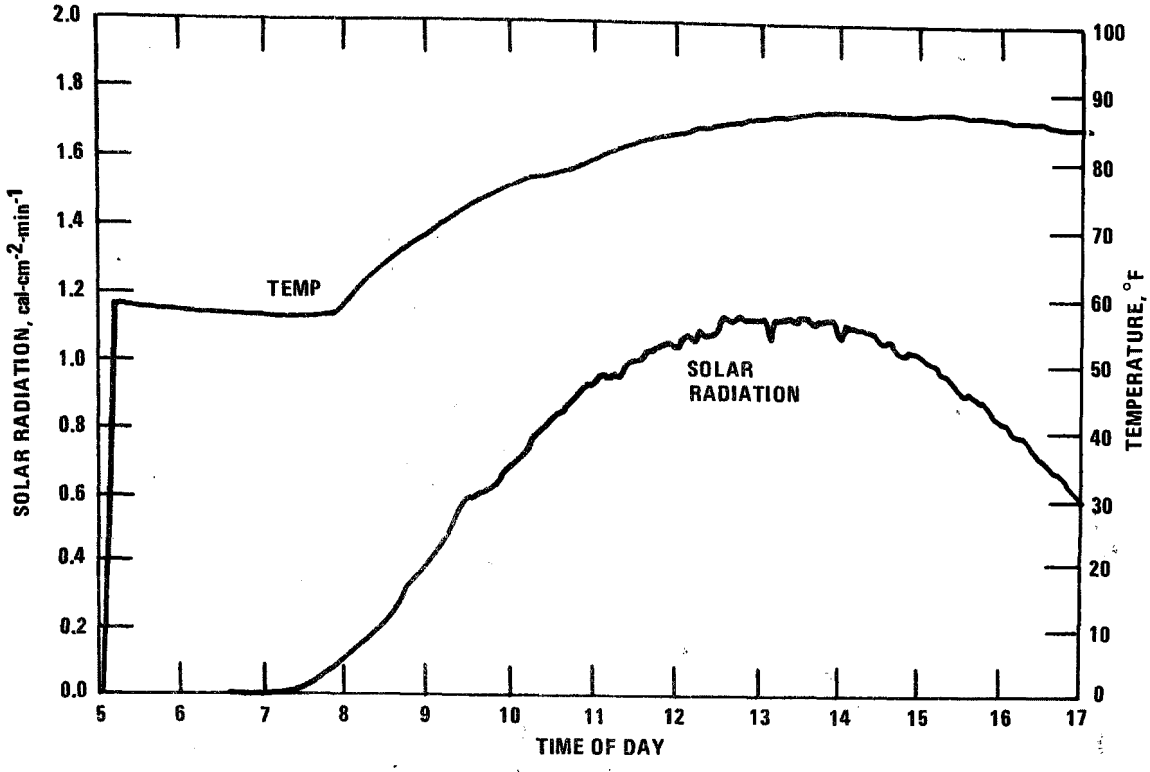

Figure 45. Diurnal variation of solar radiation and temperature, September 19, 1974.

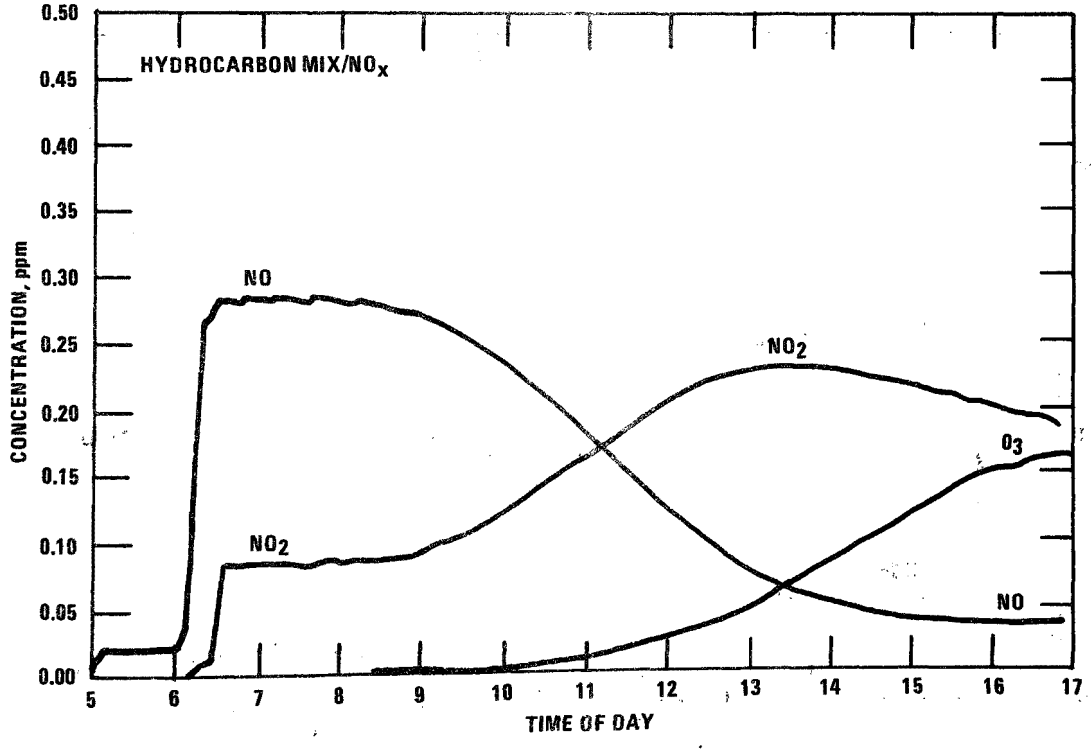

Figure 46. Concentration-time profiles, September 19, 1974.

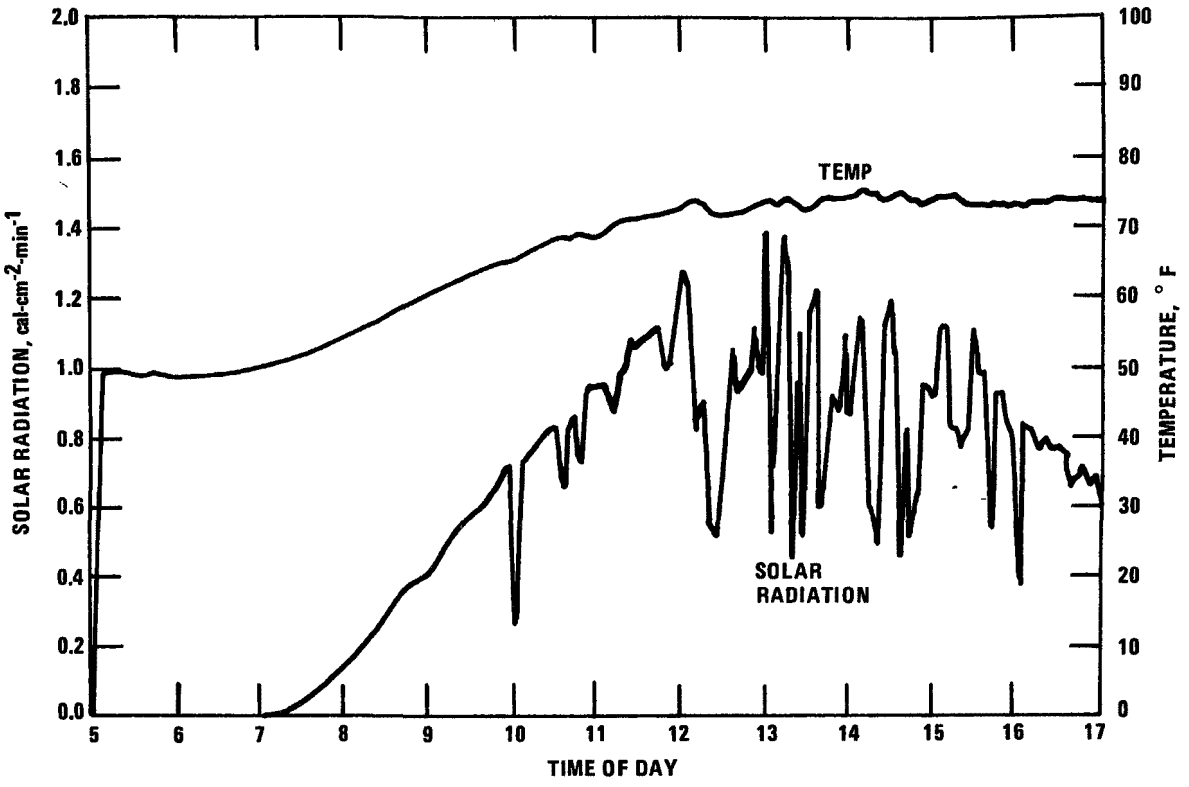

Figure 47. Diurnal variations of solar radiation and temperature, September 23, 1974.

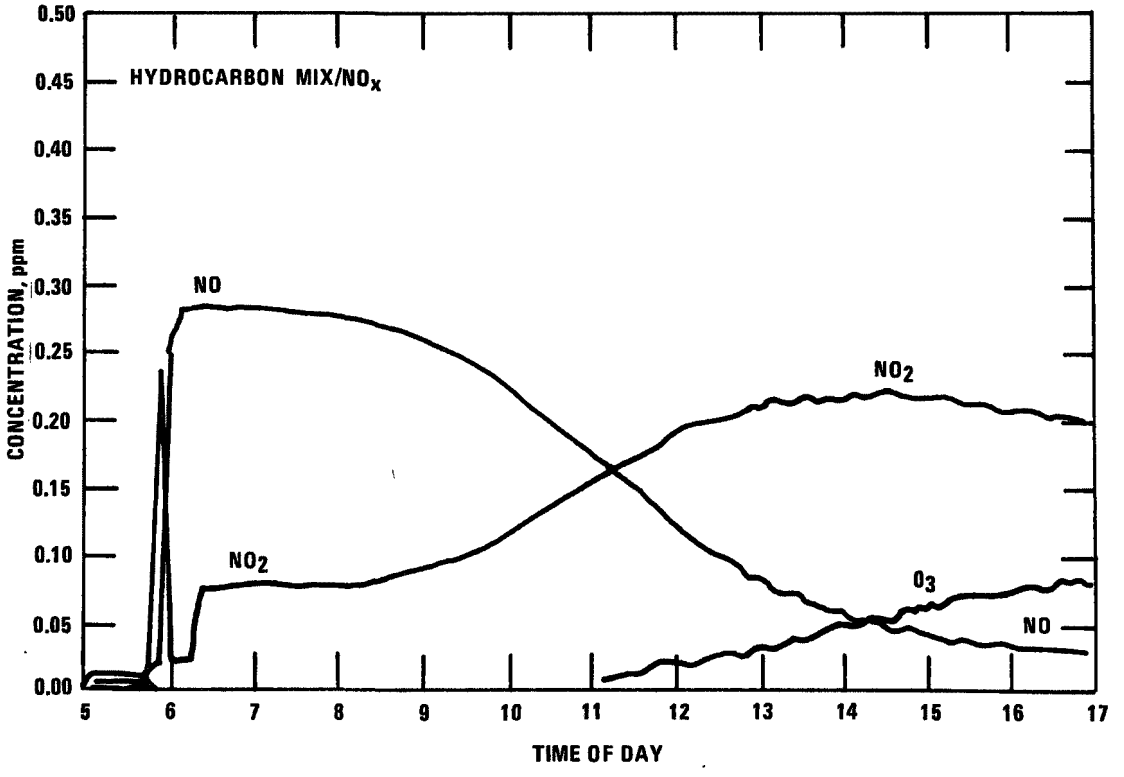

Figure 48. Concentration-time profiles, September 23, 1974.

paraffins, olefins, and sometimes toluene and m-xylene. The conversion of NO to NO_2 is much slower (approximately 2.5 less reactive than propylene) and it generates less PAN to interfere with the NO_2 afternoon readings. The lower reactivity reflects itself in a lower free radical flux, which is less competitive with O_3 for NO in the afternoon, leading to lower $[O_3]$ and higher [NO] and less consumption of NO_2.

The effect of TSR variations on NO and NO_2 profiles is also less than might be expected. Comparison of NO and NO_2 profiles for Figures 45 and 46, September 19, 1974, with Figures 47 and 48, September 22, 1974, shows near perfect matches until 12:00. The effect of the "chop" in TSR can be seen in the NO_2, NO, and O_3 profiles as each dip in light intensity causes free radical flux changes. The overall effect is a slightly delayed NO_2 peak, slightly higher NO, and approximately one-half the ozone on September 22. In Figure 49 for October 8, 1974, the large "hole" in TSR at the end of the run results in a decrease of the O_3 acceleration to zero, and thus this day did not reach the final O_3 value that September 19 did (see Figure 49). In Figure 49, it is evident that TSR effects (perhaps in combination with temperature effects) can easily decrease O_3 production by factors of one-half for what are otherwise apparently equal conditions.

With respect to the direct effects of temperature, the temperature profiles are somewhat confounded with the TSR, such that a more sophisticated approach is needed other than comparing one curve with another. This work is in progress and will be reported later. The temperature profiles in Figures 44 and 49 represent a relatively wide range of temperature profiles and there are no obvious temperature effects in the data. For example, October 6 and September 19 had very different temperature profiles with little effect evident in the chemical profiles.

With peak temperatures below 74° F, however, an effect is discernible and is illustrated in Figure 50. For these runs, the NO oxidation rate is decreased by one-half for a 14° F decrease in daily peak temperature. These runs were all full sun.

A final topic of discussion with respect to outdoor light conditions and the UNC chamber performance is the speed at which NO is converted to NO_2 under outdoor lighting conditions relative to indoor smog chamber constant light conditions, being considerably faster under constant light. UNC does not have an indoor chamber with which to run comparison studies, so a kinetics model was used to simulate the light and chemical conditions. The May 7, 1974, run (Figure 40) was chosen and a 52-step mechanism, specific for propylene, was used to model the data. The details of the mechanism were abstracted from the Dodge et al.,[9] Niki et al.,[10] and Demerjian et al.[11] models. Rate constants recommended by Garvin[12] were used where available; otherwise those of Dodge et al.[9] were used. The results are given in Figure 51. Validation of the model is hampered somewhat by the lack of additional product information in the late afternoon, but the model very closely adheres to the principles given by Dodge et al. and Demerjian et al., and it will serve to illustrate the important features. In Figure 51, the K_1 used in the model was a smooth function instead of the actually "choppy" solar radiation profile and there are differences in the NO, NO_2 profiles in these regions.

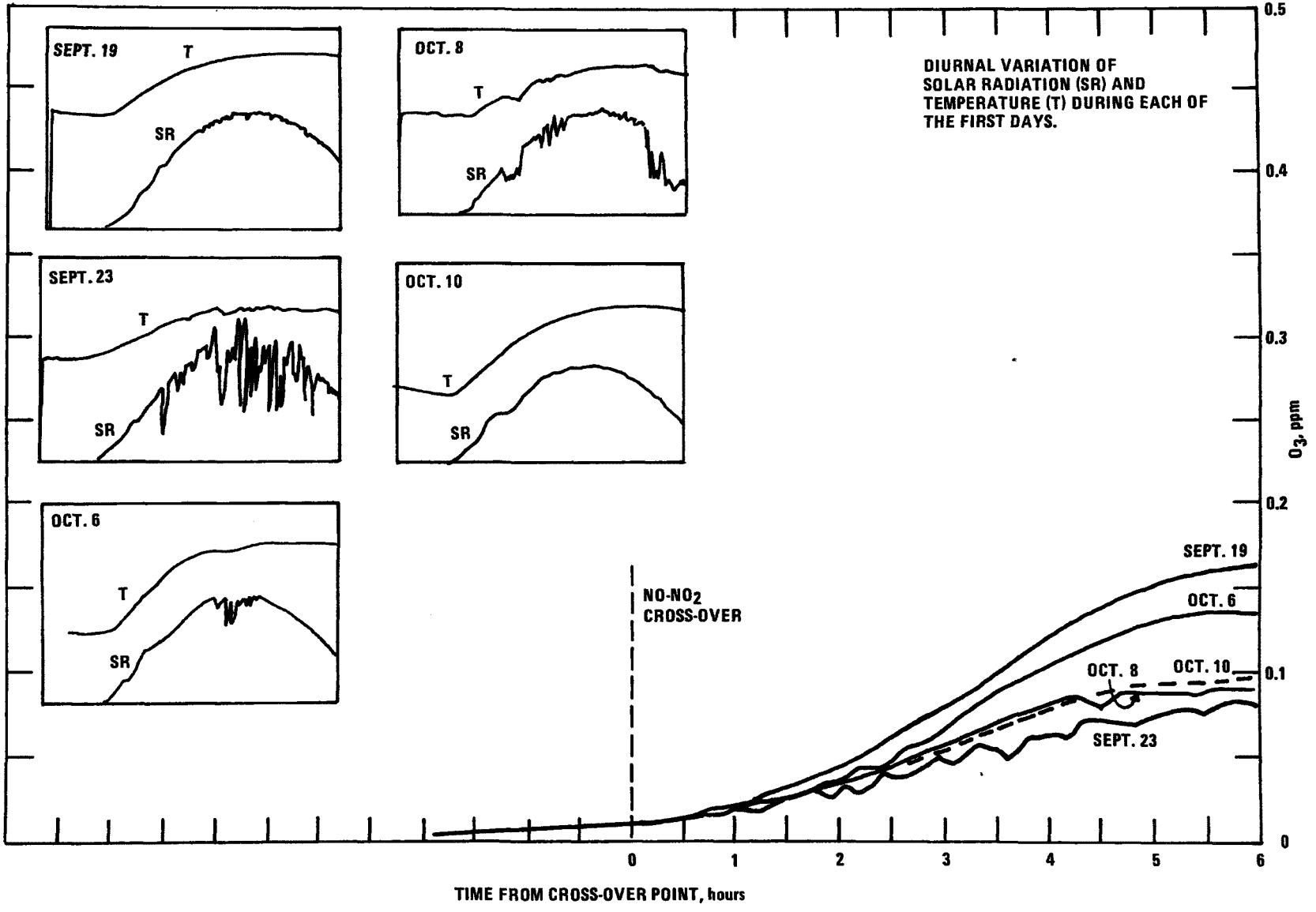

Figure 49. Comparison of ozone and solar radiation profiles for mix runs.

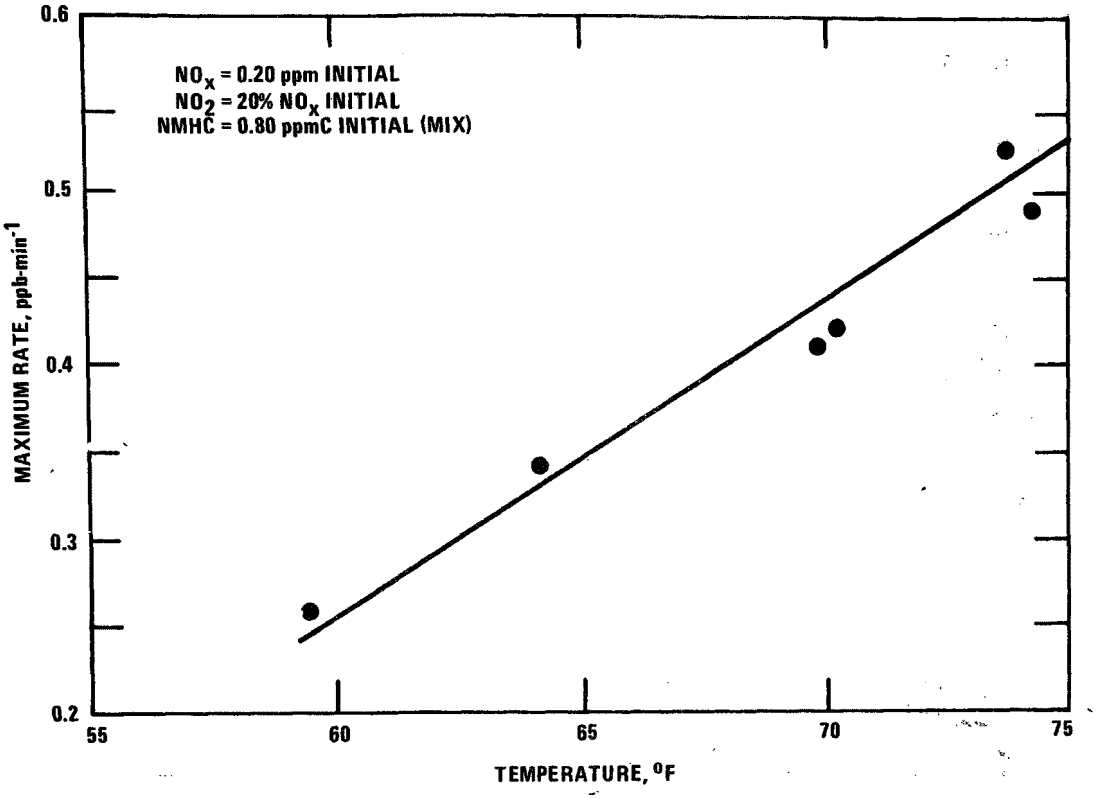

Figure 50. Effect of temperature on maximum rate of NO disappearance.

The results of operating the model under constant light intensity conditions are given in Figures 52 and 53. Comparison of Figure 51 with these figures shows that the early part of the outdoor run is between the runs for constant K_1 = 0.1 and 0.2, and the latter part of the run, from the NO_2 peak to the end, agrees fairly well with the run for constant K_1 = 0.4. These results also imply that if an indoor smog chamber is illuminated to an "average" level, that is, such that the area under the K_1-time curve is the same as the area under the outdoor K_1-time curve, high hydrocarbon reactive chemical systems will make more O_3 under the outdoor K_1 conditions than the same system would under the "average" K_1 conditions since it is the instantaneous K_1, NO_2 product that generates ozone. Low hydrocarbon, less reactive systems will make less ozone under outdoor K_1 conditions than under indoor K_1 conditions, since by the time the system reaches the NO_2 peak, K_1 is decreasing outdoors.

In all of the above models, it was necessary to assume a value near the lower limit given in Reference 12 for the reaction

$$H_2O + NO_2 + NO \longrightarrow HNO_2.$$

The photolysis of HNO_2 is considered an important initiation process in most indoor chambers; and the formation reaction above is suspected of having a heterogeneous character, and may not be elementary since it shows a second order dependence on water. The rate used in the model above was 3.5×10^{-5} ppm^{-1}min^{-1} at 20,000 ppm H_2O to be compared with the value of 1.5×10^{-2} ppm^{-1} min^{-1} at 20,000 ppm H_2O used by Dodge et al.[9] for the EPA indoor

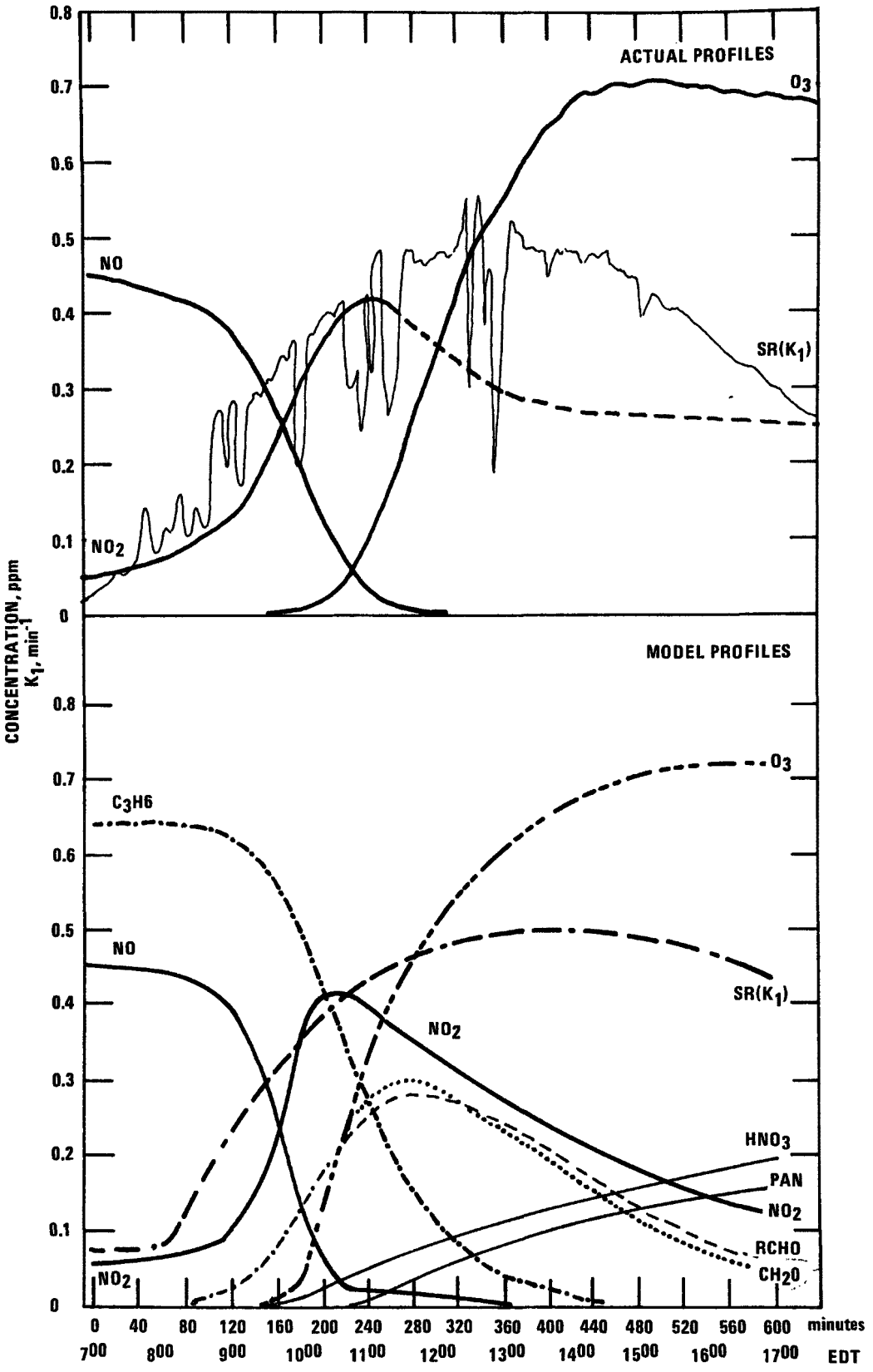

Figure 51. Comparison of kinetics model and actual data for May 7, 1974.

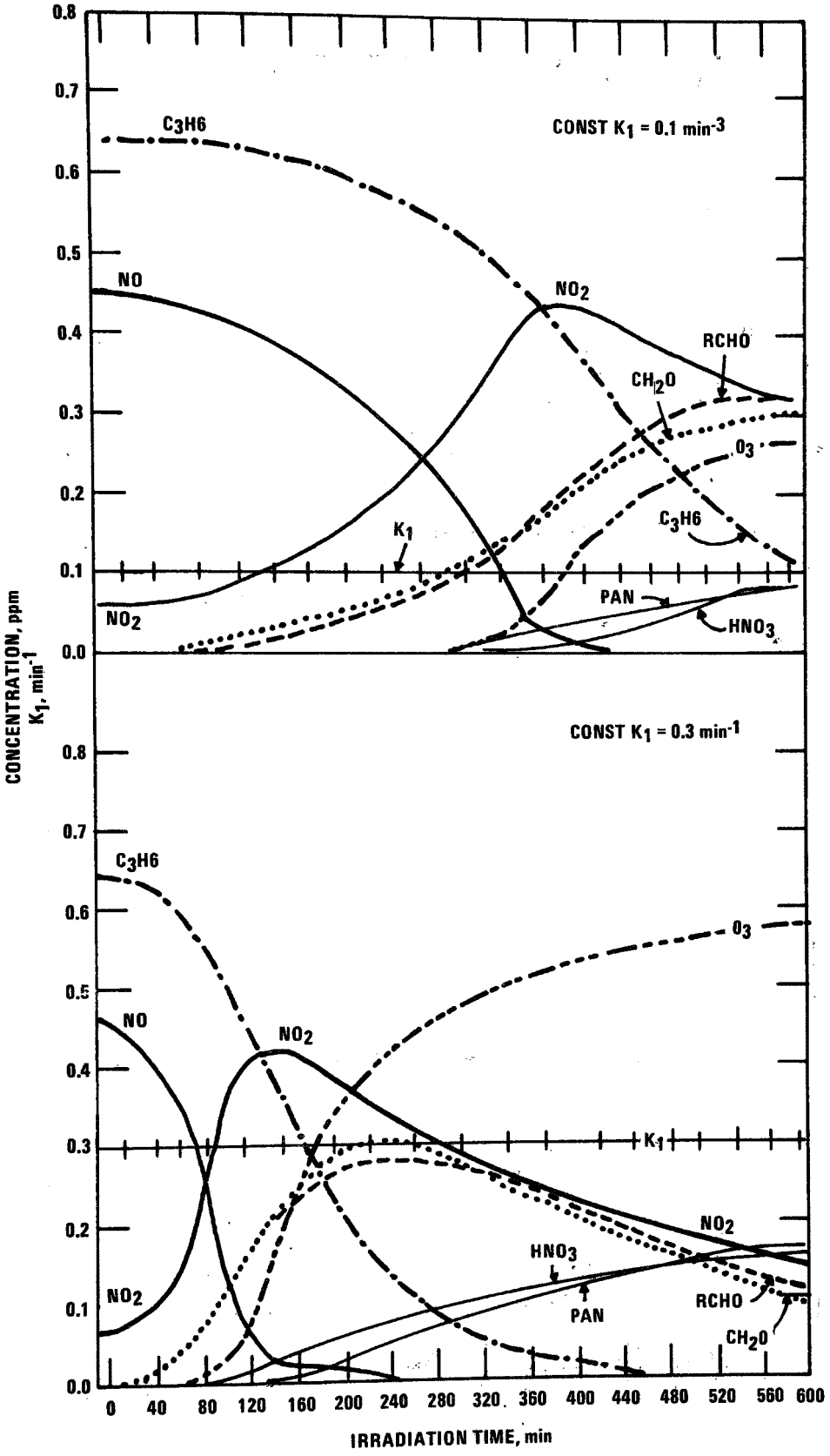

Figure 52. Model results for constant K_1=0.1, 0.3, May 7, 1974, conditions.

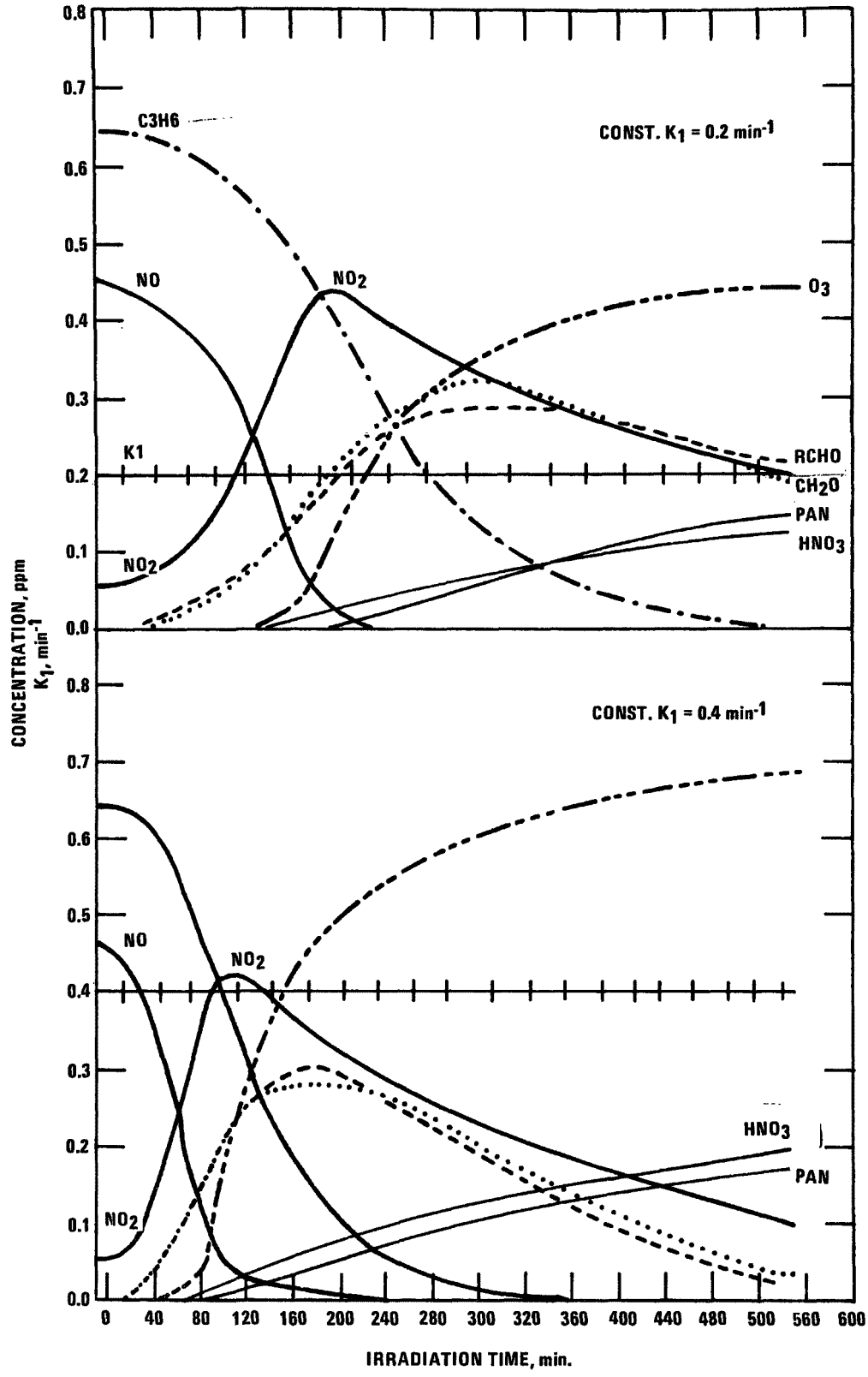

Figure 53. Model results for constant K_1 = 0.2, 0.4, May 7, 1974, conditions.

chamber. The morning humidity in the outdoor chamber is quite high, with dew points approaching air temperature frequently. If the EPA chamber value is used in the above model, the NO-NO_2 cross-over time is reduced by 240, 83, 40, and 30 min for 0.1, 0.2, 0.3, and 0.4 min^{-1} (k_1), respectively. It would seem that: (1) the model needs improvement in some unknown area, (2) the UNC chamber exhibits unusually low surface effects, (3) there are other chamber artifacts that are not clearly understood, or (4) all of the above.

It should be pointed out that none of the runs that were selected for this presentation were designed to determine the effects of TSR and temperature and, in most cases, one side of each dual run has been presented. Much more information is available in the data that have been examined herein, in terms of the side to side comparisons as well as the day to day comparisons. For example, the May 19, 1974, run was a test of the effect of constant NO_x, different NO_2 on the outcome of the experiment. The full dual profile data are shown in Figure 54.

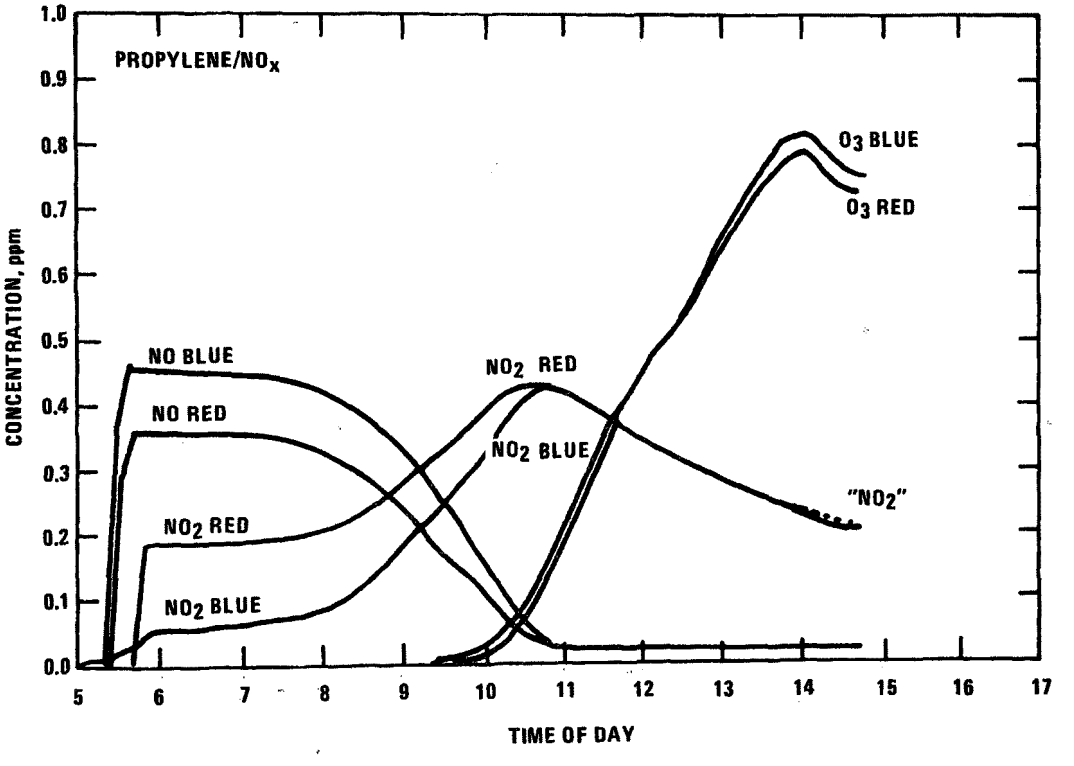

Figure 54. Concentration-time profiles for dual run in University of North Carolina chamber, effect of initial NO_2/NO_x, May 19, 1974.

In summary,

1. ϕKa and total solar radiation on a horizontal surface are highly correlated.
2. Substantial changes in total solar radiation and temperature have relatively minor effects on NO-NO_2 profiles.

3. Low solar radiation in afternoon has a direct effect on O_3 generation. The effect is approximately equivalent to operating under constant low level light intensity.

4. Peak daily temperatures below 74° F do affect the NO oxidation rate, reducing it by a factor of 0.5 at 60° F.

5. Models can fit outdoor chamber data if detailed K_1 profiles are used.

6. The UNC chamber apparently exhibits very low surface reactivity with respect to HNO_2 formation.

REFERENCES FOR CHAPTER 5

1. Environ. Sci. Technol. 6:253, March 1972.

2. A Critique of the 1975-1976 Federal Automobile Emission Standards for Hydrocarbons and Oxides of Nitrogen. National Academy of Science, Committee on Motor Vehicle Emission Standards.

3. Air Quality Criteria for Nitrogen Oxides. U.S. Environmental Protection Agency. Washington, D.C. Publication No. AP-84. January 1971.

4. J. Air Pollut. Contr. Ass. 19:929-936, 1969.

5. Hydrocarbons in Polluted Air. State Air Pollution Research Center. University of California; Riverside, Calif. CRC Project CAPA 5, 68. June 1973.

6. Holmes, J. R. et al. Measurement of Ultraviolet Radiation Intensity in Photochemical Smog Studies. Environ. Sci. Technol. 7(6):519, 1973.

7. Sickles, J. and H.E. Jeffries. University of North Carolina, Chapel Hill, N.C. Private communication. 1974.

8. Kamens, R.K. University of North Carolina, Chapel Hill, N.C. Private communication. 1974.

9. Dodge, M.C., T.A. Hecht, and J.H. Seinfeld. Further Development of Generalized Kinetic Mechanism for Photochemical Smog. Environ. Sci. Technol. 8:327, 1974.

10. Niki, H., E.E. Daby, and B. Weinstock. Mechanisms of Smog Reactions. Adv. Chem. 113:16, 1972.

11. Demerjian, K.L., J.A. Kerr, and J.G. Calvert. The Mechanism of Photochemical Smog Formation. In: Advances in Environmental Science and Technology (Vol. 4). J.N. Pitts and R.L. Metcalf (ed.). New York, John Wiley and Sons, 1974. p. 1-262.

12. Chemical Kinetics Data Survey VII; Tables of Rate and Photochemical Data for Modelling the Stratosphere. D. Garvin and R.I. Hampson (ed.). National Bureau of Standards. Washington, D.C. Report NBSIR 74-430. January 1974.

6. VALIDITY AND UTILITY OF SMOG CHAMBER DATA

INTRODUCTORY REMARKS -- *B. Dimitriades, EPA*

Since oxidant and NO_2 are the only photochemical pollutants for which control strategies have been developed, it is only natural that the discussion here be addressed first to the role that the smog chamber data played in the formulation of these control strategies. It should be stressed, however, that it would be grossly wrong to judge the smog chamber method and data based on the present and past experiences alone. In the future, it is quite likely that the smog chamber method and data will find a much greater use.

The following three presentations should provide a fairly complete and specific treatment of the questions "how can one use smog chamber data, and how valid is such use in development of oxidant control strategies, at least, relative to the aerometric data." These three presentations each represent a case study of the oxidant problem in the Los Angeles basin, and more specifically, of the problem of calculating control requirements in the South Coast Air Basin. These three presentations will describe the three different approaches that have been used to relate oxidant to the oxidant precursors; one of these approaches is based primarily on smog chamber data.

The first presentation will be given by Mr. Walter Hamming, who, as the Chief Analyst in Los Angeles County's Air Pollution Control District, is the originator of the so-called LACAPCD Viewpoint. Mr. Hamming will present the LACAPCD method for calculating control requirements for Los Angeles and will concentrate on the Hamming Transform, which is a key step in this method.

Following Mr. Hamming, Dr. Dimitriades will present briefly the method recommended by EPA for calculating control requirements in SCAB or any other location.

Finally, Mr. Holmes, of the California Air Resources Board (CARB), will present the CARB procedure for deriving air quality standards (AQS) for HC and NO_x consistent with the AQS for oxidant and NO_2. This procedure alone does not constitute the entire method for calculating control requirements, but it is a key step.

Because the subject of these presentations is an extremely complex one, and because some members of the audience may not have had the opportunity to examine this issue closely, and finally, because there is much interest in the audience's response and evaluation of the various viewpoints to be presented, it is appropriate that some introductory explanations be given.

Within the interest framework of this meeting, the issue to be discussed is an issue regarding the accuracy and reliability of methods for calculating control requirements. Clearly, it is not an issue regarding the economics or the effects of control on life-styles,

etc. Not that these things are of no interest whatever--far from it; simply, they are not and cannot be of any interest to this meeting. The question to be dealt with here is the question of what are the relative accuracies and validities of the presently available methods for calculating control requirements for oxidant abatement.

After having established this context, the two main opposing viewpoints are, in general terms, as follows: The LACAPCD Viewpoint favors a method (for calculating control requirements) that relies primarily on smog chamber data and secondarily on aerometric data. Such smog chamber data exist and give a fairly complete definition of the dependence of oxidant on HC and NO_x. To circumvent the problem of uncertainty regarding applicability of smog chamber data in the real atmosphere, the LACAPCD method includes a procedure for empirically relating the smog chamber predictions to real atmosphere observations. This procedure is the so-called Hamming Transform that Mr. Hamming will elaborate upon.

The EPA Viewpoint favors a method that relies primarily on real atmosphere data and secondarily on smog chamber data. The EPA Viewpoint places the emphasis on the inherent validity of the aerometric data and maintains that in the interest of such validity, several limitations of the EPA method can be tolerated.

Both viewpoints have their strong and weak points. EPA has been and will continue to pursue development of both approaches; certainly, there is no commitment for life to one and the same method.

THE LACAPCD VIEWPOINT (HAMMING TRANSFORM) --*W. Hamming*

Summary

Mr. Hamming submitted the following written summary of his talk.

The "Hamming Transform" is a procedure involving smog chamber ozone concentrations formed using one maximum atmospheric concentration of NO_x and nonmethane, non-natural gas fraction of total hydrocarbons found to exist at downtown Los Angeles in the 6 to 9 a.m. period of the day during the smog season; this concentration is related to the one maximum ozone concentration measured in the smog season at Pasadena or Azusa later in the day, 1 to 3 p.m.

The frequency distribution of NO_x and its related hydrocarbons is determined by (1) weather and (2) motor vehicle emissions (i.e., their rate, not total tons). As the control program changes the ratio between the NO_x and the nonmethane, non-natural gas hydrocarbons, and as hydrocarbons are reduced, and as NO_x increases before being reduced, the position of the yearly smog season frequency distribution can be viewed as moving over the "reaction field" found from smog chamber results, increasing or decreasing in length from 0, 0 in the NO_x-hydrocarbon coordinate system to the calculated yearly smog season's maximum concentration at downtown Los Angeles. For each year's smog season only one point need be used to describe each such frequency distribution.

One could choose the midpoint, or the maximum, or even a point between, but one must be consistent. The point on the frequency distribution is not representative of the day on which the highest ozone was measured, it is to be representative of the whole frequency distribution at a given NO_x-hydrocarbon ratio. In the procedure leading to the Hamming Transform, the maximum point on the frequency distribution has been used. For convenience, this point has been related to the maximum ozone in the atmosphere and in smog chamber studies.

Presentation

In his talk, Mr. Hamming offered the following discussion:

Prior to the District making any claims as to how ozone varied with HC and NO_x, Haagen-Smit showed that although ozone can be formed from hydrocarbon and oxides of nitrogen in air and sunlight, ozone formation could be squelched if the hydrocarbon were in large excess. Similarly, ozone could be reduced as NO_x, especially NO, was increased. In other words there is an NO_x/HC ratio that produces the most O_3. Further, Stanford Research Institute demonstrated (1) that maximum eye irritation occured when the ratio between NO_x and hydrocarbons from auto exhaust was just right, and (2) that aerosol formation was maximized at high hydrocarbon to NO_x ratios. Further, Dr. Tuesday of General Motors was very insistent that NO increases were a way to control ozone formation.

The District's only claim to fame in this field is that under controlled conditions using typical traffic cycles, auto exhaust was generated (dynometer) and irradiated in 1000-ft^3 chambers. The reproduction of all these effects mentioned above was possible as the NO_x/HC ratio changed

1. High residual NO_2 was formed at high NO_x/HC ratios.
2. At lower NO_x/HC ratios there was no residual NO_2, but O_3 was maximized.
3. At slightly lower NO_x/HC ratios, EI was maximized.
4. At lower NO_x/HC ratios, aldehydes were maximized.
5. At still lower NO_x/HC ratios (high HC/NO_x), aerosol formation was maximized.

The figures shown in the paper "The Pathway to Clean Air" are derived from those test runs back in the 1960-63 period.

Some 2 years ago at the National Academy of Science, Dr. Altshuller presented diagrams of oxidant-ozone formation that were very similar to the one shown in our paper mentioned above.

Your own work showing the line of 1/10 ppm O_3 for 1 hour corresponds quite well with ours, considering ours was for instantaneous peaks of 1/10 ppm.

There ought to be no question that the field of NO_x-HC that forms ozone is sufficiently well defined to be useful in the control of ambient air concentrations. If the atmosphere were defined such that it would under all conditions be to the "left" of the 1/10 line, as in

the Dimitriades paper, ozone greater than 0.08 ppm could not form. This only requires that the ratio of NO_x (in grams per mile) to HC (in grams per mile) be greater than 1, preferably 2 or 3 (0.2 ppm NO_x, 0.5 ppm HC carbomation), a ratio (in ppm) of 4:10, or preferably 1:1.

In the paper "Calculations of Atmospheric Hydrocarbon Composition in Central Los Angeles" it was stated that, from a study of gas chromatographic air samples, there were only four sources of nonmethane hydrocarbon in downtown Los Angeles (DOLA). (1) auto exhaust, (2) blowby, (3) evaporation losses, and (4) natural gas (ethane, propane, and butane). No refinery hydrocarbon emissions were found nor was there any large or consist ent indication of solvent emissions. Total pollution tonages are not the correct "measure" to use. The non-methane, non-natural gas fraction of total hydrocarbons is the correct "measure" or factor to use in terms of concentration or proportional grams per mile emitted.[1,2]

Thus, from the NO_x frequency distribution, it is simpler to calculate this factor for hydrocarbons, and this is what has been done. For each year, the actual NO_x concentrations and the calculated nonmethane, non-natural gas fraction of total hydrocarbons were used toegther to describe an atmosphere on the NO_x-HC-ozone chart, Figure 55. Each year's data have some width, but are represented for convenience by a line.

This curve or "pathway" derived from motor vehicle emissions in DOLA slightly exceeds the maximum found and is thus an "upper limit curve" or "upper bound." All atmospheric data would fall below this curve. Now if this curve can, by control efforts, be made to cross over the "Dimitriades line" as will occur if the Federal Interim Standards for auto exhaust are continued until 1980 or if the California Standards for auto exhaust are made official by EPA until 1980, then, as shown in Figure 55 or 56 the oxidant value of this "upper bound" curve can only produce less ozone than 0.08 (or if you will less than 1/10 ppm). This only means that for that year the atmosphere represented by t line from zero-zero to the point on the "upper bound" curve could only produce 1/10 ppm or less. The true Los Angeles atmosphere, being slightly lower in NO_x and HC, would produce very slightly less ozone at Pasadena or Azusa.

It should be clearly understood that the transform only works for one point a year. It is of no value for day to day forecasting of ozone concentrations. The whole frequency distribution from zero-zero to the top point (for each year) is considered as a whole and is represented by one point each year. We only choose the "top" point (the highest one) to represent the frequency distribution of which one day produced the maximum ozone that year.

Discussion

Following numerous questions from the audience and explanations from Mr. Hamming, the procedure recommended by LACAPCD for relating oxidant to the oxidant precursors was, according to the understanding of the Chairman, Dr. Dimitriades, as follows:

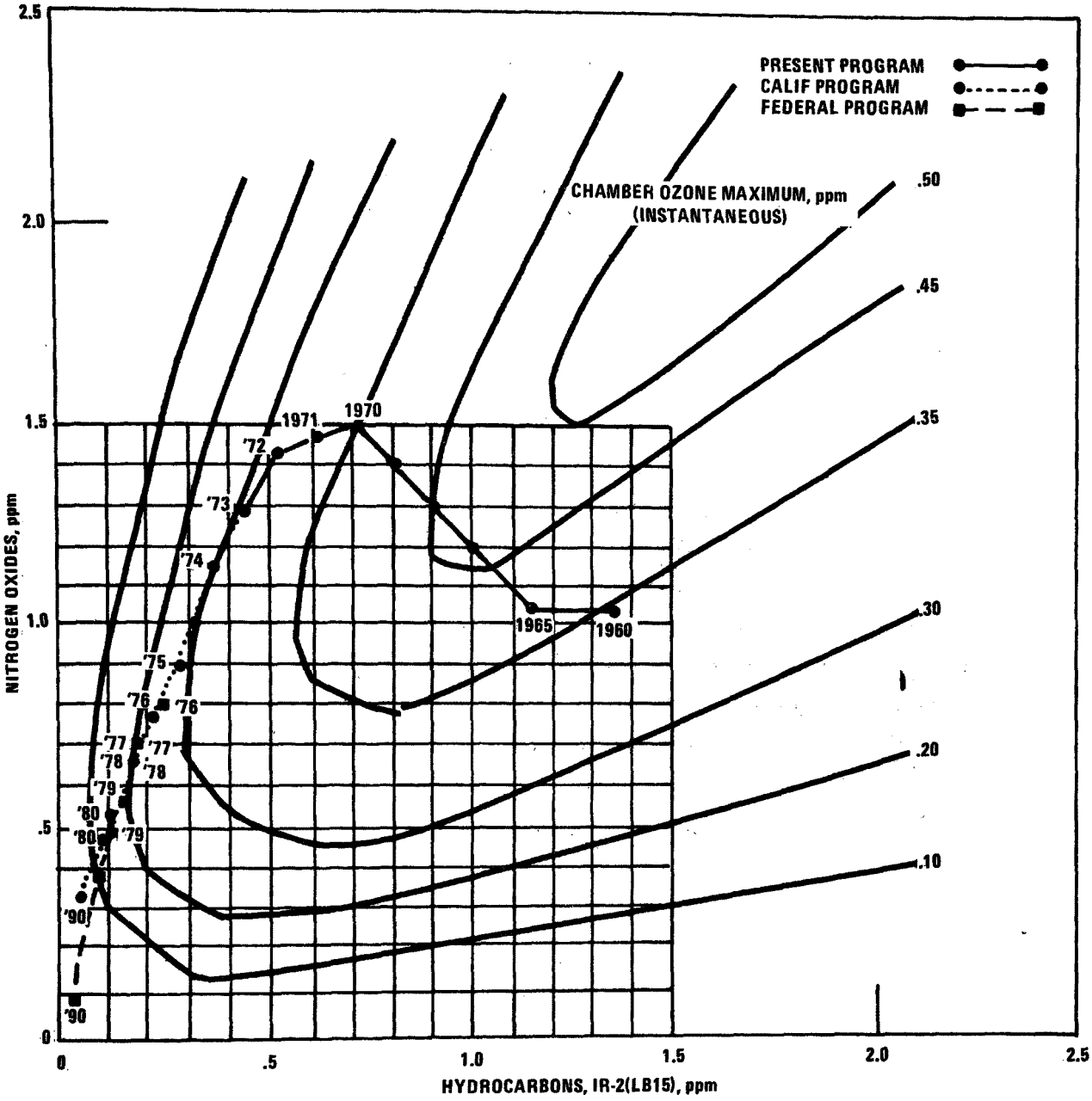

Figure 55. Ozone as a function of HC and NO_x, from smog chamber data.

The basis of the LACAPCD procedure is the O_x-HC-NO_x relationships derived from smog chamber studies[1] and depicted in Figure 55. The diagrams of Figure 55 are used to obtain the O_3 concentration value predicted by the smog chamber data for HC and NO_x concentrations equal to the maximum instantaneous concentrations observed in downtown Los Angeles (DOLA), during 6 to 9 a.m., in a given year. The concentration values for DOLA are used here because DOLA is the main source area whose air generally transports high levels of ozone into the main receptor area, Pasadena. Note that these maximum HC and NO_x concentration values are not always values of actually measured concentrations. They were calculated as follows: During the precontrol period 1960-65, the maximum instantaneous NO_x concentration--defined as the maximum on the frequency distribution plot--in

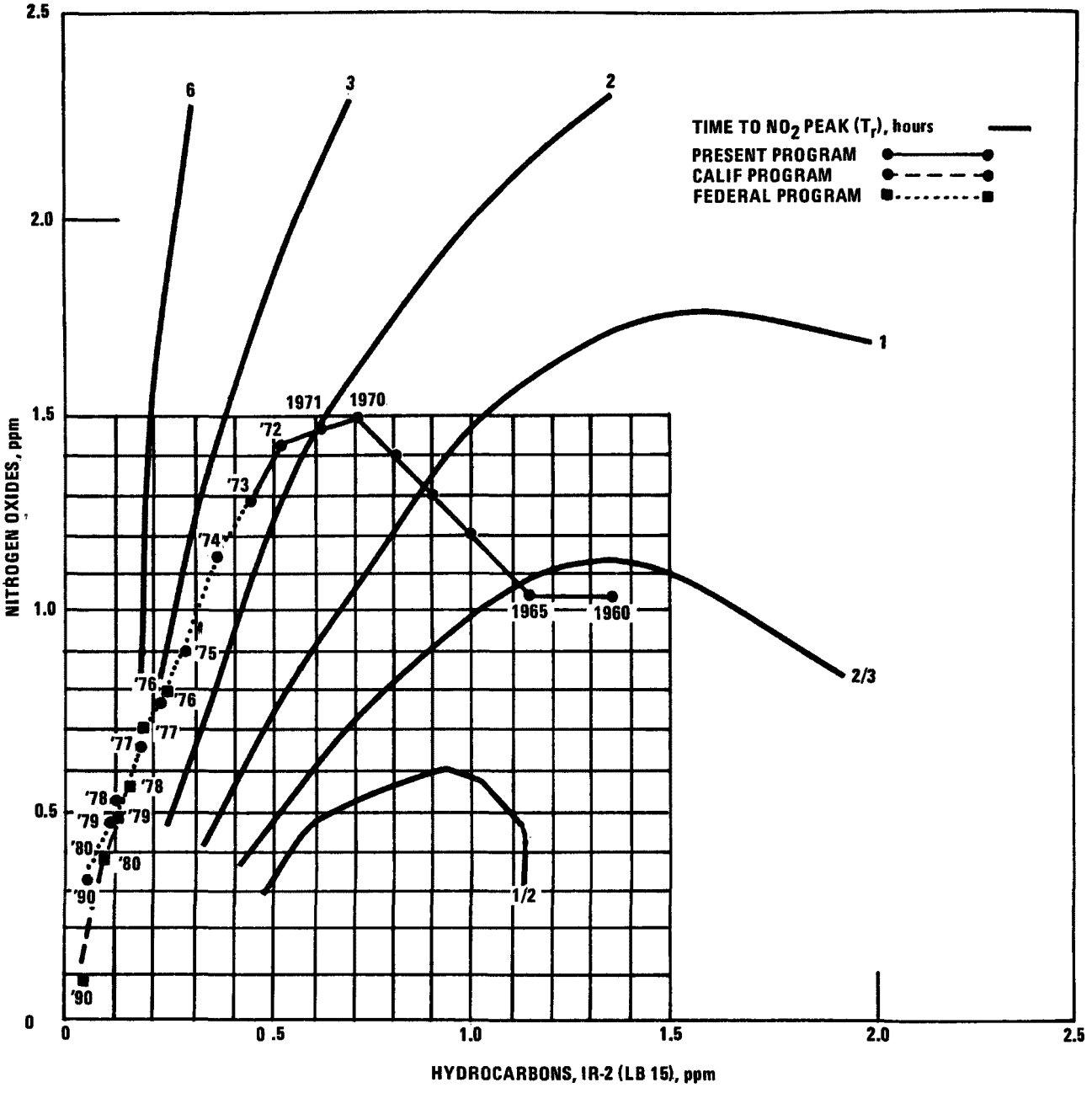

Figure 56. Time to maximum NO_2 as a function of HC and NO_x, from smog chamber data.

DOLA was 1.04 ppm; in 1955-60, the NO_x-to-HC ratio (as ppm-NO_x to ppm-hexane by non-dispersive infrared, instrument model LB-15A) in automobile emissions was 1.24 for the exhaust and 0.72 for the entire auto emissions mixture. From these data and from the auto emission factors derived for 1960-65 and for each of the subsequent years, values for the expected maximum (not to be exceeded) instantaneous concentrations of HC and NO_x were calculated for each of the subsequent years. Note that if in any year, the actually observed maximum NO_x concentration was higher than the calculated one, then this observed NO_x value was adopted instead, and was used to calculate the corresponding maximum HC concentration value.

From the O_3 concentration values read off the "chamber" plots (Figure 55), values for the O_3 concentrations expected in the ambient air are calculated by using the "Hamming Transform" equations and the diagrams of Figure 56. The Hamming Transform equations were derived as follows:

The concentration of O_3 in air was assumed to be a function of the "chamber" O_3 concentration, $[O_3]_{ch}$, as shown by Equation 1.

$$[O_3]_{air} = \frac{k_1 [O_3]_{ch} + k_2 [O_3]_{ch}}{D_f} \quad (1)$$

where k_1 is a factor greater than 1.0 that adjusts $[O_3]_{ch}$ for losses in the chamber due to unavoidable dilution, and k_2 is a factor denoting the additional ozone formation in air as a result of the continuous influx of fresh emissions as the air moves from the source area to the receptor area. D_f is a diffusion-related factor that is to be expressed in terms of a precursor concentration function; in fact, it is assumed that either one of the functions shown by Equation 2 is valid.

$$D_f = k_4[NO_x]^m [T_r]^n = k_4[S \cdot HC]^m [T_R]^n \quad (2)$$

In Equation 2, S is the presumably constant NO_x-to-HC (nonmethane, non-natural gas fraction) ratio in air, and T_r is the time to maximum NO_2 in the (smog chamber) irradiation of a given HC-NO_x mixture sample. Figure 56 is a graphical depiction of T_r as a function of HC and NO_x, as determined in the LACAPCD study.

Equations 1 and 2 are combined to yield Equation 3

$$\frac{[O_3]_{air}}{[O_3]_{ch}} = \frac{k}{[NO_x]^m [T_r]^n} \quad (3)$$

The three unknowns, k, m, and n, were determined by using smog chamber data and aerometric data. Thus, for each year the maximum NO_x concentration was estimated as described in the preceding paragraphs and its value was substituted for $[NO_x]$. From this value and from the known HC-to-NO_x ratio--obtained from auto emission factors--the maximum HC concentration was estimated and used to obtain the T_r value (from Figure 56). $[O_3]_{air}$ denotes the maximum O_3 concentration observed in Pasadena or Azusa--whichever is higher--in the year. Since there are data available for 14 years (1960-1973), it follows that there are 14 simultaneous equations that could be used to determine the unknowns k, m, and n. Nevertheless, because of their distinction (see Figure 57) only 6 year-points were used. More specifically, this is because a graphical depiction of the 14 year-points suggests that these points may fit a family of curves as shown in Figure 57. Of these curves, the one best defined is the one defined by 6 year-points (1960, 1965, 1969,1970, 1972, 1973). However, this curve does not reflect the most unfavorable meteorological conditions. Such conditions evidently occurred in 1971 when $[O_3]_{air}/[O_3]_{ch}$ had its highest value. Because of this and because the interest here is in relating O_3 to O_3-precursors for the most unfavorable meteorological conditions, the 6-point curve was transposed so as to go through the 1971 year-point. This is equivalent to first calculating values for k, m, and n, based

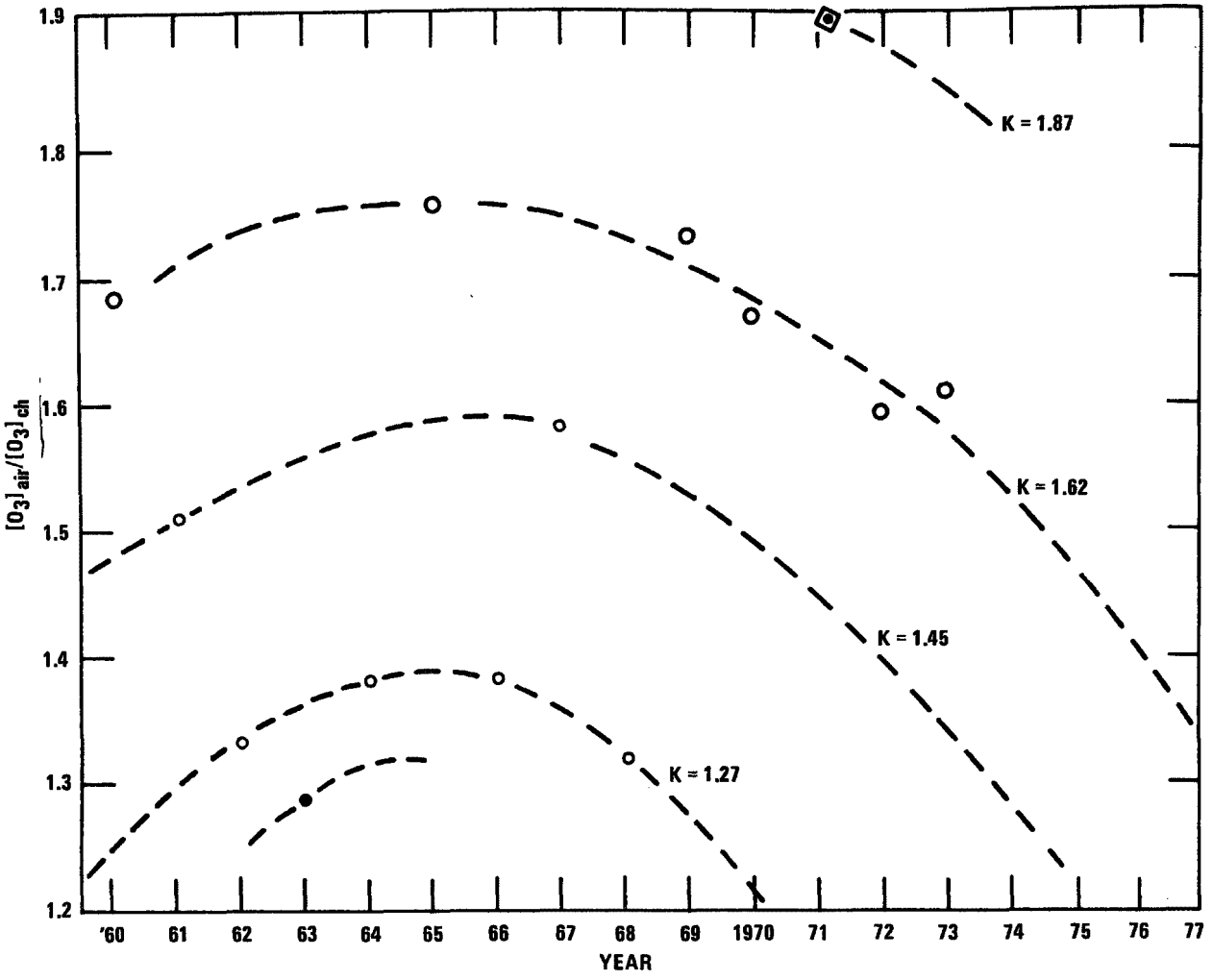

Figure 57. Variation of $[O_3]_{air}/[O_3]_{ch}$ with year.

on the 6 year-points (paired into three 2-year averages), and subsequently adjusting the k value so as to make the 6-year-point curve go through the 1971 year-point. Thus, the "Hamming Transform" equation becomes

$$\frac{[O_3]_{air}}{[O_3]_{ch}} = \frac{1.87\,[NO_x]^{0.222}}{[T_r]^{0.106}} \qquad (4)$$

for $[O_3]$ denoting maximum instantaneous O_3 concentration, or

$$\frac{[O_3]_{air}}{[O_3]_{ch}} = \frac{1.5\,[NO_x]^{0.222}}{[T_r]^{0.106}} \qquad (5)$$

for $[O_3]$ denoting maximum hourly average O_3 concentration.

THE EPA VIEWPOINT -- *B. Dimitriades, EPA*

The EPA approach to calculating control requirements for oxidant abatement involved the following steps:

1. Aerometric data from several cities were obtained and used to construct the so-called "upper limit" curve (Figure 58) that relates the 6 to 9 a.m. NMHC to the maximum 1-hour oxidant ever observed.

2. From the upper limit curve, the NMHC concentration value of 0.24 ppmC was derived as representing the maximum NMHC concentration consistent with the oxidant standard.

3. Control requirements in a region, e.g., Los Angeles, are calculated from the upper limit curve and the maximum 1-hour oxidant ever observed in the region.

The upper limit curve presently available for the Los Angeles basin was constructed from data taken at several points in the basin. These data points were plotted so as to relate the day's maximum 1-hour oxidant throughout the basin to the average of all 6 to 9 a.m. NMHC values obtained in the various monitoring stations in the basin.

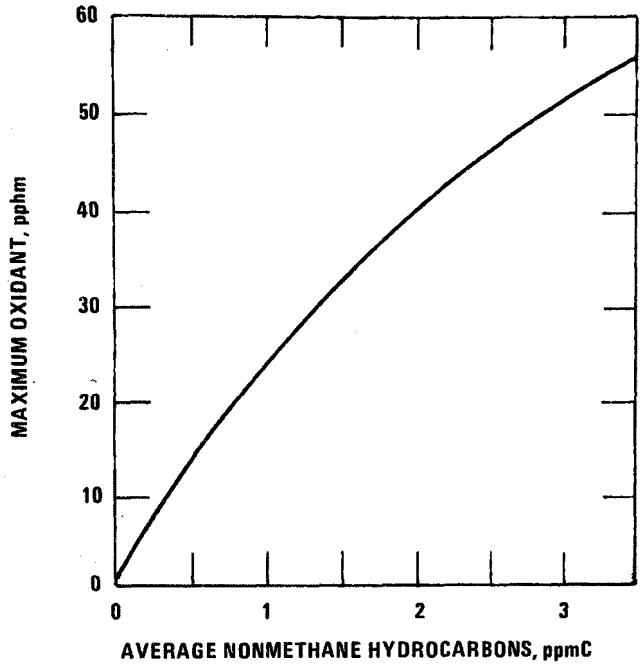

Figure 58. Upper limit oxidant values in the South Coast Air Basin as a function of average 6 to 9 a.m. nonmethane hydrocarbon concentrations, 1971 data. Oxidant concentrations are maximum 1-hour values for 12 stations; NMHC concentrations are average values for 8 stations.

The strong point of this method, according to the EPA viewpoint, is the high degree of inherent validity that results from use of real atmosphere data. While such validity is certainly not indisputable, it must be assumed that, conceptually at least, the aerometric data method should be more valid than any laboratory method.

Weaknesses of the EPA method and the EPA viewpoint regarding these weaknesses are as follows:

The EPA method has a conceptual limitation in spite of the realistic nature of its data base. This limitation arises mainly from the empirical nature of the upper limit curve. Because of this empirical nature, the upper limit curve, or any other empirical relationships of aerometric data, cannot be used with confidence to predict future air quality. To explain, the upper limit curve does not necessarily depict the dependence of oxidant on HC. The wide range of NMHC values shown in the plot reflects the variation in meteorological conditions affecting dispersion--e.g., wind speed--and not variation of the NMHC factor alone. Therefore, the upper limit curve, properly interpreted, could very well depict the dependence of oxidant on wind speed and not necessarily the dependence on NMHC. From a control standpoint, the upper limit curve, if interpreted properly, could mean that in order to reduce the oxidant down to the standard, the meteorological dispersion conditions throughout the day should be controlled in such a way that the 6 to 9 a.m. level of

NMHC is reduced down to 0.24 ppmC or less. Given this interpretation, an upper limit O_x/NO_x curve or O_x/CO curve would have just as much validity as the O_x/HC curve, since the 6 to 9 a.m. NO_x or 6 to 9 a.m. CO are just as good indicators of atmospheric dilution as the 6 to 9 a.m. HC.

In summary, then, the upper limit O_x/NMHC curve depicts either the dependence of oxidant on the dispersion factor or the dependence of oxidant on HC. The EPA viewpoint is that the upper limit curve can be assumed to depict the dependence of oxidant on NMHC.

The EPA assumption is supported by smog chamber data. Such data indicate that in simulated current atmospheres, in which the HC/NO_x is 10:1 or higher, reduction of HC or of both HC and NO_x (keeping HC/NO_x constant) will cause reduction in oxidant (Figure 59). This evidence in essence means that, insofar as the effect on ambient oxidant is concerned, the reduction of HC through emission control is, qualitatively at least, equivalent to reduction of the HC level through dispersion.

The other major limitation of the EPA method for calculating control requirements is that the method ignores the NO_x role in the oxidant formation process. The problem here is simple, and has been recognized only thanks to the smog chamber data available. If unilateral control of HC is adopted as the approach to oxidant control, then the HC-to-NO_x ratio will change with time to lower values resulting in stronger inhibition by NO. Such enhanced inhibition, in turn, will permit somewhat higher levels of HC in the atmosphere than the upper limit curve dictates. In conclusion then, the maximum NMHC level consistent with the oxidant standard should not be 0.24 ppmC but somewhat higher.

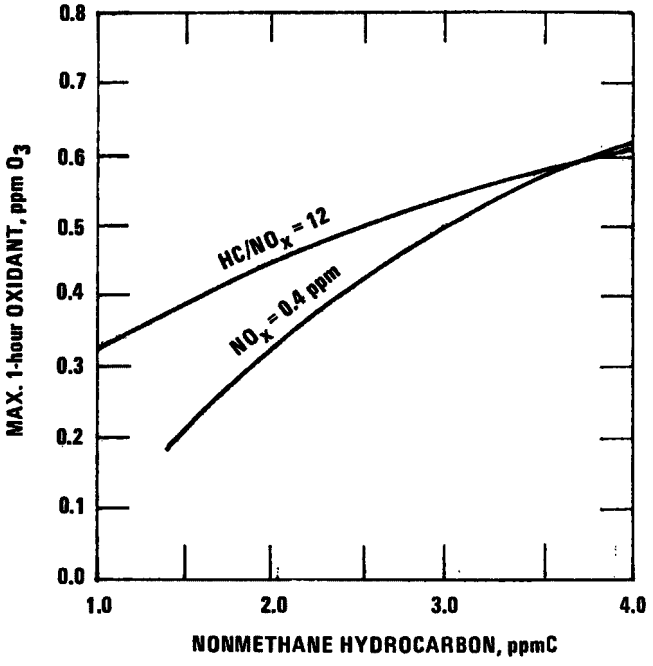

Figure 59. Smog chamber data on dependence of oxidant on NMHC under constant NO_x or HC/NO_x conditions.

EPA admits that this limitation of the EPA method is a real one. However, since the aerometric data are not sufficiently abundant to permit quantification of the NO_x role at this time, EPA feels that, for the present, this limitation should be tolerated as the lesser of the two evils. The other evil, of course, would be to use smog chamber data as the primary basis of the entire control strategy.

There are other limitations of the EPA method for calculating control requirements; however, the ones already discussed are the major ones and constitute the main points of disagreement between EPA and its critics.

To complete the presentation of the EPA veiwpoint on this issue, the following remarks are offered in regard to the proper use of the smog chamber data.

If smog chamber data are to be used to devise an oxidant control strategy, then, according to EPA viewpoint, such data should be used following the procedure illustrated in Figure 60. First, the smog chamber data are used to construct the 0.08-ppm O_3 isopleth (Figure 60). From this isopleth it can be deduced that in order to achieve the oxidant standard, ambient morning concentrations of HC and NO_x should be controlled so as to be within the shaded area of the graph. Here it should be pointed out that HC must be controlled somewhat more than what the minimum requirement is in order to ensure achievement of the oxidant standard even when the NO_x falls below its maximum value. To explain, EPA believes, and there are data to support such belief, that for HC at its maximum value, the NO_x may vary downward from its maximum value. Assuming that this HC/NO_x variation is real, it can be seen then that HC must be controlled somewhat more than this diagram requires. More specifically, HC must be controlled down to approximately 0.2 ppmC or even less. In conclusion then the smog chamber data, if used according to this EPA procedure, do not disagree with the dictates of the aerometric data analysis.

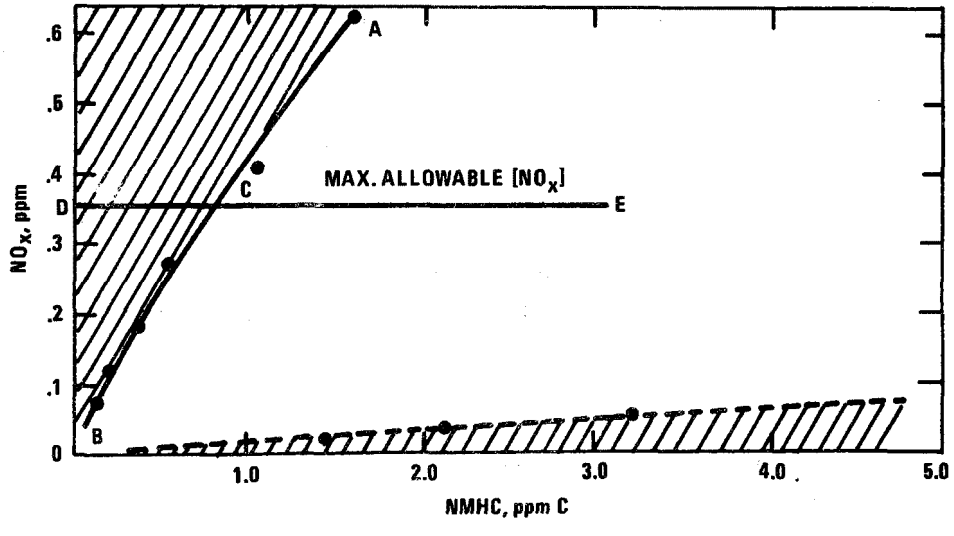

Figure 60. Equal response lines representing all combinations of NMHC and NO_x concentrations corresponding to 0.08 ppm O_3 of oxidant.

The following final remarks reflect this speaker's viewpoint, not necessarily adopted by EPA, regarding the relative validity and utility of the smog chamber and aerometric data.

While both the smog chamber method and the aerometric data method (for calculating control requirements) lack in validity at this time, the smog chamber method has a greater

potential for improvement than thought earlier. The aerometric data, in this speaker's judgment, have a certain degree of inherent validity because they are real atmosphere data. However, these data are also inherently limited in that they cannot be used to predict future levels of photochemical air quality. The fact that such data are taken from past and present day atmospheres simply makes them inappropriate for such use. For the extremely simple cases, e.g., the case of CO pollution, a trend analysis of atmospheric data may give valid predictions. However, the photochemical oxidant problem, even though it may be simpler than other photochemical pollution problems, still is too complex to be adequately defined and analyzed by aerometric data. The effects of HC/NO_x, HC composition, transport, and diurnal emission patterns, as well as the interactions among these effects, simply cannot be delineated based on aerometric data alone.

It is submitted here as a strong recommendation that (1) it should be set as a goal to develop a chamber methodology to the point that it would be possible to design photochemical pollution control strategies based on smog chamber data, and (2) aerometric data should be used as a guide in development of valid smog chamber methodology.

To obtain such aerometric data, it is recommended that field studies be specially designed and conducted to provide a few points in the true cause-effect relationship between HC, NO_x, and oxidant. Such points could then be used to validate or develop smog chamber methodology.

The "Hamming Transform" (discussed in preceding presentation) illustrates an alternative way of using atmospheric data to develop smog chamber methodology. However, I must reject this method as being inherently unreliable. The empirical nature of the correlation between smog chamber oxidant and observed ambient air oxidant makes this correlation inappropriate as a predictor of future air quality. Thus, this "transform" has the same disadvantages as those of the upper limit curve or any empirical relationship of atmospheric data, and it has the additional disadvantage that it has been derived from extremely few points. For this reason the objective here can be accomplished more reliably through specially designed field studies.

CALIFORNIA AIR RESOURCES BOARD VIEWPOINT* --

J. Holmes, F. Bonamassa, CARB

Introduction

The results of experiments conducted in a "new generation" of environmental chambers are currently becoming available. These chambers are characterized by radiation sources that closely approximate the UV portion of the solar spectrum as observed at the

*This presentation is based on a report entitled "Application of the Results of Recent Environmental Chamber Studies to the Control of Photochemical Oxidant," which is a preliminary draft. It has not been formally reviewed or released by CARB and should not be considered as representing the Board's policy. It has been given limited circulation for comment on its technical soundness and policy implications.

earth's surface and by clean, chemically inert interior surfaces that have a very low potential for decomposition of the ozone formed in the smog reaction. In this report, we summarize the results of two important studies and examine the implications of these results for the oxidant control strategy options in the South Coast Air Basin.

Environmental Chamber Studies

In this section, using some of these new data (which are still incomplete), we reexamine the relationships between hydrocarbon and NO_x concentrations with respect to ozone buildup rate, ozone concentrations, and ozone dosage. Of particular interest in this reexamination are the following aspects of the problem:

1. Ozone concentrations achieved during long (10-hour) irradiations.
2. Dependence of ozone concentration on initial NO_x concentration for long irradiation times.
3. Effect of dilution at constant $(HC)/(NO_x)$ ratio on ozone formation at various ratios.
4. Investigation of conditions under which initial NO_x concentration limits ozone potential.

The results of earlier chamber studies have defined the general relationship between oxidant formation and hydrocarbon reactivity and concentrations. For those concentrations of interest in the ambient atmosphere of the South Coast Air Basin (SCAB), any reduction in initial hydrocarbon concentration results in an increase in the time required to reach an ozone maximum and in a decrease in the maximum value attained, for a specified initial concentration of NO_x and period and intensity of UV irradiation. There are, of course, differences in reactivity among hydrocarbons. This question is beyond the scope of the present discussion, however. In general, olefins are more reactive in promoting ozone buildup, aromatics and paraffins are less reactive, and methane and acetylene are, in effect, unreactive. Carbon monoxide behaves as a very low reactivity hydrocarbon, insofar as its capability for promoting ozone buildup. Aldehydes and ketones behave as moderately reactive hydrocarbons in this regard.

The question of the effect of NO_x control on ozone buildup in the South Coast Air Basin is not a simple one. In the complex series of chemical reactions associated with photochemical smog, NO_2 serves as both an initiator and terminator of the chain reactions that cause (1) conversion of NO to NO_2, and (2) the buildup of ozone and other oxidants. Thus, for each level of nonmethane hydrocarbon there is an "optimum" level of NO_x that, in a static system, leads to maximum ozone dosage, for a specified period and intensity of UV irradiation.

Over most of the concentration range applicable to the ambient atmosphere, the results of environmental chamber studies clearly demonstrate that ozone dosage is a function of both initial hydrocarbon and NO_x concentrations and their ratio. Data relating initial

hydrocarbon and NO_x concentrations and resultant oxidant concentrations can be presented in several different ways, illustrating different aspects of the relationship. The simplest representation is the reaction profile, in which the concentration versus time behavior of the reactants and products are plotted on a two-dimensional graph. For the purposes of discussion, it is convenient to consider the overall process of photochemical smog formation to occur in three more or less well defined stages, each characterized by a different manifestation:

Stage	Typical characteristics
Phase I	Conversion of NO to NO_2
Phase II	Rapid buildup of O_3 accompanied by formation of gas-phase aldehydes and organic aerosol from olefins
Phase III	Continued buildup of O_3, but at an appreciably slower rate than in II, accompanied by formation of nitrate aerosol from NO_2

These stages are fairly sharply defined in static chamber experiments. In the atmosphere, there is appreciable overlapping of stages because fresh reactants are continually being injected into the reacting air mass.

Figure 61 shows the reaction profile for a typical smog chamber[3] run (hydrocarbon data are not shown). The initial reaction mixture contained 0.36 ppmC nonmethane hydrocarbon (NMHC) consisting of a surrogate mixture simulating auto exhaust and 0.05 ppm NO_x (an initial ratio of NMHC to NO_x about 6.9); the mixture was irradiated for 6 hours. Note that the rate of increase of the ozone concentration at the end of the run suggests that the system has appreciable potential for further ozone formation.

Figure 62 shows the reaction profile of a similar system irradiated for 10 hours. Note that ozone continues to build up at nearly a constant rate over the entire 4 hours of additional irradiation, reaching a level of 0.29 ppm, an increase of more than 50 percent over the value attained in the shorter run, 0.18 ppm.

These data were obtained by investigators at the Statewide Air Pollution Research Center, UC Riverside, under contract to the CARB.[3] The results of nearly 50 similar chamber runs demonstrate that, even at the lowest initial concentrations of hydrocarbon and NO_x, appreciable potential for ozone buildup remains in a polluted air mass after 6 hours of irradiation at full solar intensity.

Complete experimental data on the effect of initial NO_x concentration upon ozone buildup for long irradiation times are not yet available. However, estimates based upon an empirical extrapolation of the 6-hour SAPRC data[3] to longer irradiation times suggest that even at the lowest initial concentrations studied to date, 0.08 ppmC NMHC and 0.05

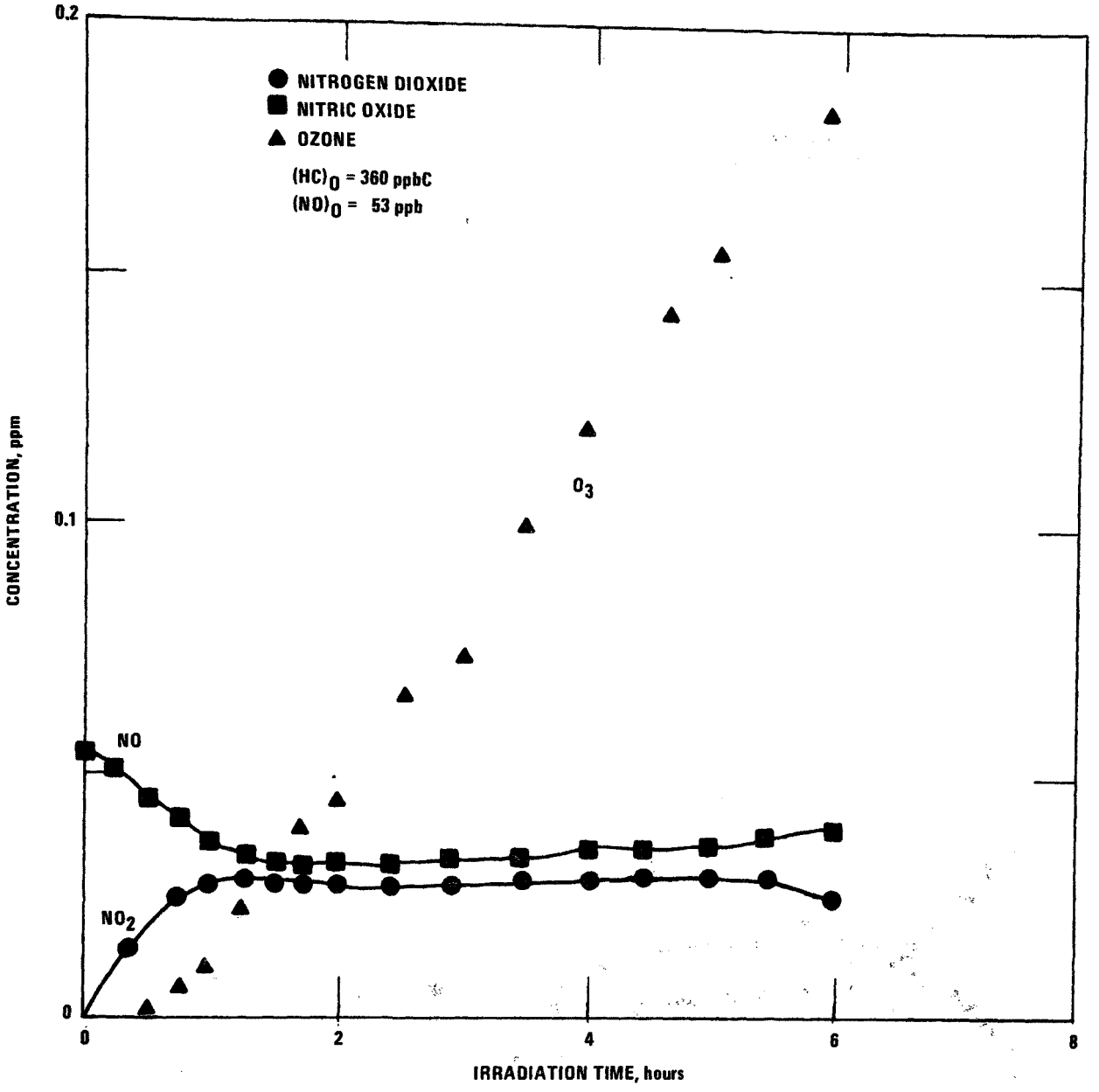

Figure 61. Reaction profile for SAPRC Run No. 42E, 6-hour irradiation.

ppm NO_x can lead to nearly 0.10 ppm ozone when the irradiation period is extended to 10 hours at full solar intensity.* These results are summarized in Table 15.

The data from Table 15, though still incomplete, have been used to generate crude ozone isopleths for 6-hour and extrapolated 10-hour irradiations (Figures 63 and 64). In addition, the final ozone buildup rates as a function of $(NMHC)_o$ and $(NO_x)_o$ have been plotted in Figure 65.

*Data cited by Leighton[4] for Los Angeles during the period around the summer solstice indicate that the total radiant flux between the hours of 6 a.m. and 6 p.m. (solar time) corresponds to 9 hours of irradiation at the maximum (solar noon) intensity.

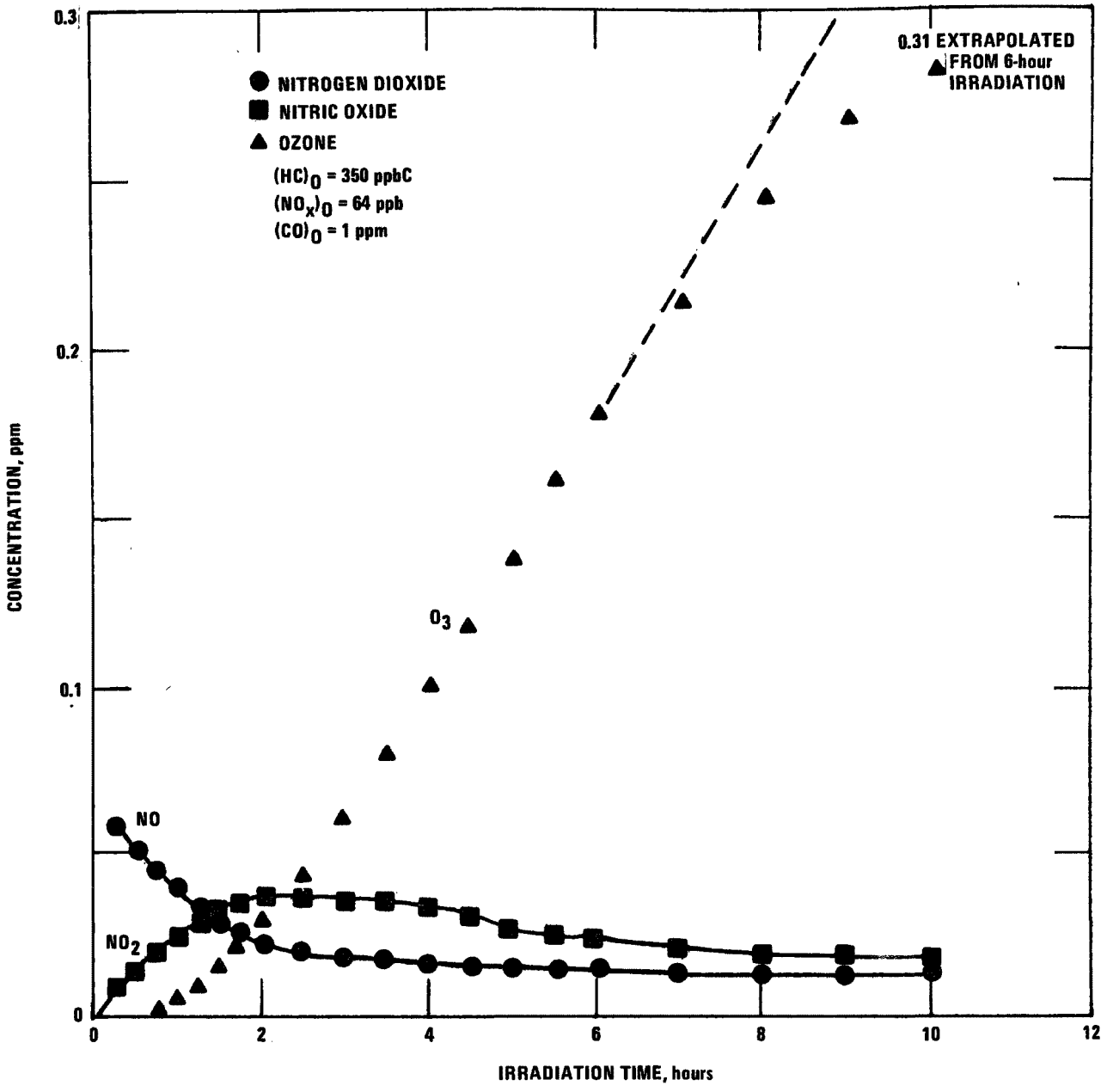

Figure 62. Reaction profile for SAPRC Run No. 48E, 10-hour irradiation.

The 6-hour data yield ozone isopleths generally in agreement with Dimitriades' extensive study of irradiated auto exhaust.[5,6] In particular, the SAPRC data reinforce Dimitriades' conclusion that initial levels of NMHC and NO_x of 0.80 and 0.33 ppm, respect tively, will not exceed the proposed levels of 0.08 ppm ozone for 1 hour and 0.25 ppm NO_2 for 1 hour. This conclusion applies only to static systems irradiated for 6 hours, however.

The ozone isopleths for the extrapolated 10-hour irradiations (Figure 64), assuming the procedure used to obatin them is reasonably valid, suggest several interesting, although tentative, conclusions:

Table 15. OZONE FORMATION, SAPRC GLASS CHAMBER

Run	$(NO_x)o$, ppm	(NMHC)o,[a] ppmC	$\frac{(NMHC)o}{(NO_x)o}$	6-hr O_3, ppm	$\frac{d(O_3)(5.5\text{-hr})}{dt}$, ppm hr^{-1}	Est.[b] of 10-hr O_3 ppm
10	0.286	1.92	6.7	0.44	0.091	0.71
11	0.362	1.97	5.4	0.26	0.073	0.48
12	0.362	1.96	5.4	0.26	0.074	0.48
13	0.167	2.08	12.5	0.48	0.057	0.65
14	-	-	-	-	-	-
15	0.095	2.11	22.2	0.41	0.019	0.47
16	0.007	2.39	341.4	0.14	0.021	0.20
17	0.082	1.96	23.9	0.39	0.024	0.46
18	0.047	2.03	43.6	0.31	0.020	0.37
19	0.038	2.18	57.4	0.20	0.017	0.25
20	0.103	0.56	5.4	0.30	0.056	0.47
21	0.160	0.67	4.2	0.24	0.068	0.44
22	0.025	0.60	24.0	0.16	0.024	0.23
23	0.283	2.28	8.1	0.33	0.075	0.55
24	0.276	0.73	2.6	0.12	0.035	0.22
25	0.009	0.81	90.0	0.14	0.019	0.20
26	0.085	0.85	10.0	0.35	0.031	0.44
27	0.088	0.61	6.9	0.27	0.047	0.41
28	0.169	0.70	4.1	0.19	0.044	0.32
29	0.285	0.64	2.2	0.07	0.029	0.16
30	0.285	0.74	2.6	0.06	0.019	0.12
31	0.268	0.60	2.2	0.06	0.018	0.11
32	0.230	0.64	2.8	0.06	0.022	0.13
33	0.269	-	-	-	-	-
34	0.088	0.63	7.2	0.25	0.041	0.37
35	0.171	0.67	3.9	0.17	0.043	0.30
36	0.191	0.58	3.0	0.12	0.030	0.21
37	0.025	0.77	30.8	0.16	0.022	0.23
38	0.198	0.63	3.2	0.10	0.036	0.21
39	0.191	0.74	3.9	0.13	0.035	0.23
40	0.052	0.73	14.0	0.25	0.020	0.31
41	0.050	0.72	14.4	0.20	0.015	0.24
42	0.052	0.36	6.9	0.18	0.031	0.27
43	0.105	0.37	3.5	0.14	0.040	0.26
44	0.031	0.43	13.9	0.11	0.020	0.17
45	0.125	0.43	3.4	0.10	0.029	0.19
46	0.050	0.08	1.6	0.06	0.014	0.10
47	0.010	0.37	37.0	0.10	0.030	0.19
48	0.064	0.35	5.5	0.18	0.043	0.31

[a] Surrogate mixture.

[b] Ozone concentration after 10 hours estimated by adding 3 x final O_3 rate to O_3 concentration at end of 6-hour irradiation.

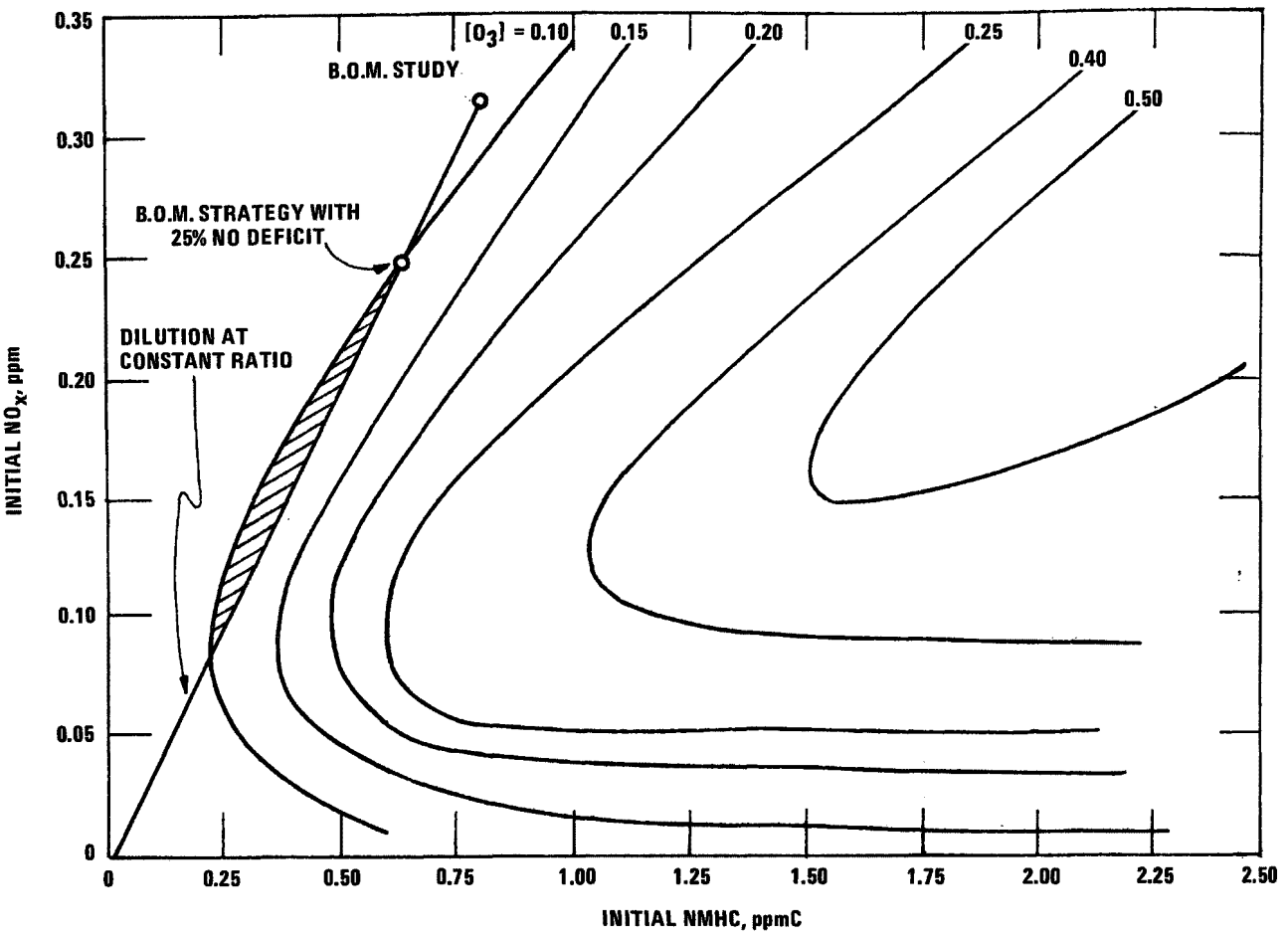

Figure 63. Ozone isopleths from 6-hour irradiations of HC-NO_x mixtures, SAPRC Runs 10 - 48 (E). [O_3] values are final 6-hour ozone concentrations (ppm).

1. Undiluted systems[5,6] suggested that the air quality standard for NMHC and NO_x will produce 0.12 to 0.15 ppm maximum ozone and exceed the 0.08 ppm standard for oxidant for well over 1 hour.
2. Very high levels of ozone (>0.5 ppm) can be produced from much lower concentrations of initial reactants than believed earlier.
3. The "optimum" ratio of NMHC to NO_x for ozone formation seems to be much lower--more nearly 7:1 than 10:1--for extended periods of irradiation.

The implications of the first item are obvious: if realistic worst-case irradiation times are used in chamber experiments, the permissible level of NMHC consistent with the 0.08 ppm oxidant standard is lower than that suggested by Dimitriades, perhaps 0.65 ppm NMHC.

On the other hand, the SAPRC data suggest that the NO_2 maximum at these levels and with an initial ratio of NO to NO_2 of about 9 to 1 is about 65 percent of the initial NO_x, so the allowable level of NO_x consistent with the 0.25-ppm air quality standard for NO_2 may be somewhat higher, perhaps as high as 0.37 ppm.

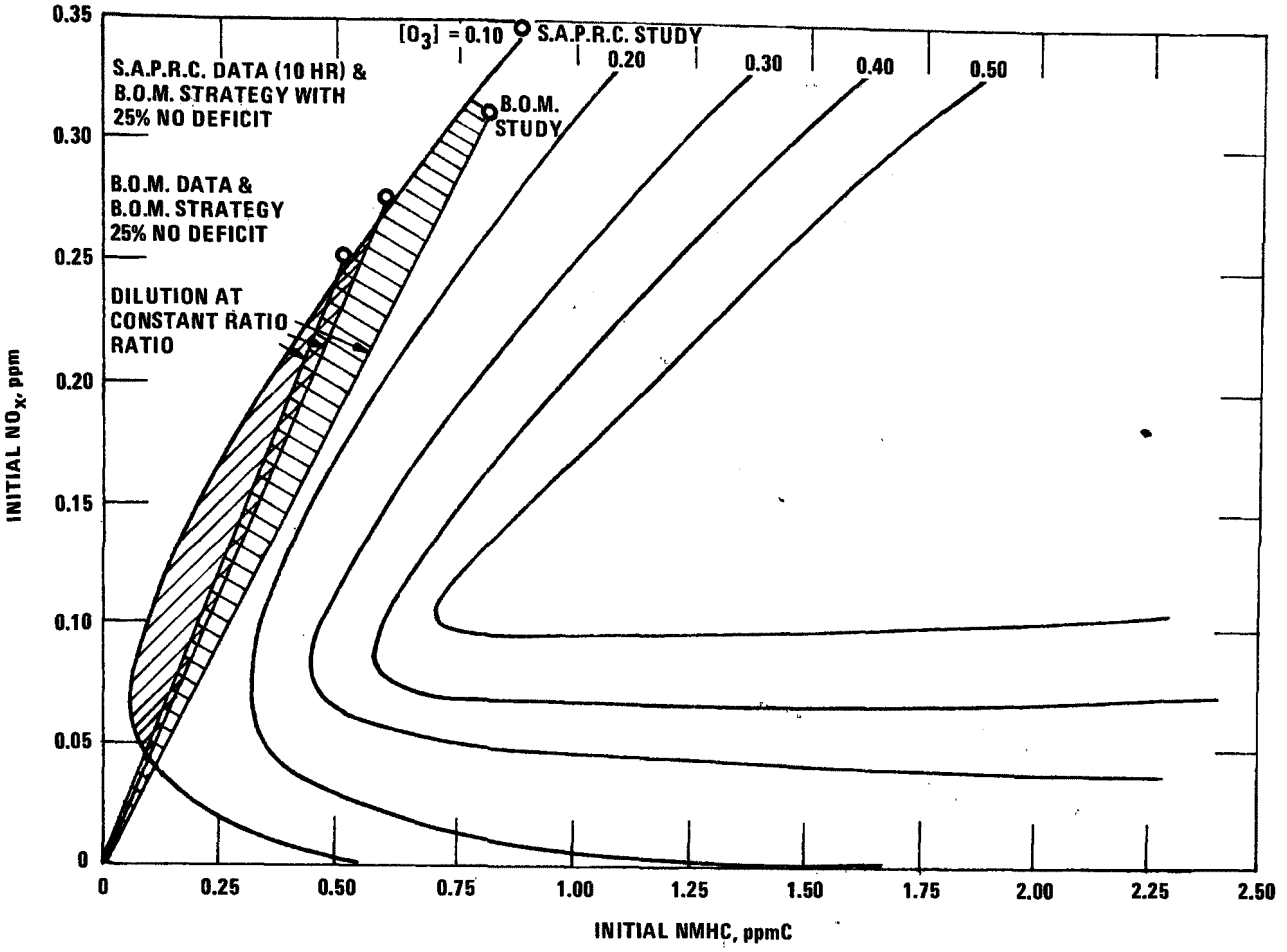

Figure 64. Ozone isopleths from 10-hour irradiations of HC-NO_x mixtures, SAPRC Runs 10 - 48 (E). $[O_3]$ values are final 10-hour ozone concentrations plus 3 times the final rate of ozone formation.

It should be pointed out, however, that the initial NO/NO_2 ratio of 9 to 1 used in the SAPRC studies is unrealistically high. Aerometric data indicate that the initial ratio in source areas of the SCAB during smog episodes can remain below 2 to 1 throughout the 6 to 9 a.m. NO emissions peak. Under these initial conditions, chamber experiments would exhibit a NO_2 maximum corresponding more closely to the value of 75 to 80 percent of the initial NO_x suggested by Dimitriades.[5,6]

The second conclusion suggests that the high ozone levels observed in the eastern portions of the SCAB can be accounted for, at least in part, by the long-term irradiation of polluted air masses moving from the urban-industrial source areas to receptor areas in San Bernardino and Riverside Counties over the span of 8 to 10 hours between the peak emission period and the time of the observed oxidant maximum.

If the third conclusion, regarding the "optimum" ratio of NMHC to NO_x for ozone formation under conditions of longer-term irradiation, is correct, this suggests that the ambient levels of NMHC and NO_x at many locations in the SCAB are currently at or near this optimum value. This, in turn, suggests that control strategies requiring reductions in the emissions of either NMHC or NO_x (or both) are likely to lead to a reduction of oxidant dosage.

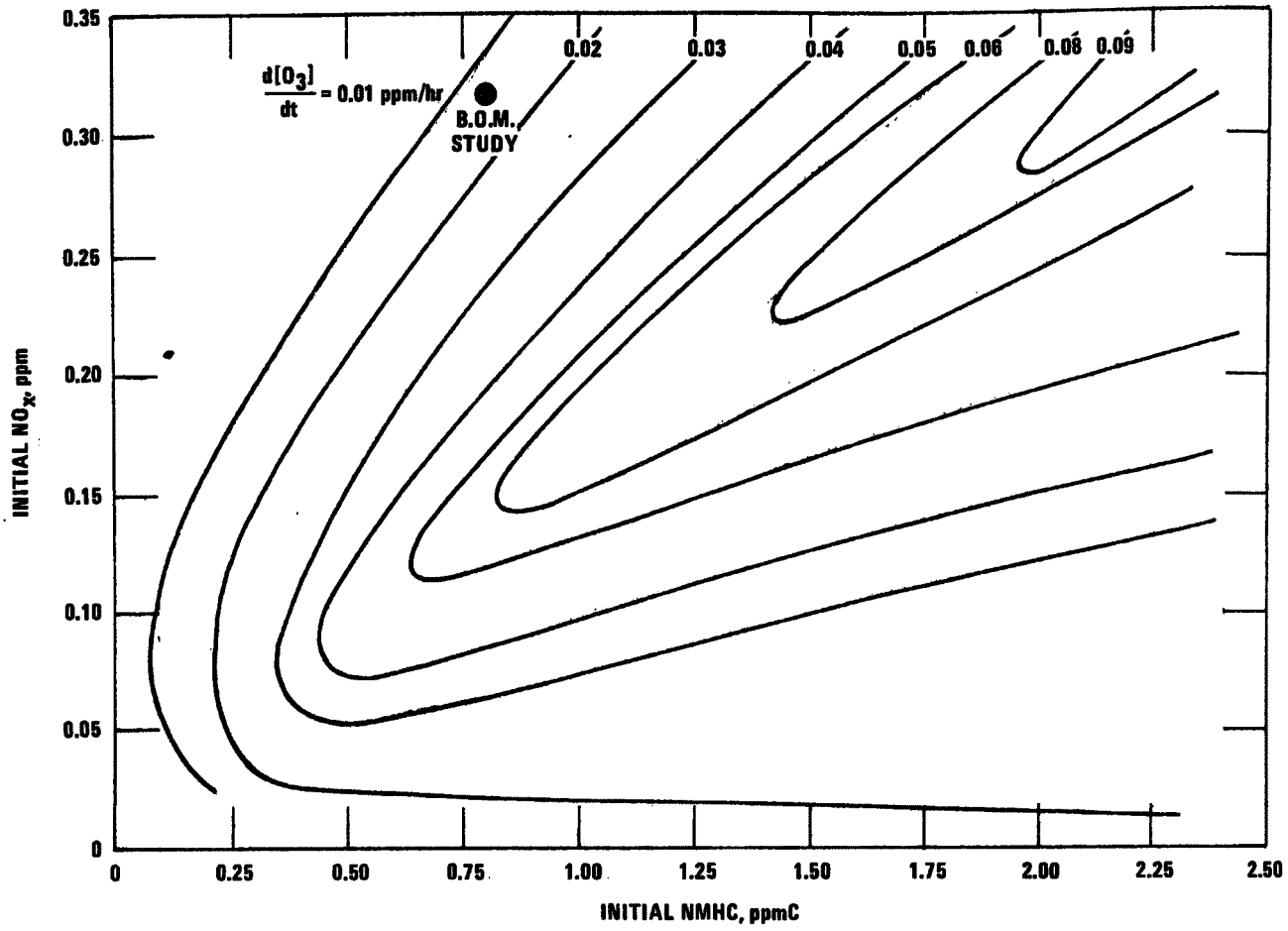

Figure 65. Ozone rate isopleths from 10-hour irradiations of HC-NO_x mixtures, SAPRC Runs 10 - 48 (E).

A recent analysis presented by Hamming et al.[1] suggests that any reduction in NO_x alone would lead to an increase in oxidant. This is somewhat misleading; such a strategy would lead to somewhat more rapid onset of ozone buildup, since Phase I of the smog formation process would be shortened, but, under similar conditions of mixing, irradiation, and dilution, the maximum hourly average ozone concentration achieved in a given air mass would be lowered, and total ozone dosage would be reduced over most of the trajectory of the air mass.

The extensive study of Dimitriades[5,6] of ozone buildup in irradiated auto exhaust at somewhat higher levels than in the SAPRC study at various NMHC to NO_x ratios provides another useful data base for determining an oxidant control strategy for the SCAB. Here again, however, the irradiations extended over only 6 hours at somewhat less than full solar intensity, so the possibilities for long-term ozone buildup were not assessed in his analysis of the data. The original reaction-profile data have not been made available to CARB, so empirical extrapolations to a 10-hour irradiation cannot be made.

The principal result of Dimitriades' study is the familiar plot of "equal response" lines (Figure 60) defining ranges of initial NMHC and NO_x concentrations at which the oxidant standard is not exceeded.

In addition to the short irradiation time, several other problems must be taken into consideration when one attempts to interpret these results in terms of a control program. Dimitriades[5] has criticized Hamming's[1] application of these results to produce a timetable for the achievement of the oxidant standard in Los Angeles County. Moreover, Dimitriades has not taken into account the effects of dilution on the reactivity of an air mass containing an initial burden of NMHC and NO_x corresponding to the target levels he proposes.

Dimitriades' data are presented in two different formats in Figure 66. In proposing levels of 0.80 ppm NMHC and 0.33 ppm NO_x he is attempting to take full advantage of the so-called inhibitory[7] effect of NO_x while just maintaining the air quality standard for NO_2.

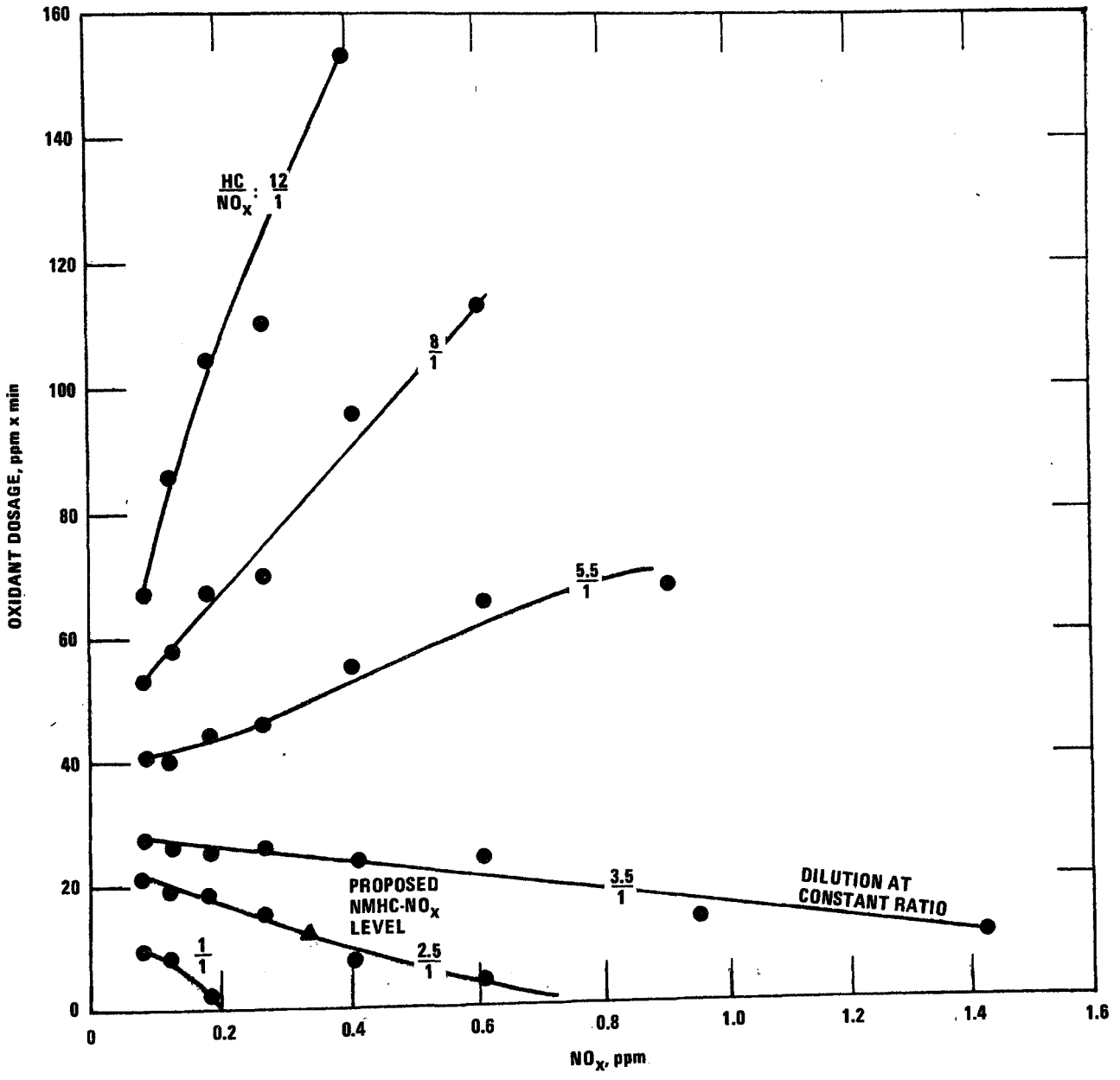

Figure 66. Oxidant-dosage reactivity of exhaust as a function of NO_x at various HC:NO_x ratios.

It is apparent from Figure 66 that dilution at constant ratio of an air mass containing the correct levels of NMHC and NO_x will increase the oxidant-dosage reactivity of the system to a point at which the oxidant standard will be exceeded unless further dilution occurs.

Dimitriades[5] points out a further problem associated with day to day variations in the relative emissions of NMHC and NO_x. Success of a strategy based on the inhibitory effect of NO requires that some minimum amount of NO be emitted to prevent or at least delay ozone buildup. This is not a trivial problem, since the abnormal traffic conditions that produce maxima in NMHC (stop and go, low average speeds) coincide with minimum NO_x emissions from autos.

Clearly, a strategy that relies upon the inhibitory effect of NO must take into account the effects of both dilution of the air mass and the possibility of a deficit in NO emissions altering the ratio of NMHC to NO_x.

Conclusions

The discussion in the preceding section points out that an oxidant control strategy based on the inhibitory effects of NO, such as that proposed by Dimitriades.[5,6] must be modified to take into account the effects of dilution, NO deficit, and long-term irradiation.

First, one must determine the effects of extended irradiation. Complete experimental data are lacking, so we have generated the empirical ozone isopleths in Figure 64 to represent such conditions. Second, the maximum allowable NO_x concentration consistent with the 0.25-ppm 1-hour maximum for NO_2 must be determined. Both the Bureau of Mines and SAPRC studies suggest that this is about 0.35 ppm NO_x.

Third, one must make some sort of worst-case estimate of the NO_x deficit expected in the day to day variations in NMHC and NO_x emissions. Auto emissions data suggest that a value of 25 percent is not unreasonable, although a thorough and continuing check of air quality data will be required to determine the validity of this estimate.

Finally, a maximum value of initial NMHC consistent with this lower value of NO_x must be determined from the isopleths in Figure 64 or, when they become available for the SAPRC data, oxidant dosage plots such as in Figure 66. The isopleth plot, Figure 64, yields a maximum allowable initial concentration of NMHC of about 0.60 ppmC.

A similar estimate using the Bureau of Mines data yields a maximum value of about 0.50 ppmC of NMHC. This lower value reflects the higher yield of NO_2 reported by Dimitriades.[5,6]

The effects on reactivity of dilution at constant ratio from the various initial mixtures shown in Figure 64 can be estimated from the relationship between the isopleths and lines drawn to the origin. The mixture corresponding to the 10-hour SAPRC data, using the Bureau of Mines strategy with a 25 percent NO deficit, goes through a reactivity maximum corresponding to about 0.14 ppm oxidant at a dilution of about 2 to 1. Similar dilution effects are predicted for the other mixtures discussed above.

On the basis of these considerations, it is our best judgment that ambient levels of NMHC and NO_x cannot exceed approximately 0.60 ppmC and 0.35 ppm, respectively, if both a standard of 0.25 ppm NO_2 (1-hour maximum) and a revised oxidant standard of 0.12 ppm are to be achieved in the South Coast Air Basin.

Unresolved Questions

The analysis and conclusions presented here do not take into account several important factors that have an influence on the ultimate levels of NMHC and NO_x required to achieve the oxidant standard. Briefly, these are:

1. The effects of carry-over or "aged smog" on the validity of the proposed limits on 6 to 9 a.m. emissions, particularly with respect to fraction of initial NO_x appearing as NO_2.
2. The effect, if any, of downward mixing of ozone trapped aloft overnight on ground level concentrations of ozone the following day.
3. The efficiency of conversion of NO_x emissions to nitrate aerosol under the proposed conditions for the achievement of the oxidant standard and the related health-effects question.

All of these questions are currently under investigation by CARB and other agencies. Our current view of the oxidant control problem may need to be altered when the results of these and other studies in progress become available.

SMOG CHAMBER STUDIES OF POLLUTANT PRECURSOR RELATIONSHIPS -- *B. Dimitriades, EPA*

Continuing and recently initiated photochemical pollutant-precursor relationship studies in EPA are as follows:

1. Oxidant-precursor Relationships and Their Dependence on Pollutant Transport Conditions--The study calls for smog chamber testing of synthetic and auto exhaust HC-NO_x mixtures under conditions similar to those in moving air masses, namely, continuous dilution, continuous injection of reactants, prolonged irradiation, and repeated irradiation. Objective is to obtain and compare O_x/HC/NO_x relationships for simulated transport and nontransport conditions.
2. Oxidant-precursor Relationships and the Impact of HC Control on Such Relationships--The study calls for smog chamber testing of synthetic and auto exhaust HC-NO_x mixtures simulating atmospheric pollutant makeup before and after application of HC control. Objective is to obtain and compare O_x/HC/NO_x relationships for simulated precontrol and postcontrol atmospheres.
3. Sulfate-precursor Relationships in Area-wide Systems and in Roadway Systems --The study calls for smog chamber testing of synthetic and auto exhaust

$NC/NO_x/SO_2$ mixtures under conditions similar to those in area-wide atmospheres and roadway atmospheres. Objective is to determine the rate of SO_2 oxidation under the conditions of the study, and to explore the effects of factors such as the HC, NO_x, and SO_2 reactant concentrations, humidity, HN_3, and primary aerosol, upon such rate.

4. Photochemical Aerosol-precursor Relationships--The study calls for smog chamber testing of synthetic $HC/NO_x/SO_2$ mixtures under conditions similar to those in urban and rural atmospheres. Objective is to determine the effect of factors such as reactant concentration, humidity, NH_3, and primary aerosol on photochemical aerosol formation.

5. NO_2-precursor Relationships and the Impact of HC Control on Such Relationships--The study--nearly completed--involves smog chamber testing of synthetic HC/NO_x mixtures in an outdoor smog chamber. Objective is to determine the dependence of photochemically formed NO_2 on reactant NO_x and HC, and to explore advantages and disadvantages of outdoor operation of smog chambers.

6. Smog Chamber Studies for Photochemical Model Development--The program involves modeling of smog chamber data taken with a variety of smog chambers and on a variety of HC/NO_x and $HC/NO_x/SO_2$ systems.

REFERENCES FOR CHAPTER 6

1. Hamming, W.J., R.L. Chass, J.E. Dickinson, and W.G. MacBeth. Motor Vehicle Control and Air Quality: The Path to Clean Air for Los Angles.. Los Angles County Air Pollution Control District, Los Angles, Calif. (Presented at 66th Annual Air Pollution Control Association Meeting. Chicago. June 24-28, 1973. Paper No. 73-73.)

2. Calculations of Atmospheric Hydrocarbon Composition in Central Los Angeles.

3. Pitts, J.N. et al. Quarterly Progress Report, CARB Contract No. 3-017. Statewide Air Pollution Research Center, University of California, Riverside, Calif. December 31, 1973.

4. Leighton, P.A. The Photochemistry of Air Pollution. New York, Academic Press, 1961. p. 31.

5. Dimitriades, B. On the Function of Hydrocarbon and Nitrogen Oxides in Photochemical-smog Formation. U.S. Bureau of Mines. Washington, D.C. Document RI-7433. 1970.

6. Dimitriades, B. U. S. Environmental Protection Agency, Research Triangle Park, N.C. Private Communication.

7. Glasson, W.A. and C.S. Tuesday. Environ. Sci. Technol. 4: 37, January 1970.

7. CONCLUSION

B. Dimitriades

A conference was conducted by EPA at its Research Triangle Park, North Carolina, Environmental Research Center, for the purpose of reviewing present status and utility of smog chamber methodology. Specific objectives of the conference were to review on-going smog chamber studies sponsored by EPA, to assess and explain performance differences among existing smog chambers, to identify methodology deficiencies, and to discuss the utility of the smog chamber method in development of photochemical pollution control strategies.

Smog chamber performance was examined in the light of recent experimental evidence that showed that disagreement in test results among different chambers must be caused, partly at least, by differences in chamber design. Thus, intensity and spectral character of radiation, surface-to-volume ratio, and nature and condition of wall surface were reported to significantly affect chamber measurements. Increased photolysis of HONO and aldehydes was offered as a mechanistic explanation of the observed enhancive effect of low wavelength radiation upon reactivity manifestations. The existence of wall-material effects was interpreted to suggest that heterogeneous reaction steps are important and, hence, should be identified and included in the reaction mechanism models. Also, such effects seem to be minimized in large chambers (several hundred cubic feet) made of Teflon film.

The analytical methods commonly used in smog chamber experimentation were reported to lack in several respects. Methods for NO_2 measurement suffer from as yet unresolved interference problems. Thus, the Saltzman method was shown--but not unequivocally proved--to suffer from O_3 interference, whereas the chemiluminescence method was found to respond to several nitrogen compounds other than NO_2 (e.g., PAN, alkyl nitrates, nitric acid). Methods used for photochemical sulfate measurement were the barium chloranilate and the barium perchlorate methods; the chloranilate method seemed to be somewhat inferior. In situ measurement by infrared spectroscopy was reported to be feasible and useful in smog chamber studies, especially for identification and measurement of unstable species. Measurement of nonmethane hydrocarbon using certain commercial instruments was reported to be inaccurate, perhaps because of improper calibration. Finally, recommendations were made to standardize among EPA contractors and grantees (1) calibration procedures of instrumental methods, (2) statistical expressions of accuracy and precision of smog chamber measurements, and (3) definitions of chemical reactivity manifestations.

Evidence regarding chamber background reactivity was summarized and interpreted to suggest that trace levels of (nonmethane) organic and NO_x contaminants (a few parts

per hundred million) could cause, upon irradiation, significant ozone accumulation and oxidation of SO_2 into sulfate. The evidence suggested, furthermore, that in such background activity, wall surface also has a role other than merely providing an interface for adsorption-desorption phenomena.

The issue of comparability of smog chamber atmosphere and real atmosphere was examined using two approaches. By one approach, comparability should be established using real atmosphere and smog chamber data on the cause-effect relationship between ozone and ozone precursors. By the other approach, comparability should be assumed, provided the dynamic character of real atmosphere is adequately simulated in the smog chamber. Within the context of this latter approach, the performance of a dual, Teflon-made smog chamber operated outdoors was discussed and reported to be promising.

The validity and utility of smog chamber data were examined in connection with a case study of the oxidant problem in California's South Coast Air Basin (SCAB). The EPA and Los Angles County viewpoints and methods for calculating control requirements were presented and contrasted. New smog chamber data generated at University of California's Statewide Air Pollution Research Center under California Air Resources Board contract were interpreted to derive air quality standards for HC and NO_x, consistent with the ozone and NO_2 standards. EPA prefers aerometric data--rather than smog chamber data--as the primary basis for deriving control requirements for oxidant abatement. Nevertheless, EPA is committed to pursuing all three investigative methods--aerometric data analysis, smog chamber method, modeling--in the effort to develop control strategies based on sound and completely scientific evidence.

The conference made it clear that in the study of photochemical pollution problems, smog chamber experimentation is indispensable for studying the photochemical pollutant formation process and for providing estimates of precursor control requirements. The conference suggested also that the present analytical measurement problems are neither critical nor insurmountable. Furthermore, the limitations of the smog chamber method due to lack of inherent validity are not necessarily prohibitive. It appears that with further research the smog chamber method could be developed to the point that smog chamber data would be equally or more valid than data taken by any other method. In the light of such a promise, EPA intends to sustain a smog chamber study program directed to several photochemical pollution problems, including the problems of ozone, NO_2, photochemical aerosol, sulfates, and nitrates.

LIST OF ATTENDANTS

A. P. Altshuller
Environmental Protection Agency
National Environmental Research Center
Research Triangle Park, NC 27711

Dick Angus
Environmental Protection Agency
Durham, NC

Stephen Aust
Bureau of Air Quality Control
Dept. of Health and Mental Hygiene
Environmental Health Administration
610 N. Howard Street
Baltimore, MD 21201

Joseph Behar
Environmental Protection Agency
P.O. Box 15027
Las Vegas, NV 89114

J. J. Bufalini
Environmental Protection Agency
National Environmental Research Center
Research Triangle Park, NC 27711

Marijon Bufalini
Environmental Protection Agency
National Environmental Research Center
Research Triangle Park, NC 27711

Peter Connell
Latimer Hall
University of California
Berkeley, CA

F. M. Covington
EPA Region IX
100 California Street
San Francisco, CA 94111

Kenneth Demerjian
Calspan Corporation
4455 Genesee Street, P.O. Box 235
Buffalo, NY 14221

M.C. Dodge
Environmental Protection Agency
National Environmental Research Center
Research Triangle Park, NC 27711

G. J. Doyle
Department of Chemistry
University of California
Riverside, CA 92502

A. H. Ellison
Environmental Protection Agency
National Environmental Research Center
Research Triangle Park, NC 27711

C. E. Feigley
Dept. of Environmental Science
and Engineering
School of Public Health
University of North Carolina
Chapel Hill, NC 27514

Don Fox
Dept. of Environmental Science
and Engineering
School of Public Health
University of North Carolina
Chapel Hill, NC 27514

Bruce Gay
Environmental Protection Agency
National Environmental Research Center
Research Triangle Park, NC 27711

Sydney Gordon
Environmental Protection Agency
National Environmental Research Center
Research Triangle Park, NC 27711

William Greenburg
Sun-Telegram
San Bernardino, CA

W. J. Hamming
2428 Lee Avenue
Arcadia, CA 91006

P. H. Hanst
Environmental Protection Agency
National Environmental Research Center
Research Triangle Park, NC 27711

T. A. Hecht
Systems Applications Inc.
950 Northgate Drive
San Raphael, CA 94903

J. Holmes
Air Resources Lab.
9528 Telstar Avenue
El Monte, CA 91731

Joel Horowitz
Environmental Protection Agency
Washington, DC

C. M. Huang
Research Analyst, Air Quality Branch
Tennessee Valley Authority
Muscle Shoals, AL 35660

R. J. Jaffe
Dept. 56-20, Bldg. 151
Lockheed M. S. Co.
Sunnyvale, CA 94088

Harvey Jeffries
Dept. of Environmental Science
and Engineering
School of Public Health
University of North Carolina
Chapel Hill, NC 27514

Richard Johnson
Environmental Protection Agency
Durham, NC

S. Joshi
Environmental Protection Agency
National Environmental Research Center
Research Triangle Park, NC 27711

Richard Kamens
Dept. of Environmental Science
and Engineering
School of Public Health
University of North Carolina
Chapel Hill, NC 27514

D. B. Kittleson
Dept. of Mechanical Engineering
University of Minnesota
Minneapolis, MN 55455

W. C. Kocmond
Calspan Corporation
4455 Genesee Street, P.O. Box 235
Buffalo, NY 14221

Richard L. Kuntz
Environmental Protection Agency
National Environmental Research Center
Research Triangle Park, NC 27711

Daniel Lillian
U.S. Army Env. Hygiene Agency
Air Pollution Engineering Division
Edgewood Arsenal, MD 21014

William Lonneman
Environmental Protection Agency
National Environmental Research Center
Research Triangle Park, NC 27711

F. J. Malcolm
School of Public Health
University of North Carolina
Chapel Hill, NC 27514

David Miller
Battelle
505 King Avenue
Columbus, OH

Ron Mueller
EPA Region IX, 100 California Street
San Francisco, CA 94111

Robert Neligan
Environmental Protection Agency
Durham, NC

John Overton
Environmental Protection Agency
National Environmental Research Center
Research Triangle Park, NC 27711

Joseph Padgett
Environmental Protection Agency
Durham, NC

Joseph Paisie
Bureau of Air Quality Control
Dept. of Health and Mental Hygiene
Environmental Health Administration
610 N. Howard Street
Baltimore, MD 21201

T. R. Powers
Exxon Research and Engineering
P.O. Box 51
Linden, NJ 07036

R. A. Rasmussen
Air Pollution Research Section
College of Engineering
Washington State University
Pullman, WA 99163

P. C. Reist
Dept. of Environmental Science
and Engineering
School of Public Health
Univerity of North Carolina
Chapel Hill, NC 27514

L. A. Ripperton
Research Triangle Institute
Research Triangle Park, NC 27709

Joe Sickles
Dept. of Environmental Science
and Engineering
School of Public Health
University of North Carolina
Chapel Hill, NC 27514

J. Singh
Dept. of Environmental Science
Rutgers University
New Brunswick, NJ 08903

John Spence
Environmental Protection Agency
National Environmental Research Center
Research Triangle Park, NC 27711

C. W. Spicer
Battelle
505 King Avenue
Columbus, OH

E. P. Stahel
Dept. of Chemical Engineering
North Carolina State University
Raleigh, NC 27607

E. R. Stephens
Statewide Air Pollution Research Center
University of California
Riverside, CA

R. K. Stevens
Environmental Protection Agency
National Environmental Research Center
Research Triangle Park, NC 27711

R. S. Tsai
Commonwealth of Puerto Rico
Economic Development Administration
Research and Development Dept.
G.P.O. Box 3088
San Juan, Puerto Rico 00936

Charles Walters
Environmental Protection Agency
National Environmental Research Center
Research Triangle Park, NC 27711

Hal Westberg
College of Engineering
Research Division
Washington State University
Pullman, WA 99163

W. E. Wilson
Environmental Protection Agency
National Environmental Research Center
Research Triangle Park, NC 27711

Arthur Winer
Statewide Air Pollution Research Center
University of California
Riverside, CA 92502

Ted Winfield
Environmental Protection Agency
National Environmental Research Center
Research Triangle Park, NC 27711

T. Yang
Calspan Corporation
4455 Genesee Street
P.O. Box 235
Buffalo, NY 14221

TECHNICAL REPORT DATA
(Please read Instructions on the reverse before completing)

1. REPORT NO.	2.	3. RECIPIENT'S ACCESSION NO.
EPA-600/3-76-029		

4. TITLE AND SUBTITLE	5. REPORT DATE
SMOG CHAMBER CONFERENCE PROCEEDINGS	April 1976
	6. PERFORMING ORGANIZATION CODE

7. AUTHOR(S)	8. PERFORMING ORGANIZATION REPORT NO.
Basil Dimitriades (Chairman)	

9. PERFORMING ORGANIZATION NAME AND ADDRESS	10. PROGRAM ELEMENT NO.
Environmental Sciences Research Laboratory Office of Research and Development U.S. Environmental Protection Agency Research Triangle Park, NC 27711	1AA008
	11. CONTRACT/GRANT NO.

12. SPONSORING AGENCY NAME AND ADDRESS	13. TYPE OF REPORT AND PERIOD COVERED
Environmental Sciences Research Laboratory Office of Research and Development U.S. Environmental Protection Agency Research Triangle Park, NC 27711	Final Oct. 24-25, 1974
	14. SPONSORING AGENCY CODE EPA-ORD

15. SUPPLEMENTARY NOTES

16. ABSTRACT

Smog chamber methodology was reviewed with respect to its present status and utility in developing photochemical pollution control strategies. Measurement of NO and O_3 in chamber atmospheres was judged to be satisfactory; measurement of NO_2, non-methane hydrocarbon, and sulfate presented problems. Surface effects and background contamination problems were minimal in large (hundreds of cubic feet) chambers made of Teflon film. Compared to indoor chambers, outdoor chamber operations were less costly and yielded more valid data in some respects. Specific sets of smog chamber data were used to estimate oxidant-related control requirements for California's South Coast Air Basin. Such estimates were judged to be more useful relative to those based on aerometric data analysis in that the role of NO_x in oxidant formation was considered quantitatively. Other applications of smog chamber methodology in photochemical air pollution research were discussed.

17. KEY WORDS AND DOCUMENT ANALYSIS

a. DESCRIPTORS	b. IDENTIFIERS/OPEN ENDED TERMS	c. COSATI Field/Group
Air Pollution * Test chambers * Design * Reviews Evaluation Contamination * Photochemical reactions		13B 14B 05B 07E

18. DISTRIBUTION STATEMENT	19. SECURITY CLASS *(This Report)*	21. NO. OF PAGES
RELEASE TO PUBLIC	UNCLASSIFIED	129
	20. SECURITY CLASS *(This page)*	22. PRICE
	UNCLASSIFIED	

EPA Form 2220-1 (9-73)